# A Computer Simulation and Molecular-Thermodynamic Framework to Model the Micellization of Ionic Branched Surfactants in Aqueous Solution

by
Shangchao Lin

B.S., Mechanical Engineering, University of Michigan, 2006

Submitted to the Department of Mechanical Engineering
in partial fulfillment of the requirements for the degree of

Master of Science

at the

MASSACHUSETTS INSTITUTE OF TECHNOLOGY

SEPTEMBER 2008



Signature of Author . . . . . .
Department of Mechanical Engineering
August 21, 2008

Certified by . . . . . .
Daniel Blankschtein
Professor of Chemical Engineering
Thesis Supervisor

Accepted by . . . . . .
Nicolas G. Hadjiconstantinou
Associate Professor of Mechanical Engineering
Thesis Reader

Accepted by . . . . . .
Lallit Anand
Professor of Mechanical Engineering
Chairman, Committee for Graduate Students

# A Computer Simulation and Molecular-Thermodynamic Framework to Model the Micellization of Ionic Branched Surfactants in Aqueous Solution

by

Shangchao Lin

Submitted to the Department of Mechanical Engineering
on August 21, 2008, in partial fulfillment of the
requirements for the degree of
Master of Science

## Abstract

Surfactants, or surface active agents, are chemicals exhibiting amphiphilic behavior toward a solvent. This amphiphilic character leads to increased activity at interfaces and to self-assembly into micellar aggregates beyond a threshold surfactant concentration, referred to as the critical micelle concentration (CMC), in bulk solutions. As a result of these unique attributes, surfactants are used in many pharmaceutical, industrial, and environmental applications, including biological separations, fat metabolism during digestion, drug delivery, and water purification. Selection of the appropriate surfactant for a given application is often motivated by the need to control bulk solution micellization properties, such as the CMC and the micelle shape and size. The ability to make molecular-level predictions of these surfactant properties would allow formulators in industry to speed up the design and optimization of new surfactant formulations.

In this thesis, a combined computer simulation/molecular-thermodynamic (CS－MT) modeling approach was developed and utilized to study the micellization behavior of ionic branched surfactants, which are a class of surfactants of great industrial relevance in applications such as detergency, emulsification, and enhanced-oil recovery. In the CS－MT modeling approach, molecular dynamics (MD) simulations are used to obtain input parameters for molecular-thermodynamic (MT) modeling of surfactant micellization. This approach is motivated by the limitations inherent in computer simulations (the high computational expense associated with modeling self-assembly) and in MT modeling approaches (their restriction to structurally and chemically simple surfactants).

One key input required for traditional MT modeling is the identification of the hydrated ("head") and the dehydrated ("tail") portions of surfactants in a self-assembled micellar aggregate. Using the results of MD simulations of surfactants in a micellar environment, a novel head and tail identification method was developed based on the determination of a conceptual micelle core－water interface. The introduction of an interfacial region consisting of partially hydrated, neutral atomic groups required formulating an improved surfactant tail packing approach.

Another key input required in the CS－MT modeling approach is the fractional degree of hydration of each atomic group in the ionic branched surfactants considered in this thesis, which can be used to accurately quantify the hydrophobic driving force for micelle formation in aqueous media. Fractional hydration profiles were obtained by conducting two MD simulations, one in a bulk water environment and the other in a micellar environment. By investigating the radial distribution function (RDF) between each surfactant group and hydrating atoms which are capable of forming hydrogen-bonds and coordinate-bonds, an updated cutoff distance for counting hydrating contacts was selected. These simulated fractional hydration profiles were then utilized as inputs in the MT model, which enables calculation of the minimum free energy associated with micelle formation, from which the CMC and the optimal micelle shape and size can be predicted at the molecular level.

The MD simulations were shown to extend the applicability of the traditional MT modeling approach to more complex surfactant systems than had been possible to date. A rich variety of ionic branched surfactants were modeled using the new CS－MT modeling approach, including two homologous series of simple secondary alkyl sulfonates and three classes of more complex ionic branched surfactants possessing aromatic moieties. For each of the ionic branched surfactants modeled, the predictions of the CS－MT modeling approach were found to be in reasonable agreement with the experimental data, including accounting for the chemical and structural complexities of the branched surfactants more accurately. The CS－MT modeling approach developed in this thesis not only extends our ability to make accurate molecular-level predictions of the micellization behavior of complex surfactants, but it also contributes to our overall fundamental understanding of the solution behavior of surfactants.

Thesis Supervisor: Daniel Blankschtein
Title: Professor of Chemical Engineering

# Contents

# List of Figures

# List of Tables

# Acknowledgments

My work in this thesis represents more than one year of effort as a Master student in the Blankschtein Group at MIT. In that time, I have had the opportunity to work with a number of individuals who have contributed in various ways to my personal and professional development. I look forward to continuing to work with many of them during my forthcoming doctoral research.

First, I would like to express my deep appreciation for the hard work and dedication of my thesis advisor, Professor Daniel Blankschtein, who introduced me to the discipline of colloid and interface science and guided me throughout the process of creating this thesis while stimulating my creativity and encouraging independent investigation. His patience and kindness continue to motivate and inspire me in my work and personal life. Professor Blankschtein also provided substantial help in organizing and presenting the results of this thesis. Without him, this thesis would not have been possible.

I would like to acknowledge two past students who influenced my research. Dr. Brian Stephenson, my predecessor in the group, was an important source of advice in the early stages of my project. Brian's doctoral research provided the starting point for my own work, and, although many aspects of the theory have changed with time to accommodate increasingly complex surfactant structures, Brian's contributions remain visible and the inspiration arising from his dedication to research constant. I would also like to thank Dr. Arthur Goldsipe, who developed the micellization software that I have used extensively in my research.

I would like to thank my collaborator on various aspects of this project, Jonathan Mendenhall, who is currently a doctoral candidate in the Blankschtein Group. Jonathan has worked on many of the computer programs required for the generation of the results presented here, and he developed the novel neutral atom packing model required for the accurate prediction of branched surfactant micellization properties. We have had many fruitful discussions regarding surfactants and computer simulation techniques, and I look forward to many more to come.

For help in proofreading this thesis in the early stages of its writing, and providing valuable constructive criticism, I would like to thank here both Jonathan and Jaisree Iyer, a new Ph.D. student in the Blankschtein Group. I greatly appreciate their help.

My sincere thanks are extended also to all past and present members of the Blankschtein Group who I have had the opportunity to interact with. They have provided a pleasant and supportive

environment in which to work. I hope that all past group members — Brian, Arthur, Srinivas, Saswata, Amanda, Leo, Vibha, and Hitoshi — all enjoy great success in their careers. I wish the current group members — Jonathan, Jennifer, Baris, and Jaisree — success in their present and future research endeavors.

Above all, I would like to thank my family — my grandparents, parents, and relatives, who have supported me throughout my time in the United States and away from home with their unfailing love and confidence in my efforts. My parents in particular always show interest in my daily life and have been supportive throughout my upbringing in our hometown of Suzhou, a beautiful Chinese city where I lived for 20 years, my undergraduate education at Shanghai Jiao Tong University in Shanghai, China and at the University of Michigan, and my current education at MIT.

Words cannot describe my deep appreciation for my wife Ying, whose love, understanding, encouragement, and persistent confidence in me has lifted burdens from my shoulders and supported me throughout, even as her words had to cross the great distance between Shanghai and Boston. I wish that we could have been together during the past three years that we have been in love. It is her unselfishness, her intelligence, her beauty, and her passion for our future that stirs and inspires me. In this simple way, I would like to express my gratitude: "Ying, I love you!"

Finally, I am grateful to DuPont for the research funding they have provided for this work through the DuPont-MIT Alliance. I am also grateful to the Department of Mechanical Engineering at MIT, who provided me with the opportunity to study here and complete this Master.

# Chapter 1

# Introduction

## 1.1 Background and Motivation

Surfactants, or surface active agents, are molecules consisting of a hydrophilic moiety, referred to as the head, and a hydrophobic moiety, referred to as the tail [1–3]. The surfactant head can be anionic, cationic, zwitterionic, or nonionic. The surfactant tail can consist of linear or branched hydrocarbons. In addition, aromatic groups, such as benzene rings, and haloalkanes, such as fluorocarbons, may be present in the surfactant tail. When dissolved in water, surfactant molecules self-assemble into aggregates above a threshold concentration, referred to as the critical micelle concentration (CMC) [1–3]. Above the CMC, the surfactant molecules form aggregates, known as micelles, that coexist with singly-dispersed surfactant molecules, known as monomers. The surfactant molecules comprising the micelle have their hydrophobic tails partly shielded from water in the aggregate interior (the micelle core), and their hydrophilic heads exposed to water at the aggregate surface (the micelle core–water interface) [1–3]. The self-assembly of surfactant molecules in water into spherical micelles is illustrated schematically in Figure 1-1. Surfactant self-assembly in water is driven primarily by the hydrophobic effect, a phenomenon wherein hydrophobic molecules tend to segregate from water as reflected in the tendency of oil to separate from water [1–3]. The hydrophobic effect is due to the disruption of the hydrogen-bonding network of water around hydrophobic molecules, and will be discussed in detail in Section 2.2. The amphiphilic, dual nature of surfactants towards water leads to the segregation of the hydrophobic tails from water and to the exposure of the hydrophilic heads to water, which results in the formation of micelles above

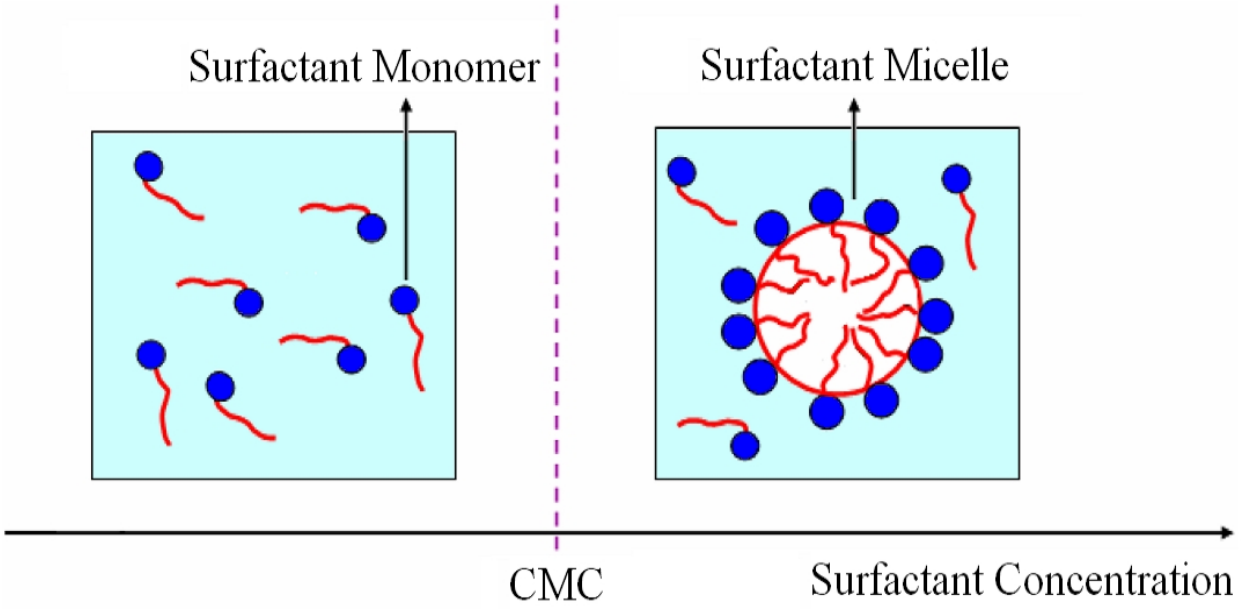


Figure 1-1: At surfactant concentrations which exceed the CMC, surfactant monomers self-assemble in water into micellar aggregates. (Color code for the surfactant molecule: blue – surfactant head and red – surfactant tail).

the CMC (see Figure 1-1). Other important driving forces for the micellization process include van der Waals, hydrogen-bonding, steric, and electrostatic (in the case of ionic and zwitterionic surfactants which carry charges) interactions [1–3].

Upon surfactant micellization, the concentration of free surfactant monomers in aqueous solution becomes independent, or only weakly dependent, on the total concentration of added surfactant molecules [2–4]. This is because from an enthalpic and entropic point of view, it is more favorable that the added surfactant molecules contribute either to the growth of existing micelles or to the increase in the population of similarly-sized micelles. The CMC depends on the chemical structure of the surfactant and the solution conditions, including the temperature, the pressure, and (particularly in the case of ionic surfactants) the solution ionic strength. Micelles may form in a number of different geometries. Indeed, in addition to spherical micelles, surfactants can form cylindrical and discoidal micelles depending on the surfactant chemical structure and on the solution conditions [2–4]. In the case of spherical micelles, the distribution of micelle sizes (aggregation numbers) is rather monodisperse, while in the case of cylindrical or discoidal micelles, the distribution of micelle sizes can be quite polydisperse [2, 3]. Spherical or globular micelles

are typically observed when total surfactant concentrations are low and/or when the repulsions between the surfactant heads are strong [2, 3]. At higher surfactant concentrations, one-dimensional growth into cylindrical micelles, or two-dimensional growth into discoidal micelles, may occur. In the case of ionic surfactants, the presence of counterions from added salts, which reduces the extent of electrostatic repulsions between the surfactant heads, can result in sphere-to-cylinder or sphere-to-disk micelle shape transitions [2–4].

Another important and practically relevant phenomenon observed in aqueous surfactant systems is solubilization (or "encapsulation") of sparingly water-soluble organic solutes in the hydrophobic cores of surfactant micelles [5, 6]. The micellar solubilization of such solutes increases their effective solubility in the aqueous solution. The solubilized solutes, or "solubilizates", may in turn impact micelle properties, including the CMC, and the shape and average size of micelles [5, 6].

A rich variety of industrial, environmental, energy-related, pharmaceutical, and biological processes make use of surfactants [5, 6], often because of their ability to enhance the effective solubility of sparingly water-soluble organic compounds via micellar-assisted solubilization. The ability of surfactants to aid in the mixing of hydrophobic and hydrophilic molecules is used extensively in the chemical industry in applications such as the removal of oily materials from a substrate (known as detergency), reaction-rate enhancement in polymerization reactions, and separation processes [5, 6]. In environmental applications, surfactant micelles can be used to solubilize and separate toxic ingredients in waste water for water purification [7–9]. In energy production, surfactants are used as one of the main reagents in fluids injected into underground formations during chemical flooding to achieve enhanced oil-recovery by reducing the oil–water interfacial tension [10–12]. Surfactants are also used in the pharmaceutical industry to encapsulate water-insoluble drugs in aqueous vehicles for oral or intravenous delivery into a patient's body [13]. Examples of biological processes involving surfactants include the role of phospholipid biosurfactants in the gastrointestinal tract during digestion, and the body's use of bile salts to solubilize cholesterol [5]. These important applications have encouraged researchers to synthesize, tune, and optimize new, more complex surfactants in order to attain improved performance characteristics.

Branched surfactants, that is, surfactants consisting of branched tails, constitute an important and practically relevant class of complex surfactants which are used extensively in the chemical

industry. Branched surfactants can originate as side products when synthesizing linear surfactants, such as Genapol UD 079, a commercial nonionic surfactant synthesized from paraffin hydrocarbons [14, 15]. The paraffin hydrocarbons typically consist of alkane mixtures comprising a distribution of linear and branched structures. The cost of purifying the paraffin hydrocarbons to produce linear alkanes is prohibitively expensive for most applications involving such commercial surfactants.

As shown in Figure 1-2, unlike linear surfactants, branched surfactants have side chains (SC's) attached to one, or to multiple, positions in the surfactant molecule, such as to the hydrophilic, nitrogen-carrying head (Figure 1-2 (a)), to the hydrophobic group close to the sulfonate head (Figure 1-2 (b)), or to the hydrophobic group on the primary hydrocarbon chain (Figure 1-2 (c)). Our group is interested in studying the micellization behavior of surfactants possessing branched tails for three practical reasons: (i) branched surfactants, such as Triton X-100 (Figure 1-2 (d), left) and Silwet L-77 (Figure 1-2 (d), right), are of great industrial relevance as ingredients in various product formulations, and are commonly used as stabilizers, emulsifiers, or wetting agents [16–19], (ii) branched surfactants, such as phospholipids (Figure 1-2 (e)), are of biological relevance in forming cell membranes which are an essential building block of cells, tissues, and organs [1, 20], and (iii) unlike linear surfactants, branched surfactants allow chemical formulators enhanced flexibility in designing new chemical architectures, as demonstrated recently by the great interest in the design of gemini surfactants (Figure 1-2 (f)) to improve solubilization capacity by varying the spacer length [21–25]. An important characteristic of branched surfactants, which affects micelle shape, is that the bulky surfactant tail separates the surfactant heads far from each other, and therefore, decreases the repulsions between the surfactant heads [26–29]. As a result, branched surfactants tend to aggregate into micelle shapes of lower curvature, including cylindrical and discoidal micelles, or to form planar bilayers in the case of phospholipid cell membranes [1, 20].

Since surfactant micellization (which serves as the basis of micellar-assisted solubilization) is such an important, widespread phenomenon, developing a fundamental understanding of the factors that affect micellization is of great academic and practical relevance. The development of theoretical modeling approaches would significantly reduce the time and cost associated with experiments aimed at designing and optimizing new surfactant formulations. Currently, this formulation process is mostly conducted in industry through tedious and time consuming trial-and-error

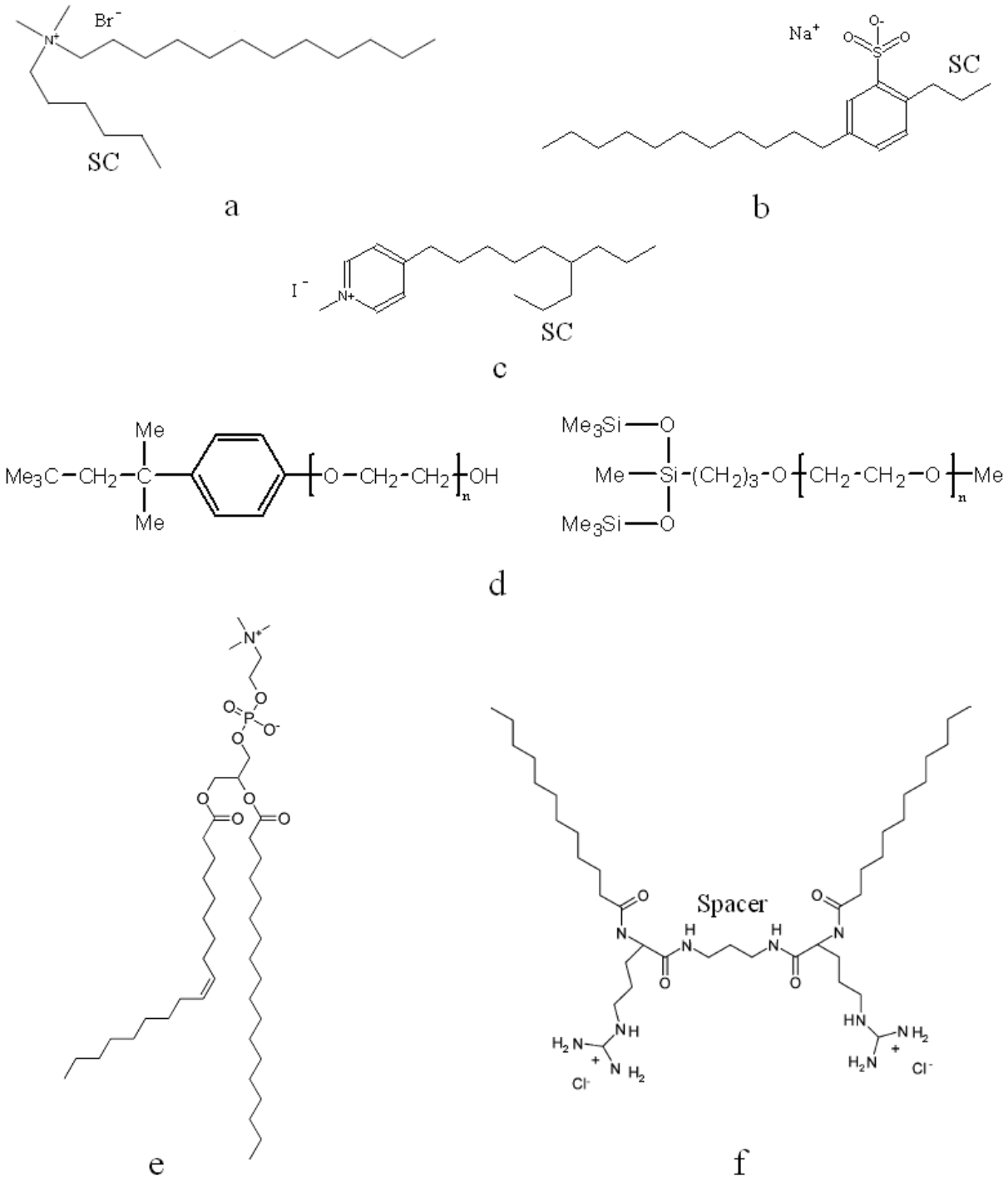


Figure 1-2: Examples of branched surfactants: (a) branched dimethylammonium bromide ($DC_6AB$), (b) sodium dialkyl benzene sulfonate, (c) alkyl pyridinium iodide, (d) Triton X-100 (left) and Silwet L-77 (right), (e) lecithin (phosphatidylcholine), and (f) arginine-based gemini surfactant. The "SC" in (a), (b), and (c) denotes side chain, and the “Me” in Triton X-100 and Silwet L-77 denotes a methyl group.

experimentation, or by using simple rules of thumb, which are not based on solid generalizable principles. Theoretical models developed in the past have aimed to: (i) provide molecular-level understanding of the micellization process, and (ii) predict micellar solution properties, including the CMC, the micelle geometry, and the microstructure of the micellar aggregates. In many cases, theoretical predictions of the CMC, the micelle shape, and the micelle size can also be correlated with practically relevant surfactant performance characteristics [3, 30, 31]. For example, researchers have reported correlations between the geometry of micelles and the micellar solution viscosity [3, 30]. Recently, the monomer and the micelle concentrations have been reported to correlate with the adverse ability of surfactants to induce skin irritation [31].

## 1.2 Introduction to Theoretical Models of Surfactant Micellization

In this section, an overview of the theoretical approaches that have been developed to model micellization is presented. Emphasis is given to molecular-thermodynamic (MT) models because these represent the most successful and predictive models of micellization that have been developed to date.

### 1.2.1 Brief Overview of Theoretical Models of Micellization

Many researchers have carried out theoretical investigations of surfactant micellization in aqueous solution in order to predict micellar solution properties as well as the microstructure of the micellar aggregates [32–36]. In several of these investigations, the surfactant chemical structure and the solution conditions (surfactant concentration, temperature, salt type and concentration, and counterion type) are used as inputs to make the necessary predictions. In particular, Tanford did groundbreaking work to develop a phenomenological theory of micellization, which provides significant insight into the physical process of micelle formation [1]. Subsequently, Israelachvili developed a geometric packing theory to model micellization, which allows predictions of micelle shape based on the surfactant geometry [2]. Following Tanford and Israelachvili, MT modeling approaches were developed and have been used by a number of researchers, particularly, by Nagarajan and

Ruckenstein [28, 33, 37–45]. In the MT modeling approach, the free energy of micellization is divided into several free-energy contributions, all of which can be computed molecularly, given the chemical structure of the surfactants and the solution conditions. The free energy of micellization corresponds to the free-energy change per surfactant molecule associated with transferring the surfactant monomers and the counterions (in the case of ionic surfactants) from the bulk aqueous solution to the micellar environment. The MT modeling approach developed by Nagarajan and Ruckenstein permits prediction of the CMC, the micelle shape, and the micelle size for a variety of simple surfactant systems, including nonionic, ionic, and zwitterionic surfactants [33]. More recently, the Blankschtein group has made important progress in the MT modeling of surfactant solution behavior [32, 46–56]. Most recently, a novel, combined computer simulation–molecular-thermodynamic (CS–MT) modeling approach was developed by Stephenson et al., which involves the use of computer simulations (CS) to obtain input parameters for the molecular-thermodynamic (MT) modeling of surfactant micellization [57–60]. The CS–MT modeling approach has been successfully applied to model a broad class of surfactants having linear hydrocarbon tails attached to single nonionic, anionic, cationic, or zwitterionic heads, including octyl sulfinyl ethanol (OSE), dodecyl octa(ethylene oxide) ($C_{12}E_8$), sodium dodecyl sulfate (SDS), cetyltrimethylammonium bromide (CTAB), and dodecylphosphocholine (DPC) [59, 60].

### 1.2.2 Limitations of the Current Molecular-Thermodynamic Modeling Approaches

Although significant progress has been made to date, MT approaches advanced to model surfactant micellization have been successfully applied only to relatively simple surfactants. The most severe limitation associated with MT modeling is the requirement of *a priori* knowledge of the hydrated and the dehydrated portions of surfactants within a micelle. This information is used to assign a head and a tail to each of the surfactant species present, and is one of the most important inputs required to evaluate the free-energy change associated with micelle formation. Based on experimental evidence, it is possible to anticipate which portions of a surfactant molecule will be hydrated in the case of simple chemical structures. For example, surfactants with linear hydrocarbon tails attached to a single charged anionic, cationic, or zwitterionic head have all the $CH_2$ groups

in the hydrocarbon, except for the one adjacent to the charged head, in the surfactant tail [48, 49]. On the other hand, nonionic surfactants typically have all the $CH_2$ groups in the hydrocarbon in the surfactant tail [33, 61].

However, in the case of more complex surfactant chemical structures, such as those shown in Figure 1-2, it is much more difficult to make reasonable *a priori* surfactant head and tail assignments. Indeed, for surfactants which contain branching in the tail region, this difficulty reflects the more constrained conformations of the shorter, side chain (SC) because of its connectivity to the longer, primary chain (see Figure 1-2), a constraint that is not present in the case of surfactants which possess linear tails. In particular, it is challenging to determine the hydration state of the shorter, side chain in sodium dialkyl benzene sulfonate (see Figure 1-2 (b)). This reflects the fact that the longer, primary chain in sodium dialkyl benzene sulfonate needs to fill out the incompressible micelle core, and as a result, the smaller side chains are often forced to reside at the micelle core–water interface due to the constraint imposed by their geometric attachment to the primary chain. However, it is unclear *a priori* which side chain atoms will locate inside the micelle core (thereby undergoing significant dehydration) and which side chain atoms will reside at the micelle core–water interface (thereby remaining hydrated). Similarly, the hydration state of the benzene ring attached to the sulfonate group in the same surfactant is unclear. Indeed, it is very likely that only part of the benzene ring will reside fully within the micelle core. This example demonstrates that, in order to generalize MT modeling to more chemically and structurally complex surfactants, knowledge of the hydration states of chemical moieties in the self-assembled, equilibrium micellar state is required. Obtaining the required information is beyond the capability of simple group-contribution methods, because the hydration state (and, therefore, the head and tail identification) of various moieties within a complex surfactant is intimately related to the manner in which these moieties are connected to each other. The CS–MT modeling approach was developed in order to model such complex surfactants [59, 60].

## 1.3 Introduction to Computer Simulation Methods

Computer simulations of molecular systems are used to estimate equilibrium or dynamic properties of the systems. Computer simulations allow investigations of complex, many-body systems for

which analytical, closed-form solutions do not exist. Two of the most popular computer simulation methods used today are molecular dynamics (MD) and Monte Carlo (MC) simulations. Both methods can be used to determine equilibrium properties, while the MD method can also be used to determine dynamic properties. Frequently, properties of interest depend on the positions and momenta of all the particles present in a system. Given this dependence, the instantaneous value of the property of interest, $A$, can be expressed as $A(p^N(t), r^N(t))$, where $p^N(t)$ represents the momenta of the $N$ particles at time $t$, and $r^N(t)$ represents the positions of the $N$ particles at time $t$. The instantaneous value of the property $A$ may fluctuate with time, and it is frequently useful to determine the time average value of the property through integration [62]:

$$A_{ave} = \lim_{\tau \to \infty} \frac{1}{\tau} \int_{\tau=0}^{\tau} A\left(p^N(t), r^N(t)\right) dt \tag{1.1}$$

In MD simulation, the time evolution of a system is determined by solving Newton's equations of motion. To this end, a potential energy model (referred to as a force field) must be used to describe the intermolecular and intramolecular interactions of each of the system components. The forces acting on each particle in the system are determined through differentiation of the potential energy model. Once the force acting on each particle is known, trajectories which describe how the positions, velocities, and accelerations of the particles respond to these forces are computed numerically by incrementing forward in time with small time steps and using an integration technique such as the velocity Verlet or the leap-frog algorithm [63]. At the end of an MD simulation with $S$ time steps, averaged properties are determined as follows [62]:

$$A_{ave} = \frac{1}{S} \sum_{i}^{S} A\left(p^N(i), r^N(i)\right) \tag{1.2}$$

An alternative to determining a time average value of the property A of interest is to calculate the ensemble average, or the expectation value. In this approach, a large number of replicas of the system of interest are considered simultaneously. The ensemble average, usually determined in an MC simulation, can be expressed mathematically as follows [62]:

$$\langle A \rangle = \iint A\left(p^N, r^N\right) \rho(p^N, r^N) dp^N dr^N \tag{1.3}$$

where $\rho(p^N, r^N)$, the probability density of the ensemble, is the probability of finding a configuration with momenta $p^N$ and positions $r^N$. Although only a double integral sign is shown, in practice, the integration is carried out over all $6N$ momenta and positions of the particles present in the system. Therefore, in this approach, the average value of the property $A$ is determined by averaging over all possible configurations of the system rather than by taking a time average. In accordance with the ergodic hypothesis, which is one of the fundamental axioms of statistical mechanics, the ensemble average $\langle A \rangle$ can be considered equal to the time average $A_{ave}$ under certain conditions. In particular, in MD simulations, the ergodic hypothesis holds by assuming no correlation among each system trajectory frame that one outputs for studying. Therefore, the average, or expectation value, of the property $A$ is obtained from MD simulations as follows [62]:

$$\langle A \rangle = A_{ave} = \frac{1}{M} \sum_{i}^{M} A\left(p^N(i), r^N(i)\right) \tag{1.4}$$

where $M$ is the number of trajectory frames outputted for studying. Note that $M$ may be equal to the number of simulation time steps $S$, or it may be the number of trajectory frames outputted at regular time steps.

### 1.3.1 Brief Overview of Computer Simulation Studies of Micellization

In recent years, a growing number of researchers have investigated the use of computer simulations to examine the structural characteristics of micelles and to model the self-assembly of surfactants in aqueous solution. The majority of the research reported to date has used either molecular dynamics (MD) or Monte Carlo (MC) simulations. In theory, MD and MC simulations based on atomistic force fields have the advantage of being able to model arbitrarily complex chemical structures. However, computer simulation of micelle formation is computationally challenging because: (i) micellar systems may consist of many surfactant and solvent molecules (typically comprising millions of atoms), (ii) micellar systems have a high liquid-like density (continuous simulation under infinite dilution condition does not work), and (iii) the time scales involved in surfactant self-assembly are quite long (on the order of milliseconds [1], while a computer simulation time step is typically on the order of femtoseconds). As a result of (i) - (iii) above, it has been necessary to either simulate coarse-grained systems over long time periods to gain simplified

insight into the self-assembly process, or to simulate small systems over short time periods using more realistic, fully-atomistic models of the system components and of the intramolecular interactions [64–73]. Additional areas of research include the use of computer simulations to directly estimate the free energy of micellization [74], or the use of computer simulations of preformed surfactant micelles to study post-equilibrium micellar microstructures [75–85]. Recently, Stephenson et al. have performed: (i) computer simulations of preformed surfactant systems [59, 60], (ii) computer simulations of surfactant self-assembly [86], and (iii) direct computer-simulation estimations of the free energy of micelle formation [87, 88].

### 1.3.2 Introduction to Computer Simulation–Molecular-Thermodynamic (CS–MT) Models

As discussed in Section 1.3.1, determining the free energy of micellization through computer simulations is challenging and computationally expensive. To circumvent the limitations associated with implementing a purely computer simulation approach, Mohanty et al. developed a computational approach to determine the free energy of micellization that combines computer simulations and molecular-thermodynamic modeling [89]. Mohanty et al. used this approach to model a surfactant system consisting of the cationic surfactant cetyltrimethylammonium bromide (CTAB) and the salt sodium salicylate (NaSal). Mohanty et al. obtained reasonable estimates of the effect of the salicylate ions on the CMC, on the micelle geometry, and on the micelle size. It is important to note that Mohanty et al. only accounted for the presence of water using a mean-field term calculated separately from simulations using the method of Bocker et al. [83]. Although the results obtained, particularly for the sphere-to-wormlike micelle shape transition, appear quite reasonable, given the large number of approximations made during the simulations (including the implementation of approximate constraints to maintain the structure of the micelle shell region, the use of approximate models to account for the interactions of the micellar components with counterions and water, and the approximate MT modeling of the micelle core region), the level of agreement obtained with the experimental data exceeded expectations.

Most recently, Stephenson et al. have used the CS–MT modeling approach, with the motivation discussed in Sections 1.1 and 1.2 in mind, to determine the free energy of micellization [57–60, 90].

Development of a hybrid CS–MT modeling approach is motivated by the limitations inherent in computer simulations (the high computational expense associated with direct modeling of self-assembly) and in molecular-thermodynamic modeling approaches (their restriction to structurally and chemically simple surfactants). The CS–MT modeling approach was developed to more accurately quantify the hydrophobic driving force, which is the primary driving force for surfactant self-assembly in aqueous solution. In the CS–MT modeling approach, atomistic molecular dynamics (MD) simulations are used to quantify the hydration changes that take place during self-assembly [57–60]. This hydration information is then used in an MT model to quantify the hydrophobic effect, which is decomposed into two components: (i) the free-energy change associated with the dehydration of the entire surfactant molecule that accompanies micelle self-assembly (as captured in $\hat{g}_{dehydr}$), and (ii) the change in hydration free energy experienced by the surfactant tail in the micelle core during micelle self-assembly (as captured in $\hat{g}_{hydr}$).

A key input required for the MT modeling approach is the identification of the hydrated and the dehydrated portions (head and tail) of surfactants in a self-assembled micelle. It is important to note that although surfactant molecules consist of hydrophobic moieties and hydrophilic moieties, one often finds that the hydrophilic moiety is not necessarily completely hydrated and that the hydrophobic moiety is not necessarily completely dehydrated. This information was originally obtained by conducting MD simulations of surfactant molecules at a water–oil interface (serving as a proxy of the micelle core–water interface) [57]. Instead, in the modified CS–MT modeling approach described in this thesis to model branched surfactants, I have developed a new approach for head and tail identification by conducting MD simulations of surfactants in a micellar environment. From the MD simulation results, I have found that some groups in the surfactant molecule tend to reside near the micelle core–water interface. These groups cannot be easily identified as being part of the surfactant head or as being part of the surfactant tail, since they are neither as dehydrated as groups that belong to the tail nor as hydrated as groups that belong to the head. Therefore, these partially hydrated groups have been designated as "neutral atom" groups in the surfactant molecule, and a modified MT model was developed in collaboration with J. D. Mendenhall in the Blankschtein group to model the free energy of micellization of surfactants possessing conventional head and tail groups in addition to neutral groups. This new assignment of each atomic group as head, tail, or neutral allows for the extension of the CS–MT modeling approach to

more complex surfactant systems than has been possible to date.

The CS–MT modeling approach was formulated to allow prediction of the free-energy change associated with the formation of surfactant aggregates of any shape and size by performing only two MD simulations: one of the surfactants in bulk water and the other of the surfactants in a micelle of spherical shape and an arbitary size [58]. In the CS–MT modeling approach implemented in this thesis, to model branched surfactants, a modified method for analyzing MD simulation results was introduced to maintain consistency with the general approach used previously in the literature [78, 91–95]. The new, modified CS–MT modeling approach was validated by using it to model the micellization behavior of two homologous series of simple ionic branched surfactants in aqueous solution, and the micellization behavior of three classes of complex ionic branched surfactants in aqueous solution. For each of the branched surfactant systems modeled, the modified CS–MT model predictions were found to be in reasonable agreement with the experimental data.

The remainder of the thesis is organized as follows. In Chapter 2, the theoretical background on surfactant self-assembly is reviewed, including a description of the traditional MT model (Section 2.1) and the CS–MT model (Section 2.2). In Chapter 3, the computer simulation approach used to obtain the hydration information required in the CS–MT model is presented, including: (i) an overview of the modeling approach (Section 3.1), (ii) a description of the simulation methods and parameters (Section 3.2), (iii) a description of the system preparation process and equilibrium criterion (Section 3.3), and (iv) a description of the method used to analyze the MD trajectories (see Section 3.4). In Chapter 4, predictions of surfactant properties used as inputs in the CS–MT model are presented, including: (i) a discussion of the head and tail identification method (Section 4.1), (ii) estimations of four surfactant geometric parameters (Section 4.2), and (iii) a description of the group-contribution method used to compute the interfacial tension associated with the micelle core–water interface (Section 4.3). In Chapter 5, the CS–MT modeling results are presented, including the MD simulation results of the fractional hydration profiles as inputs to the CS–MT model (Section 5.1), and the MT modeling results for the ionic linear and branched surfactants considered in this thesis with available experimental data for comparison (Sections 5.2 and 5.3). Finally, concluding remarks and future work are presented in Chapter 6.

# Chapter 2

# Theoretical Background

## 2.1 Traditional Molecular-Thermodynamic (MT) Model of Micellization

The traditional molecular-thermodynamic model of micellization relies on a thermodynamic framework to describe the micellar solution [48]. This framework allows the calculation of micellar solution properties, such as the CMC, the distribution of micelle shapes and sizes, and microstructural characteristics of the micelle (such as its core-minor radius) from the free energy of micellization. In Section 2.1.1, I discuss the thermodynamic framework that relates the free energy of micellization to various micellar solution characteristics. In Section 2.1.2, I review the traditional MT model that has been used in the past to calculate the free energy of micellization associated with micelle formation in aqueous media [48, 49, 61].

### 2.1.1 Thermodynamic Framework

The thermodynamic framework considered here is applicable to single-component, nonionic, zwitterionic, and ionic surfactants with single-type counterions bound at the micelle surface. Consider a thermodynamically equilibrated solution of $N_w$ water molecules and a distribution $\{N_{n_s n_c}\}$ of micellar aggregates (referred to as $n_s n_c$-mers) at temperature $T$ and pressure $P$, where $n_s$ is the number of surfactant molecules (component $s$) and $n_c$ is the number of bound counterions (component $c$) in each micelle.

According to the multiple-chemical equilibrium model of micellization [2], each micelle can be considered as a distinct chemical species in equilibrium with the other micelles, with the individually-dispersed surfactant molecules (the surfactant monomers), and with the unbound counterions present in the aqueous solution. Accordingly, at thermodynamic equilibrium, the solution free energy attains its minimum value when [48]:

$$\mu_{n_s n_c} = n_s \mu_s + n_c \mu_c \tag{2.1}$$

where $\mu_{n_s n_c}$ is the chemical potential of an $n_s n_c$-mer, $\mu_s$ is the chemical potential of a surfactant monomer, and $\mu_c$ is the chemical potential of an unbound counterion. Note that in the case of nonionic and zwitterionic surfactants, no counterions are present, and therefore, $n_c = 0$ throughout. The chemical potential, $\mu_{n_s n_c}$, in Eq. 2.1 can be calculated by taking the partial derivative of the total solution free energy with respect to $N_{n_s n_c}$, keeping the number of molecules of other species, the temperature, and the pressure constant [48, 49]. The chemical potential of a surfactant monomer, $\mu_s$, and of an unbound counterion, $\mu_c$, are obtained by setting $\{n_s = 1; n_c = 0\}$ and $\{n_c = 1; n_s = 0\}$, respectively, in the resulting expression for $\mu_{n_s n_c}$ [48, 49].

Using the resulting expressions for $\mu_{n_s n_c}$, $\mu_s$, and $\mu_c$ in Eq. 2.1, the following expression is obtained for the population distribution of $n_s n_c$-mers, or $n_s \beta$-mers, if it is expressed in terms of the degree of counterion binding ($\beta$, defined as $\beta = n_c / n_s$):

$$X_{n_s n_c} = X_{n_s \beta} = \left(\frac{1}{e}\right) X_s^{n_s} \exp\left(-\frac{n_s g_{mic}\left(S, l_c, \beta\right)}{k_B T}\right) \tag{2.2}$$

where

$$g_{mic} = \left(\frac{\mu^0_{n_s n_c}}{n_s} - \mu^0_s - k_B T - \beta \mu^0_c\right) - \beta k_B T \ln X_c \tag{2.3}$$

In Eq. 2.2, $X_s = N_s / N$ is the mole fraction of monomeric surfactant, and $X_{n_s n_c} = N_{n_s n_c} / N$ is the mole fraction of micelles composed of $n_s$ surfactant molecules and $n_c$ counterions, where $N = N_s + n_s N_{n_s n_c}$. In Eqs. 2.2 and 2.3, $g_{mic}$ is the free-energy of micellization per surfactant molecule, $k_B$ is the Boltzmann constant, and $T$ is the absolute temperature. In Eq. 2.3, $\mu^0_i$ is the standard-state chemical potential of species $i$ ($n_s n_c$, $s$, or $c$).

The free energy of micellization, $g_{mic}$, reflects the free-energy changes associated with trans-

ferring the surfactant monomers and the counterions in their corresponding standard states from the aqueous solution to form a micelle in its standard state (the term in the brackets in Eq. 2.3), as well as with the translational entropic penalty associated with localizing the counterions (the second term in Eq. 2.3), when that micelle is formed [48]. As shown in Eq. 2.2, $g_{mic}$ is a function of the micelle shape factor ($S$, where $S$ = 1, 2, and 3 for discoidal, cylindrical, and spherical micelles, respectively), the micelle core-minor radius ($l_c$), and the degree of counterion binding ($\beta$).

At the values of $S$, $l_c$, and $\beta$ that minimize $g_{mic}$ (denoted as $S^*$, $l_c^*$, and $\beta^*$), $g_{mic}$ has a minimum value denoted as $g_{mic}^*$. Due to the exponential dependence of $X_{n_s n_c}$ on $n_s g_{mic}$ in Eq. 2.2, small deviations of $g_{mic}$ from $g_{mic}^*$ results in large changes in $X_{n_s n_c}$. At $g_{mic}^*$, $X_{n_s n_c}$ attains its maximum value, which indicates that the population distribution of these $n_s n_c$-mers (corresponding to the optimal micelle geometry) is dominant. Accordingly, by solving for $g_{mic}^*$, the optimal micelle shape, $S^*$, the optimal core-minor radius, $l_c^*$, and the optimal degree of counterion binding, $\beta^*$, can be predicted at the molecular level. In addition, the surfactant CMC in mole fraction units is given by [48]:

$$CMC \approx \exp\left(\frac{g_{mic}^*(S^*, l_c^*, \beta^*)}{k_B T}\right) \tag{2.4}$$

Note that due to the exponential dependence of the CMC on $g_{mic}^*$, small errors in the predicted $g_{mic}^*$ result in large deviations in the predicted CMC values. As a result, a comparison of the predicted and the experimental CMC's serves as a very sensitive quantitative indication of the accuracy with which $g_{mic}^*$ can be predicted molecularly.

### 2.1.2 Traditional MT Model of Surfactant Micellization

The evaluation of $g_{mic}$, using as little experimental information as possible, has been the subject of much investigation. The traditional MT model can be used to predict $g_{mic}$ based on the chemical structures of the surfactants and the counterions in the aqueous solution. As discussed in Section 1.2.2, important inputs to the MT model are the hydrated and the dehydrated portions of each surfactant in the micellar environment [57]. The free energy of micellization, $g_{mic}$, as a function of $S$, $l_c$, and $\beta$, can be minimized with respect to each of these variables to enable the prediction of micelle characteristics and of CMC's. In the traditional MT modeling approach, $g_{mic}$ is expressed

as the sum of the following six free-energy contributions [96]:

$$g_{mic} = g_{tr} + g_{int} + g_{pack} + g_{st} + g_{elec} + g_{ent} \tag{2.5}$$

Each of the six contributions in Eq. 2.5 arises from a distinct step in a thermodynamic cycle used to model the process of micelle formation. The various steps involved are shown schematically in Figure 2-1, which depicts the micelle formation process for a cationic surfactant in aqueous solution. An analogous thought process may be used to model the formation of a multi-component surfactant micelle [37] or of a surfactant micelle containing solubilizates [39].

In the first step shown in Figure 2-1, the cationic surfactant heads are conceptually separated from the surfactant tails and subsequently discharged along with the negative counterions in the bulk aqueous solution. The corresponding discharge free energy is denoted as $g_{discharge}$ [48, 49], which is one contribution to the electrostatic free energy, $g_{elec}$.

In the second step shown in Figure 2-1, a hydrophobic micelle core composed of the surfactant tails is formed. This step is modeled as the sum of three free-energy contributions: $g_{tr}$, $g_{int}$, and $g_{pack}$. The transfer free-energy contribution, $g_{tr}$, represents the free-energy change associated with transferring the surfactant tails from the bulk aqueous solution to a bulk solution of surfactant tails [1]. The interfacial free-energy contribution, $g_{int}$, represents the free-energy change associated with forming an interface between the bulk solution of surfactant tails (the precursor of the micelle core) and the bulk aqueous solution [48]. The packing free-energy contribution, $g_{pack}$, represents the free-energy change required to fix one end of the surfactant tails at the micelle core–water interface. This free-energy contribution is estimated using a mean-field model first introduced by Ben-Shaul, Szleifer, and Gelbart [97–99]. It requires sampling the conformations and orientations of a surfactant tail, which is fixed at one end and subject to the constraint that the hydrophobic micelle core has a uniform density, which is enforced by a set of lateral pressures that act on the surfactant tail.

In the third step shown in Figure 2-1, the surfactant heads are transferred back to the surface of the micelle (with free-energy contributions, $g_{st}$ and $g_{tr,head}$) and recharged along with the counterions (with a free-energy contribution, $g_{charge}$) [48, 49, 100]. The steric free-energy contribution, $g_{st}$, accounts for the steric penalty associated with placing the surfactant heads in close proximity at

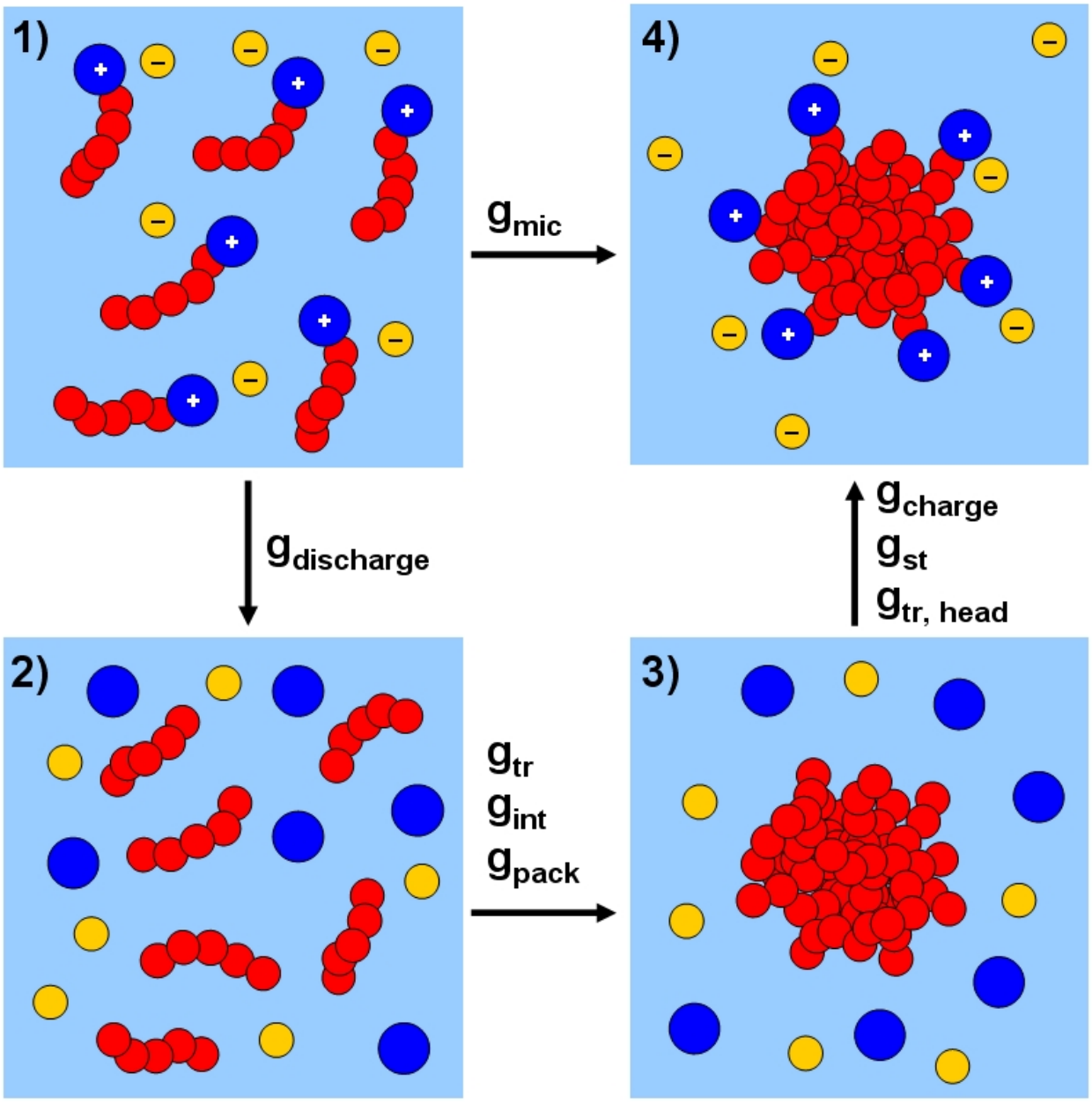


Figure 2-1: Sequence of steps followed in the molecular-thermodynamic cycle used in the CS-MT modeling approach. This sequence is presented in the context of the micellization of a cationic surfactant in aqueous solution. Between frames (1) and (2), the surfactant heads (the large blue circles carrying positive charges) are separated from the surfactant tails (the chains consisting of five red circles), and the surfactant heads and the counterions (the small yellow circles carrying negative charges) are discharged (as reflected in $g_{discharge}$). Between frames (2) and (3), the surfactant hydrophobic tails are grouped to form the micelle core (as reflected in $g_{tr}$, $g_{int}$, and $g_{pack}$). Between frames (3) and (4), the surfactant heads are reattached to one end of the surfactant tails (as reflected in $g_{st}$ and $g_{tr,head}$), and the surfactant heads and their associated counterions are recharged (as reflected in $g_{charge}$).

the micelle core–water interface [61]. In reattaching the surfactant heads to the tails at the micelle core–water interface, the heads are transferred to a slightly different environment from that corresponding to the bulk water reference state. The free-energy change associated with this transfer is expressed as $g_{tr,head}$. In the traditional MT modeling approach, the surfactant heads are assumed to remain fully hydrated in both the bulk water environment and in the micellar state, and therefore, $g_{tr,head}$ is approximated as being equal to zero. As a result, the free-energy contribution, $g_{tr,head}$, is not listed in Eq. 2.5. We define the electrostatic free-energy contribution, $g_{elec}$, in Eq. 2.5 as being equal to the sum of $g_{discharge}$ and $g_{charge}$ [48, 49]. Note that the entropic free-energy contribution, $g_{ent}$, although included in Eq. 2.5, is not shown in Figure 2-1 because, in general, (e.g., for multi-component surfactant systems or surfactant systems containing solubilizates) it may contribute to the thermodynamic cycle at several steps. For the single-component surfactant system considered here, the entropic free-energy contribution only includes the translational entropy loss of the bound counterions [48, 49]. A more detailed description of the conceptual thought process implemented in the traditional MT modeling approach can be found in Refs. [61] and [48].

The sequence of steps outlined above have been used by alkyl group for many years to model the process of micelle formation at the molecular level. An important assumption underlying the thermodynamic cycle shown in Figure 2-1 is that the hydration states of the surfactant tails is not allowed to change when separating them from the surfactant heads in aqueous solution, and subsequently reattaching them in the micellar environment. Therefore, the hydration states of the surfactant tails are assumed to be the same in frames (1) and (2), as well as in frames (3) and (4), in Figure 2-1. The transition from frame (2) to frame (3) in Figure 2-1 reflects the formation of the hydrophobic micelle core. The changes in hydration incurred in the formation of this micelle core represent the primary hydrophobic driving force for micelle formation in aqueous media. In traditional MT modeling, this driving force is modeled by two terms, $g_{tr}$ and $g_{int}$. Since a more general and accurate calculation of the hydrophobic contribution to the free energy of micelle formation is the central goal of this chapter, I will discuss the traditional MT modeling approach used to calculate $g_{tr}$ and $g_{int}$ in more detail in the following two sections. For a detailed discussion of the other free-energy contributions appearing in Eq. 2.5, the interested reader is referred to Refs. [61], [48], and [96].

**The Transfer Free-Energy Contribution, $g_{tr}$**

In the traditional MT modeling approach, only the surfactant tails contribute to $g_{tr}$. Therefore, to determine this free-energy contribution, it is first necessary to identify the head and the tail of each surfactant present in the micelle. Various approaches for such identification were developed in the past [49,57,61], and a new approach to identify head and tail based on the concept of an equimolar Gibbs dividing surface was developed as part of this thesis and will be discussed in detail in Section 4.1. After identifying the surfactant tails, $g_{tr}$ is estimated on a per surfactant molecule basis. For example, in a micelle containing a single surfactant type, the transfer free-energy contribution is estimated as follows [61]:

$$g_{tr} = k_B T \ln(s) \tag{2.6}$$

where $s$ is the aqueous solubility of the surfactant tail expressed on a mole fraction basis. For linear alkyl tails, correlations have been developed from linear hydrocarbon solution data to express solubility as a function of alkyl chain length, temperature, and the concentration of added salt in aqueous solution [61, 101, 102]. For more complex surfactants, either experimental solubility data or group-contribution methods may be used to estimate the tail solubility [57,90]. For a linear alkyl tail at temperature $T$, the following expression for the transfer free energy has been developed [61]:

$$g_{tr} = \left[ (3.037 - 1.05 n_t) \frac{298}{T} - (5.06 + 0.444 n_t) \right] k_B T \tag{2.7}$$

where $n_t$ is the number of carbons in the surfactant tail. This expression for the transfer free energy can be used to estimate, $g_{tr_i}$, the contribution to $g_{tr}$ from each carbon group in the surfactant tail. Specifically, by rewriting Eq. 2.7 in terms of $n_{CH_2}$, the number of $CH_2$ groups (that is, $n_t - 1$), and $n_{CH_3}$, the number of $CH_3$ groups (that is, 1) in the surfactant tail, we obtain the following expression:

$$g_{tr} = \left[ \left( \frac{592}{T} - 5.504 \right) n_{CH_3} - \left( \frac{313}{T} + 0.444 \right) n_{CH_2} \right] k_B T = n_{CH_3} g_{tr_{CH_3}} + n_{CH_2} g_{tr_{CH_2}} \tag{2.8}$$

Use of Eq. 2.8 yields $g_{tr_{CH_2}} = -1.494\ k_B T$ and $g_{tr_{CH_3}} = -3.518\ k_B T$ at 25°C, two useful results that are used in the CS–MT modeling approach discussed in Section 2.2.

**The Interfacial Free-Energy Contribution,** $g_{int}$

All the surfactant tail groups which are transferred from the aqueous solvent to the micelle core will reside for some time at the micelle core surface. As a result, when the bulk surfactant tail solution is exposed to the aqueous environment, a micelle core–water interface will form, and the surfactant tails residing at this interface will be partially rehydrated. The free-energy penalty associated with rehydrating these tail groups is referred to as the interfacial free-energy contribution, $g_{int}$, and is modeled in the traditional MT approach using a micelle core–water interfacial tension. In a micelle containing a single surfactant type, $g_{int}$ is computed on a per surfactant molecule basis using the following expression [48]:

$$g_{int} = \sigma_s(a - a_0) \tag{2.9}$$

where $\sigma_s$ is the curvature-dependent interfacial tension between a bulk phase of surfactant tails and water, $a$ is the area available to each surfactant molecule at the micelle core–water interface, and $a_0$ is the interfacial area that is shielded by the surfactant heads on a per surfactant molecule basis [61]. The curvature-dependent interfacial tension, $\sigma_s$, is determined using the Gibbs-Tolman-Koenig-Buff equation [103–106]:

$$\sigma_s = \frac{\sigma_0}{\left[1 + \frac{(S-1)\delta}{l_c}\right]} \tag{2.10}$$

where $\sigma_0$ is the interfacial tension between a surfactant tail phase and water at a flat interface (having a typical value of about 50 mN/m for hydrocarbons), $\delta$ is the Tolman distance [104], and $S$ is the shape factor introduced in Section 2.1.2. An empirical correlation was used to determine $\sigma_0$ as a function of the alkyl chain length and the solution temperature, although, if available, experimental $\sigma_0$ values may be used [107]. The Tolman distance, $\delta$, is computed using the following expression [61]:

$$\delta(n_t) = \frac{\delta(11) l_{\max}(n_t)}{l_{\max}(11)} \tag{2.11}$$

where $\delta(11)$ is the Tolman distance corresponding to $n_t = 11$, which has been determined to be approximately 2 Å [61], and $l_{\max}(n_t) = (1.265 n_t + 1.54)$ Å is the fully-extended length of the surfactant tail [1].

## 2.2 The Computer Simulation–Molecular-Thermodynamic (CS–MT) Modeling Approach

In this section, I will discuss the CS–MT modeling approach originally developed by Stephenson et al. [58–60], which incorporates hydration information obtained from computer simulation as an input to the molecular-thermodynamic theory. This modeling approach allows better quantification of the hydrophobic driving force for micelle self-assembly in aqueous media than the traditional MT modeling approach, which was reviewed in Section 2.1.2. As part of this thesis, a new method to obtain hydrating contacts and a more rigorous approach to make head and tail identifications have been developed, and will be discussed in Sections 3.4.3 and 4.1.

### 2.2.1 Theoretical Framework

As discussed in Section 2.1.2, and shown in Eq. 2.5, in the traditional MT model, the free energy associated with the hydrophobic effect, $g_{HE}$, is expressed as the sum of the two free-energy contributions, $g_{tr}$ and $g_{int}$. In order to more accurately quantify the hydrophobic effect, Stephenson et al. proposed replacing the sum of $g_{tr}$ (including the $g_{tr,head}$ term) and $g_{int}$ (see Figure 2-1) with the sum of: (i) the free-energy contribution associated with dehydration, $g_{dehydr}$, and (ii) the free-energy contribution associated with hydration, $g_{hydr}$, as follows [58]:

$$g_{HE} = g_{tr} + g_{int} = g_{dehydr} + g_{hydr} \tag{2.12}$$

The models used to calculate $g_{dehydr}$ and $g_{hydr}$ are presented in Section 2.2.3 and 2.2.4, respectively. As discussed in Section 1.3.2, since only two MD simulations were performed to obtain the hydration data for a surfactant micelle, $g_{HE}$ computed from these simulations is only applicable to a micellar aggregate having a given shape and size matching those of the simulation. Accordingly, Eq. 2.12 should be rewritten as follows:

$$\hat{g}_{HE} = g_{tr} + \hat{g}_{int} = \hat{g}_{dehydr} + \hat{g}_{hydr} \tag{2.13}$$

where the "ˆ" indicates that each free-energy contribution is calculated for the simulated micellar

aggregate, rather than for the optimal micelle. As a result, the MD simulations conducted as part of the CS–MT modeling approach do not allow prediction of the optimal micelle shape and size by themselves. Nevertheless, a central feature of the traditional MT model discussed in Section 2.1.2 is its ability to predict $g_{mic}(S, l_c, \beta)$ as a function of micelle shape and size. This functional dependence enables the minimization of $g_{mic}$, and therefore, the prediction of the optimal micelle geometry. As discussed by Stephenson et al. [58], with the exception of the transfer free-energy contribution, $g_{tr}$, all the other five free-energy contributions to $g_{mic}$ in Eq. 2.5 are functions of the micelle shape and size. In other words, $g_{tr}$ is independent of the structural characteristics of the micelle. Since the MD simulation provides a more accurate quantification of the hydrophobic effect (and, therefore, a more accurate estimation of $g_{tr}$), the transfer free-energy contribution can be better computed using the hydration data obtained from the MD simulation than using the traditional MT model. As a result, $g_{tr}$ computed using the traditional MT approach can be replaced by $g_{tr,CS-MT}$, the transfer free-energy contribution computed using the MD simulation results. The transfer free-energy contribution, $g_{tr,CS-MT}$, can then be used as an input to the MT model in order to predict the optimal micelle geometry. Specifically, using Eq. 2.13, it follows that:

$$g_{tr,CS-MT} = g_{tr} = \hat{g}_{HF} - \hat{g}_{int} = \hat{g}_{dehydr} + \hat{g}_{hydr} - \hat{g}_{int} \tag{2.14}$$

where $\hat{g}_{int}$ is the traditional MT prediction of the interfacial free-energy contribution corresponding to the simulated micellar aggregate. The free energy of micellization, $g_{mic}$, computed using the CS–MT modeling approach, can be obtained by replacing $g_{tr}$ in Eq. 2.5 with $g_{tr,CS-MT}$. Specifically,

$$g_{mic} = g_{tr,CS-MT} + g_{int} + g_{pack} + g_{st} + g_{elec} + g_{ent} \tag{2.15}$$

with $g_{tr,CS-MT}$ computed using Eq. 2.14 for the simulated micellar aggregate. The other five free-energy contributions in Eq. 2.15 are computed using the traditional MT model as discussed in Section 2.1.2. After minimizing $g_{mic}$ with respect to $S$, $l_c$, and $\beta$, one can determine the optimal micelle characteristics $(S^*, l_c^*, \beta^*)$, as well as the CMC using Eq. 2.4.

### 2.2.2 The Degree of Hydration, $f_i$

Before introducing the two free-energy contributions associated with the hydrophobic effect, $\hat{g}_{dehydr}$ and $\hat{g}_{hydr}$, I will first discuss the method used to quantify the degree of hydration. The hydrophobic effect associated with the formation of a micelle in aqueous solution originates from the disruption of hydrogen-bonding network structures formed by so-called "hydrophobic bonds" [108]. The strength of these hydrophobic bonds can therefore be quantified by studying the local hydrogen-bonding network around each hydrophobic group in order to obtain a corresponding degree of hydration. In the CS–MT model, the relative degree of hydration is quantified using the concept of the fractional hydration, $f_i$, for each atomic group, *i*, in the surfactant molecule, defined as follows:

$$f_i = \frac{\text{number of hydrating contacts with group } i \text{ in the micellar state}}{\text{number of hydrating contacts with group } i \text{ in the bulk water environment}} \tag{2.16}$$

Note that a "hydrating contact" is defined as the contact of surfactant group $i$ with an atom that: (i) is capable of forming hydrogen bonds, or (ii) is capable of forming coordinate covalent bonds. Note also that $f_i = 0$ indicates complete dehydration of group $i$ in the micellar state (in the traditional MT model this is assumed to be the case for every group $i$ the surfactant tail), while $f_i = 1$ indicates that the degree of hydration of group $i$ in the micellar state is the same as in the bulk water environment (in the traditional MT model this is assumed to be the case for every group in the surfactant head). On the basis of this definition, group $i$ may establish hydrating contacts with the oxygen and the hydrogen atoms in a water molecule, with a positively charged or a negatively charged ion, or with a hydrogen-bonding atom (oxygen, nitrogen, or fluorine as acceptors, and hydrogens attached to them as donors) in a hydrophilic group in the surfactant head. It is important to note that the difference between hydrophilic groups and hydrophobic groups is that the former contain some atoms that are capable of forming hydrogen bonds while the latter do not contain such hydrogen-bonding atoms. The specific manner in which $f_i$ is estimated by counting hydrating contacts using computer simulation results will be discussed in detail in Section 3.4.2. Using the fractional hydration definition given in Eq. 2.16, I discuss next the evaluation of the free-energy contributions, $\hat{g}_{dehydr}$ and $\hat{g}_{hydr}$, associated with a more rigorous quantification of the hydrophobic effect.

### 2.2.3 The Free Energy of Dehydration, $\hat{g}_{dehydr}$

The dehydration free-energy contribution in Eq. 2.12 needs to account for the change in free energy associated with the dehydration of the entire surfactant molecule upon self-assembly. As discussed in Section 2.1.2, in the traditional MT model, the surfactant heads are assumed to remain fully hydrated in the micellar state, while the surfactant tails are assumed to become fully dehydrated based on the assumption of a completely "dry" micelle core. However, in reality, and as oberved in MD simulations [77, 78, 91, 109], every atomic group in the surfactant tail will experience, on average, some degree of hydration upon micelle formation, which reflects water penetration into the micelle core. Using the hydration information obtained through computer simulation, it is no longer necessary to make the approximation made in the traditional MT model that all the atomic groups in the surfactant tail are fully dehydrated. Accordingly, Stephenson et al. proposed a more general approach to quantify $\hat{g}_{dehydr}$, the free-energy contribution associated with the dehydration of any group in the surfactant molecule, regardless of whether the group is in the head or in the tail [58]. Specifically,

$$\hat{g}_{dehydr} = \sum_{i=1}^{n} (1 - f_i)\, g_{tr_i} \tag{2.17}$$

where $n$ is the total number of groups in the surfactant molecule, $(1 - f_i)$ is the fractional dehydration associated with group $i$ upon micelle formation, and $g_{tr_i}$ is the free-energy change associated with transferring group $i$ from the aqueous solution to a bulk phase of group $i$ (that is, the transfer free-energy contribution of group $i$ to $g_{tr}$).

To compute $\hat{g}_{dehydr}$ using Eq. 2.17, it is necessary to accurately estimate $g_{tr_i}$ for each group in the surfactant molecule. By assuming that the solubility of a hydrophilic group is similar to that of a water molecule, that is, has a value of unity in mole fraction units, it follows that hydrophilic groups make a negligible contribution to the free energy of dehydration [59]. Accordingly, in the case of the ionic linear and branched surfactants considered in this thesis, only hydrophobic groups, which include the CH, $CH_2$, $CH_3$, and benzene carbon, contribute to $\hat{g}_{dehydr}$. As a result, $n$ in Eq. 2.17 is equal to the total number of hydrophobic groups. As discussed earlier, the values of $g_{tr_{CH_2}} = -1.494\ k_BT$ and $g_{tr_{CH_3}} = -3.518\ k_BT$ were obtained using the same solubility correlations for linear alkyl tails that are used in the traditional MT modeling approach [61]. Note that $g_{tr_{CH}}$ was estimated using solubility correlations for branched alkyl tails, which yields $g_{tr_{CH}} =$

$-0.444\ k_BT$ at 25°C [1]. The $g_{tr_i}$ value of benzene carbons (including CH and C groups) was estimated using a group-contribution method by assuming that each benzene carbon group makes the same contribution to the transfer free energy. Based on the aqueous solubility of a benzene ring, it then follows that $g_{tr_{C,CH(Benzene)}} = -1.433\ k_BT$ at 25°C. Note that in order to implement the CS–MT model directly, Stephenson et al. made the reasonable approximation that the $g_{tr_i}$ value of a hydrophobic group in the surfactant head is identical to the $g_{tr_i}$ value of the same type of hydrophobic group in the surfactant tail [59].

### 2.2.4 The Free Energy of Hydration, $\hat{g}_{hydr}$

The hydration free-energy contribution in Eq. 2.12 is necessary to account for the difference in the free energy associated with hydrating contacts established in bulk water and after incorporation into the micelle core. Each hydrating contact has a different free energy in the two states because the size of a single surfactant tail (usually, a hydrophobic chain) is much smaller than the size of the micelle core. This difference in size, in turn, results in a different extent of disruption of the surrounding water molecules in the two states, leading to a difference in the hydration free energies of the two states. The size dependence of hydration thermodynamics is a well-known phenomenon, and has been modeled theoretically in an approach developed by Lum, Chandler, and Weeks (the LCW Theory) [110]. The LCW theory indicates that, for small oil-like hydrophobic solutes (typically smaller than 1 nm in radius), the solute volume is sufficiently small that it does not disrupt the hydrogen-bonding network in the surrounding water molecules. For larger solutes (or clusters of solutes), the solute–water interface has sufficiently low curvature that it disrupts the hydrogen-bonding network near this interface, which in turn, increases the free energy associated with each hydrating contact [111].

As discussed in Sections 2.1.2 and 2.2.3, unlike a cluster of solutes (the "dry" micelle core model), water can actually penetrate into the micelle core. As a result, on average, all the atomic groups in the surfactant tails comprising the micelle core will contribute to the formation of the micelle core–water interface, and therefore, to the free energy of hydration, $\hat{g}_{hydr}$. The following

model has been proposed by Stephenson et al. to compute $\hat{g}_{hydr}$ [58]:

$$\hat{g}_{hydr} = \sum_{i=1}^{n_{core}} SASA_i f_i \Delta g_{wc_i} \tag{2.18}$$

where $n_{core}$ is the number of atomic groups in the surfactant molecule that adsorb onto, or are incorporated into, the micelle core (in other words, the number of groups in the surfactant tail), $SASA_i$ is the solvent accessible surface area of group $i$, $f_i$ is the fractional hydration of group $i$ as defined in Eq. 2.16, and $\Delta g_{wc_i}$ is defined as the difference in the "microscopic interfacial tension" (the interfacial free energy per unit SASA) associated with hydration in the micellar state and in the bulk water environment for group $i$. Note that $SASA_i$ was computed for each group $i$ in the surfactant tail (CH, $CH_2$, and $CH_3$ groups) based on MD simulation results of the bulk water environment (for details, see Section 3.3.1).

For amphiphilic solutes (which contain both a head and a tail), only those hydrophobic groups in the surfactant tail that are actually incorporated into the micelle core contribute to $\hat{g}_{hydr}$. Surfactant head groups that extend away from the micelle core into the aqueous solution are modeled as having the same free energy associated with hydrating contacts in the micellar state as in the bulk aqueous state (that is, they do not contribute to $\hat{g}_{hydr}$ or, equivalently, $\Delta g_{wc_i}$ equals to zero for such groups). This assumes that the extent of disruption of the hydrogen bonding/coordinate bonding network of the solution in both states is very similar. Similarly, in the case of hydrophilic groups in the surfactant tail, one may assume that these groups do not disrupt the hydrogen-bonding network as much as the hydrophobic groups, and therefore, have a negligible contribution to $\hat{g}_{hydr}$ (that is, $\Delta g_{wc_i}$ is negligible for such groups), and therefore, $n_{core}$ in Eq. 2.18 is equal to the number of hydrophobic groups in the surfactant tail.

In general, $\Delta g_{wc_i}$ depends on the chemical nature of group $i$. However, Stephenson et al. concluded that, as a result of the chemical similarity of the CH, $CH_2$, and $CH_3$ groups in a branched surfactant tail, $\Delta g_{wc_i}$ can be approximated as being equal for all these groups [58]. Note that the size difference between the CH, $CH_2$, and $CH_3$ groups is accounted for through the $SASA_i$ term in Eq. 2.18. With this approximation in mind, in what follows, $\Delta g_{wc_i}$ is assumed to be independent of $i$ (denoted as $\Delta g_{wc}$) when modeling the various ionic linear and branched surfactants considered in this thesis.

Stephenson et al. predicted $\Delta g_{wc}$ theoretically for oil aggregates and evaluated the accuracy of the CS–MT modeling results, including testing the validity and range of applicability of Eqs. 2.15, 2.17, and 2.18, as well as the validity of the computer simulation approach that will be discussed in Chapter 3. The following theoretical model was proposed for $\Delta g_{wc}$:

$$\Delta g_{wc} = \sigma_{core} - \sigma_{bulk} = \frac{\sigma_s A_{core}}{SASA_{core}} - \left( -\frac{g_{tr_i}}{SASA_i} \right) \tag{2.19}$$

where $\sigma_{core}$ is the "microscopic interfacial tension" associated with the micelle core–water interface, $\sigma_{bulk}$ is the "microscopic interfacial tension" associated with group $i$ (CH, $CH_2$, or $CH_3$)–water interface in the aqueous solution, $\sigma_s$ is the curvature-dependent macroscopic interfacial tension of the micelle core–water interface (computed using Eq. 2.10), $A_{core}$ is the area of the micelle core computed geometrically based on the volume of the micelle core subject to the assumption of a perfectly smooth spherical micelle core surface, and $SASA_{core}$ is the solvent accessible surface area of the micelle core. Note that $SASA_{core}$ was computed for the entire micelle core (the aggregate of surfactant tails) based on MD simulation results of the micellar state (for details, see Section 3.3.2).

In Eq. 2.19, $\sigma_{core} = \frac{\sigma_s A_{core}}{SASA_{core}}$ and $\sigma_{bulk} = -\frac{g_{tr_i}}{SASA_i}$ (recall that $g_{tr_i} < 0$). Note that $\sigma_{core}$ was defined to be equal to the interfacial free energy of the micelle core–water interface, $\sigma_s A_{core}$, per unit $SASA_{core}$, and $\sigma_{bulk}$ was defined to be equal to the opposite value of the transfer free energy of group $i$, $g_{tr_i}$, per unit $SASA_i$. The difference between $\sigma_{core}$ and $\sigma_{bulk}$ is equal to the free-energy difference per unit SASA associated with the hydrating contacts in the micellar state and in the bulk water environment.

The validity of Eq. 2.19 hinges on whether it is physically reasonable to evaluate $\Delta g_{wc}$ on a per unit SASA basis, thereby invoking the concept of a microscopic interfacial tension, or microscopic interfacial free energy per unit area. A number of researchers, including Tanford, have modeled solubility as a function of SASA for linear and branched alkyl chains with reasonable accuracy, suggesting that the relatively simple model proposed in Eq. 2.19 is adequate [112,113]. As a result, one can assume that the solvation free energy of group $i$ (the negative transfer free energy of group $i$, $-g_{tr_i}$) of an alkyl chain in the bulk water environment is proportional to the SASA of group $i$ in the alkyl chain, $SASA_i$. Although $\sigma_{bulk}$ is approximately constant due to the proportionality

between $-g_{tr_i}$ and $SASA_i$, given the dependence of $\sigma_s$ on the alkyl tail length and on the micelle core curvature, $\sigma_{core}$ is also expected to be a function of alkyl tail length and curvature, which indicates that the ratio of $\frac{A_{core}}{SASA_{core}}$ may also be a function of these variables. Therefore, Stephenson et al. reported results for $\frac{A_{core}}{SASA_{core}}$ for 15 oil aggregates of different shapes (spheres, cylinders, and slabs) and sizes [58], which can be used to approximately compute $\Delta g_{wc}$ for branched alkyl tails. The validity of Eq. 2.19 was discussed in greater detail in the recent work of Stephenson et al. with respect to the values of $\sigma_{core}$ and $\sigma_{bulk}$, as determined from the computer simulation results [58], and the interested reader is referred to this work for details.

# Chapter 3

# Molecular Dynamics (MD) Simulations in the CS–MT Modeling Approach

## 3.1 Modeling Approach to Quantify the Degree of Hydration

To quantify the hydrophobic effect driving the formation of branched surfactant micelles in aqueous solution, I have used atomistic-level, molecular dynamics (MD) simulations to quantify the change in hydration of each group of atoms (such as, a $CH_2$ group) in the surfactant molecule when it is transferred from the aqueous solution to the micellar state. As described in Section 2.2, this quantification requires carrying out two independent simulations: the first of a single surfactant molecule in a simulation cell of water, which I will refer to hereafter as the "bulk water simulation", and the second of the same surfactant molecule in a micellar state, which I will refer to hereafter as the "micelle simulation". Each micelle simulation was carried out by first preforming a spherical micelle of convenient aggregation number (for more details, see Stephenson et al. [59] and Section 3.3.3). The micelle was then simulated for 15 to 20 ns, which provided sufficient time for the surfactant molecules to rearrange and come to local equilibrium within the micelle. Note that the spherical geometry of the preformed micelle may not correspond to the actual optimal micelle geometry (for example, the optimal micelle shape could be cylindrical). As a result, the computer simulation results do not permit direct prediction of the optimal micelle shape and size that would be observed experimentally. Nevertheless, Stephenson et al. suggested that by using the CS–MT modeling approach (see Section 2.2), obtaining information about the hydration state of a micelle

of a single geometry is sufficient to allow prediction of the optimal micelle shape and size [58]. To this end, during the simulation, the aggregate must remain stable as a spherical micelle, and should not break apart into monomers or into several small aggregates. Based on past experience, the chosen simulation time (15 ns) is short enough to avoid kinetic breakup and/or micelle shape transitions, yet long enough to allow local equilibration in the micelle.

In addition, micelle simulations were used to make head and tail identifications of the surfactant molecules comprising a micelle. Note that approximate head and tail identifications were made initially based on oil–water interface simulations, as discussed in Stephenson et al. [57]. Considering that the head and tail assignment should be independent of the hydration state of the surfactant monomers in aqueous solution, I developed a new method to make head and tail assignments based solely on the micelle simulations (for details, see Section 4.1).

The chemical structures of the ionic branched surfactants modeled using MD simulations are shown in Figure 3-1. In addition to the two series of x-y-SAS branched surfactants, the micellization behaviors of a $C_{10}$-SAS linear surfactant and a $C_{12}$-SAS linear surfactant were modeled for comparison. In surfactants A and B, the benzene sulfonate group is attached to the $C_{12}$ hydrocarbon chain at different locations. In surfactants C and D, the two branched tails are located at different positions on the benzene ring, one closer to the surfactant head and the other farther from it. In surfactants E and F, the branching is located near the end of the primary hydrocarbon chain. The difference between surfactants E and F is that the length of the side chain, and its attachment to the primary hydrocarbon chain, are different.

The sodium secondary alkyl sulfonates (including the x-y-SAS branched surfactants) are produced on the order of 160,000 tons/year, primarily in Europe and Japan [3]. These surfactants possess excellent performance characteristics in laundry detergent applications; however, they are too expensive relative to the traditional LAS (linear alkyl benzene sulfonates) surfactants for use in powdered detergent applications. Their primary use is in concentrated liquid formulations, where their high solubility in water makes them more desirable [3]. Major domestic applications of SAS branched surfactants include use in liquid laundry detergents, dishwashing liquids, shampoos, and other personal care products. Industrial applications include cleaners, emulsifiers for PVC polymerization, and products for the textile industries [3]. Extensive theoretical and experimental studies have been carried out to investigate the micellization and the solubilization behavior of these

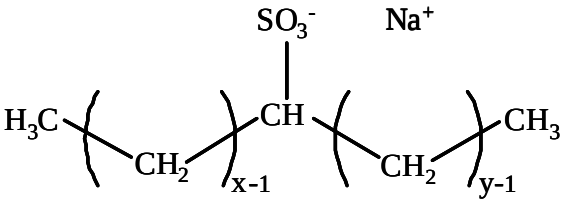


Secondary Alkyl (Paraffin) Sulfonate (x-y-SAS)

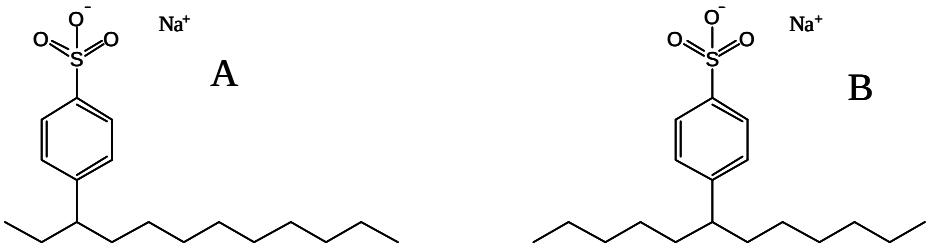


Sodium 4-($C_{12}$-Alkyl) Benzene Sulfonates

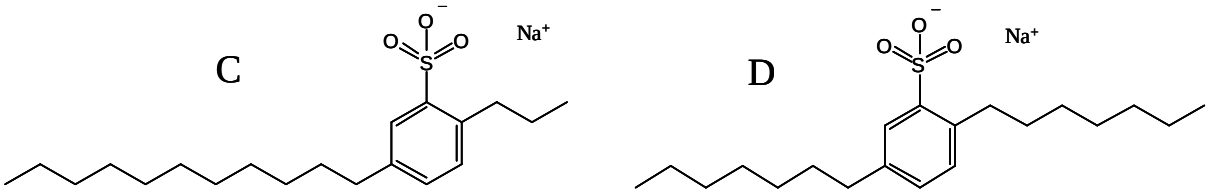


Sodium 2,5-Dialkyl Benzene Sulfonates

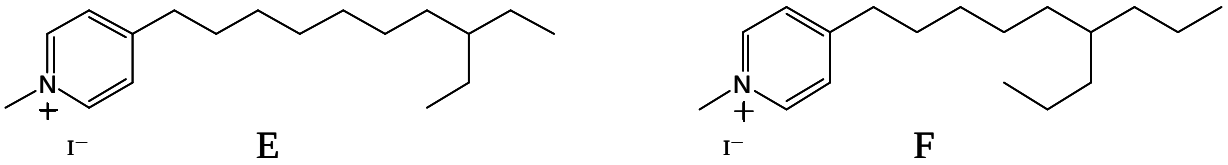


1-Methyl-4-($C_{12}$-Alkyl) Pyridinium Iodides

Figure 3-1: Ionic branched surfactants modeled in this thesis. The two series of simple ionic branched surfactants include sodium secondary alkyl (paraffin) sulfonates (denoted as x-y-SAS), where in one series, the length of the primary hydrocarbon chain is kept fixed ($y = 9$) while $x = 2, 4, 6, 8,$ or 9, and in the second series, the total length of the two portions of the hydrocarbon chain is kept fixed ($x + y = 11$) while $x = 1, 2, 3, 4,$ or $5$. The three classes of complex ionic branched surfactants consist of two sodium 4-($C_{12}$-alkyl) benzene sulfonates (denoted as surfactants A and B), two sodium 2,5-dialkyl benzene sulfonates (denoted as surfactants C and D), and two 1-methyl-4-($C_{12}$-alkyl) pyridinium iodides (denoted as surfactants E and F).

surfactants [114–116].

The branched sodium alkyl benzene sulfonate class of surfactants, which includes surfactants A and B (see Figure 3-1), are used as one of the main reagents in fluids injected into underground formations during chemical flooding for the purpose of achieving enhanced oil-recovery by reducing the oil–water interfacial tension [3, 117]. Great efforts have been made to investigate the adsorption, micellization, and solubilization behaviors of these surfactants [117–120].

The sodium dialkyl benzene sulfonate class of surfactants, which includes surfactants C and D (see Figure 3-1), are used as ingredients in some industrial formulations for detergent applications [121, 122], and their micellization behavior has been studied experimentally [123].

The branched alkyl pyridinium iodide class of surfactants, which includes surfactants E and F (see Figure 3-1), are reported to be efficient solubilizers for nontoxic *in vitro* gene delivery [124]. Theoretical and experimental studies have been carried out extensively to investigate the micellization and solubilization behaviors of these surfactants [29, 125–129].

## 3.2 Simulation Methods and Parameters

All simulations were conducted using a 2008 developers' version of the GROMACS (Groningen Machine for Chemical Simulations) 3.3.3 software package [63, 130]. All the ionic linear and branched surfactants considered here were modeled using the OPLS-AA (All-Atom, Optimized Potential for Liquid Simulations) force field [131], and water was modeled using the SPC/E (Simple Extended Point Charge) model. The SPC/E model represents an improvement over the SPC (Simple Point Charge) model through a correction implemented to account for the self-polarization of water [132]. The OPLS-AA force field defines both the bonded (bond stretching, bond angle, and dihedral angle) interactions and the nonbonded (Lennard-Jones and Coulombic) interactions between each atom within a surfactant molecule.

In order to compute Coulombic interactions, atomic charges need to be assigned to all the atoms in the surfactant molecule. For the two series of paraffin branched surfactants (x-y-SAS surfactants), atomic charges to the anionic sulfonate groups and to the hydrocarbon groups were assigned based on the default atomic charge values recommended in the OPLS-AA force field. However, the head structures of the complex branched surfactants consisting of aromatic groups

did not have suggested charges in the OPLS-AA force field. Therefore, the atomic charges for these heads (the anionic benzene sulfonate group and the cationic pyridinium group) were estimated using the CHelpG (Charges from Electrostatic Potentials using a Grid based method) algorithm as implemented in Gaussian 03 [133]. In this quantum mechanical (QM) algorithm, atomic charges are fitted to reproduce the electrostatic potential at a number of points around the molecule on its van der Waals surface [133]. This algorithm is frequently used to estimate atomic charges for molecular mechanics simulations [134].

In a separate study by Stephenson et al. [57], the authors concluded that assigning atomic charges to the hydrocarbon groups in an alkyl chain using CHelpG yields simulation results that are less physically realistic than those obtained by assigning atomic charges based on the recommended OPLS-AA force field. Therefore, the CHelpG algorithm was not used to assign atomic charges for the hydrocarbon tails of these surfactants. In a related study, Stephenson et al. investigated the sensitivity of the head and tail assignments obtained through computer simulation to the method used to assign atomic charges [57, 90]. In general and perhaps, not surprisingly, the authors found that the results are sensitive to the atomic charges used, and that the charge assignments recommended in the OPLS-AA force field yield more reasonable results than those obtained using the CHelpG algorithm. However, if a specific atomic group in the surfactant molecule does not have suggested charges in the OPLS-AA force field, Stephenson et al. found that applying the CHelpG algorithm to determine charges yields reasonably accurate results [57].

A previous study found that implementing the CHelpG algorithm by using the $rb3lyp$ density function and the $6-31+G(3df)$ basis set could provide good atomic charges to match the atomic charges suggested in the OPLS-AA force field [57, 131, 135]. Based on this finding, the CHelpG algorithm, along with the $rb3lyp$ density function and the $6-31+G(3df)$ basis set, were used to assign atomic charges [134]. Note that the $rb3lyp$ density function uses the non-local correlation provided by the LYP (Lee, Yang, and Parr) expression [136, 137], as well as the restricted Becke's three parameter functional for local correlation [138]. Note also that the $6-31+G(3df)$ basis set was selected because of the presence of multiple third orbital electrons in the sulfur atom of the surfactant molecule [139–141]. A summary of the atomic charges used to model the ionic linear and branched surfactants considered in this thesis is presented in Table 3.1.

Van der Waals interactions were treated using a cutoff distance of 0.9 nm, and electrosta-

| Surfactant Type | Atom Type | Force Field | Atomic Charge (e) |
|---|---|---|---|
| **Linear SAS and x-y-SAS** | C of $CH_3$ | OPLS_135 | $-0.180$ |
| | C of $CH_2$ | OPLS_136 | $-0.120$ |
| | C of CH (Attached to $SO_3^-$) | OPLS_499 | $0.085$ |
| | H of $CH_n$ | OPLS_140 | $0.060$ |
| | S of $SO_3^-$ | OPLS_493 | $0.916$ |
| | O of $SO_3^-$ | OPLS_494 | $-0.687$ |
| **A and B** | C of CH (Attached to Benzene) | OPLS_515 | $0.055$ |
| | C of Benzene | OPLS_145 | $-0.115$ |
| | C of Benzene (Attached to $SO_3^-$) | OPLS_499 | $-0.082$ (CHelpG) |
| | H of Benzene | OPLS_146 | $0.115$ |
| | S of $SO_3^-$ | OPLS_493 | $0.852$ (CHelpG) |
| | O of $SO_3^-$ | OPLS_494 | $-0.590$ (CHelpG) |
| **C and D** | C of $CH_2$ (Attached to Benzene) | OPLS_149 | $-0.005$ |
| **E and F** | C of CH | OPLS_137 | $-0.060$ |
| | C of $CH_2$ (Attached to Pyridinium) | OPLS_136 | $-0.023$ (CHelpG) |
| | C of $CH_3$ (Attached to $N^+$) | OPLS_135 | $-0.256$ (CHelpG) |
| | H of $CH_3$ (Attached to $N^+$) | OPLS_140 | $0.156$ (CHelpG) |
| | C1 and C5 of Pyridinium | OPLS_521 | $0.037$ (CHelpG) |
| | H1 and H5 of Pyridinium | OPLS_524 | $0.149$ (CHelpG) |
| | C2 and C4 of Pyridinium | OPLS_522 | $-0.184$ (CHelpG) |
| | H2 and H4 of Pyridinium | OPLS_525 | $0.164$ (CHelpG) |
| | C3 of Pyridinium | OPLS_523 | $0.245$ (CHelpG) |
| | $N^+$ | OPLS_520 | $0.114$ (CHelpG) |

Table 3.1: Summary of the atomic charges used to model the ionic linear and branched surfactants considered in this thesis. "CHelpG" in parentheses indicates that the atomic charges were computed using the QM method. The force field parameters of $CH_2$ and $CH_3$ are listed just for x-y-SAS, but were used for all the other surfactant molecules unless specified otherwise in parentheses. The force field parameters listed for surfactants A and B were used for surfactants C and D as well. The carbon atoms in the pyridinium ring are denoted as C1 to C5 clockwise starting from the nitrogen atom. The hydrogen atoms in the pyridinium ring are assigned according to the carbon atoms to which they are attached.

tic interactions were described using 3D PME (Particle-Mesh Ewald) summation [142, 143]. A long-range dispersion correction was implemented to more accurately calculate the energy and the pressure of the system. Shirts et al. have shown that the van der Waals cutoff selected is accurate for the OPLS-AA force field with the inclusion of long-range dispersion corrections for the energy and the pressure of the system [144, 145]. In modeling short-ranged, non-bonded interactions, a neighbor list with a cutoff of 0.9 nm was maintained and updated every 10 simulation steps. For unconstrained chemical systems (with flexible bond lengths, bond angles, and dihedral angles), very small time steps of approximately 1 fs must be taken because of the high frequency of bond vibrations [146, 147]. However, in order to increase computational efficiency, each simulation was carried out with fixed bond lengths using the SHAKE algorithm as implemented in GROMACS [148], which allowed the simulation time step to increase from 1 fs to 2 fs. Due to data storage limits, the simulated trajectories were saved and output every 10000 time steps (i.e. 20 ps) for all the data analyses presented here.

All simulations were conducted in the isothermal–isobaric $NPT$ (constant number of particles, constant pressure, and constant temperature) ensemble. The characteristic state function of this ensemble is the Gibbs free energy, which was used to quantify the free energy of micellization. In each simulation, the cell temperature was maintained at a constant value (selected to match the experimental temperature of the simulated micellar system considered) using a Berendsen-thermostat temperature coupling algorithm, which mimics weak coupling to an external heat bath with first-order kinetics with a time constant of 0.1 ps [149]. A Berendsen pressure coupling algorithm was used to maintain each simulation cell at the desired pressure of 1 bar, which exponentially relaxed the pressure with a time constant of 2 ps [149].

## 3.3 System Preparation and Equilibration

### 3.3.1 Bulk Water Simulation

The bulk water simulation for each of the ionic linear and branched surfactants considered here was initialized by placing a single surfactant molecule in a cubic simulation cell and surrounding it with water molecules. The simulation cell was selected to be sufficiently large such that there was

always at least 2 nm of water separating the surfactant molecule from its periodic image. Computer simulation studies of the propagation of water ordering away from an interface suggest that such a separation distance should be sufficient to prevent the surfactant molecule from interacting with its periodic image [150]. For the ionic linear and branched surfactants considered here, the size of the cubic simulation cell varied from 3 nm to 3.5 nm, to accommodate the 1 nm sized surfactant molecules. After brief equilibration under $NPT$ conditions (until the simulation cell volume stabilized), a 5 ns data-gathering simulation was carried out.

### 3.3.2 Micellar Aggregate Simulation

The method used to carry out the ionic linear and branched surfactant micelle simulations was more complex. A spherical micelle was preformed by placing a number of surfactant molecules in close proximity to each other with each surfactant head oriented radially outwards from the center of the micelle. The surfactant molecules were placed such that the surfactant heads were approximately uniformly spaced at the micelle surface. After preforming the surfactant micelle, a sufficient number of water molecules were added around the micelle such that the micelle was separated from its periodic image by at least 2 nm. The size of the cubic simulation cell varied from 4.5 nm to 4.7 nm, to accommodate the approximately 2.5 nm sized surfactant micelle. The number of surfactant molecules (which is equal to that of the counterions in the ionic linear and branched surfactants considered here), the number of water molecules, and the total number of atoms included in the simulation cell for each surfactant micelle are listed in Table 3.2. Note that in the micelle simulations of $C_{10}$-SAS, 4-7-SAS, and 5-6-SAS, the separation of a single surfactant molecule from the micellar aggregate was observed (as reflected in the numbers 14 (13) reported in Table 3.2). With this in mind, any separated single surfactant molecules and associated counterions were ignored in all future data analyses of the micelle simulations.

After preforming each spherical micelle, an energy minimization was conducted to remove close contacts between surfactant molecules. Next, an extended equilibration run under $NPT$ conditions was conducted for 10 ns. Results by other researchers when conducting atomistic-level simulations of micelles in aqueous solution suggest that a simulation time of 10 ns should be more than adequate to equilibrate a spherical micelle [76]. After the 10 ns equilibration under $NPT$

| Surfactant Type | No. of Surf. Molecules | No. of Water Molecules | Total No. of Atoms |
|---|---|---|---|
| **$C_{10}$-SAS** | 14 (13) | 2782 | 8850 |
| **2-9-SAS** | 14 | 2762 | 8874 |
| **4-9-SAS** | 14 | 2744 | 8904 |
| **6-9-SAS** | 14 | 2714 | 8898 |
| **8-9-SAS** | 14 | 2703 | 8949 |
| **9-9-SAS** | 14 | 2690 | 8952 |
| **$C_{12}$-SAS** | 14 | 2764 | 8880 |
| **1-10-SAS** | 14 | 2762 | 8874 |
| **3-8-SAS** | 14 | 2750 | 8838 |
| **4-7-SAS** | 14 (13) | 2769 | 8895 |
| **5-6-SAS** | 14 (13) | 2788 | 8922 |
| **Surfactant A** | 15 | 3053 | 9939 |
| **Surfactant B** | 15 | 3037 | 9891 |
| **Surfactant C** | 18 | 2579 | 8781 |
| **Surfactant D** | 10 | 2713 | 8719 |
| **Surfactant E** | 22 | 2597 | 8935 |
| **Surfactant F** | 14 | 2732 | 8924 |

Table 3.2: The number of surfactant and water molecules and the total number of atoms corresponding to each of the simulated ionic linear and branched surfactant micelles considered. The numbers in parentheses correspond to the actual numbers of surfactant molecules composing the micelle (see text).

conditions, a 5 ns data-gathering simulation was carried out. Equilibration was confirmed by monitoring the solvent accessible surface area (SASA) of the entire micelle (see Section 2.2.4), where SASA was computed using the double cubic lattice method as implemented in GROMACS [151]. The solvent accessible surface was traced out by a probe sphere of radius 0.2 nm (as justified in Ref. [58]) that was rolled around each molecule within the micelle to identify the solvent accessible region [63]. Note that I consider SASA to be the most important metric to gauge equilibration, because this property is directly proportional to the degree of hydration of the micelle, and obtaining accurate hydration information is the central objective of the computer simulations in the CS–MT modeling approach. Plots of the simulated SASA profiles as a function of simulation time during 15 ns of simulation are reported in Figure 3-2 for all the ionic linear and branched surfactants considered here. To facilitate comparison of the results, in Figure 3-2, the reported SASA values for each surfactant were normalized by the average SASA value for that surfactant. The lack of noticeable drift in SASA values towards the end of the 10 ns equilibration simulation run confirms that water contact data gathered during the subsequent 5 ns of data gathering should be

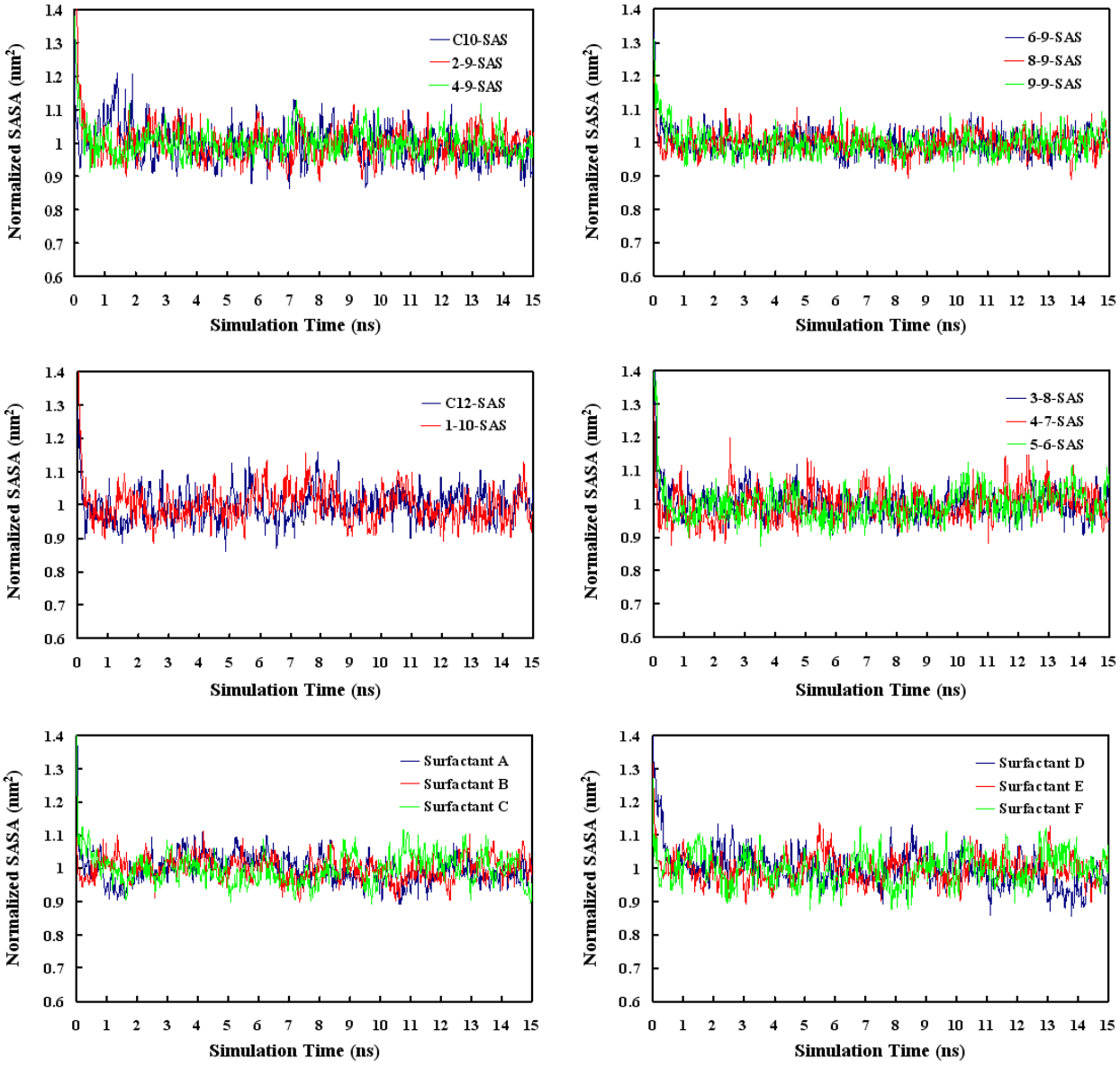


Figure 3-2: Normalized solvent accessible surface areas (SASA's) of the simulated surfactant micelles as a function of simulation time during 15 ns of simulation for all the ionic linear and branched surfactants considered in this thesis.

representative of the hydration state of the micelle in its equilibrium configuration.

Snapshots of the post-equilibration configurations of each simulated ionic linear and branched surfactant micelle are shown in Figure 3-3. Note that each surfactant molecule is depicted using the van der Waals radius of each atom.

### 3.3.3 Selection of the Simulated Micelle Geometry

The reason why spherical, rather than cylindrical or discoidal, micelles were selected for simulation was discussed by Stephenson et al. [59], where oil aggregates of different shapes and sizes were simulated and compared with each other in terms of the transfer free energy, $g_{tr,CS-MT}$ (see Section 2.2.1). The authors concluded that any micelle geometry (spherical, cylindrical, or discoidal) and aggregation number may be used to obtain hydration information as input to the CS–MT modeling approach; however, selection of the spherical geometry was found to greatly reduce the computational difficulty [58, 59]. With this in mind, I have also carried out the micelle simulations reported here using a micelle spherical geometry. Each of the ionic linear and branched surfactant micelles was constructed with a sufficiently small aggregation number to ensure that it would remain spherical during the simulation. For the complex ionic branched surfactants with aromatic groups (see Figure 3-1), this was accomplished by estimating the expected aggregation number of a spherical micelle given: (i) the estimated surfactant tail length based on the primary chain length (which corresponds to the micelle radius, and therefore, determines the micelle core volume), and (ii) the tail volume of each surfactant molecule based on the overall hydrocarbon chain volume [2]. For the other branched surfactants, such as, the x-y-SAS surfactants, where the surfactant head area is small enough that enlongation into ellipsoidal micelles is possible at the expected aggregation numbers [2], smaller aggregation numbers were used in the micelle simulations. Therefore, for the x-y-SAS surfactants, spherical micelles were preformed with the smallest aggregation number of 14, a value estimated for 5-6-SAS (which has the smallest $l_{\max}$, the fully-extended tail length in its series) and 9-9-SAS (which has the largest tail volume in its series). Note that the aggregation numbers for 5-6-SAS and 9-9-SAS were estimated using the same method used for the complex ionic branched surfactants, and their estimated aggregation numbers were found to be similar. In addition, note that spherical micelle simulations with larger aggregation numbers were also

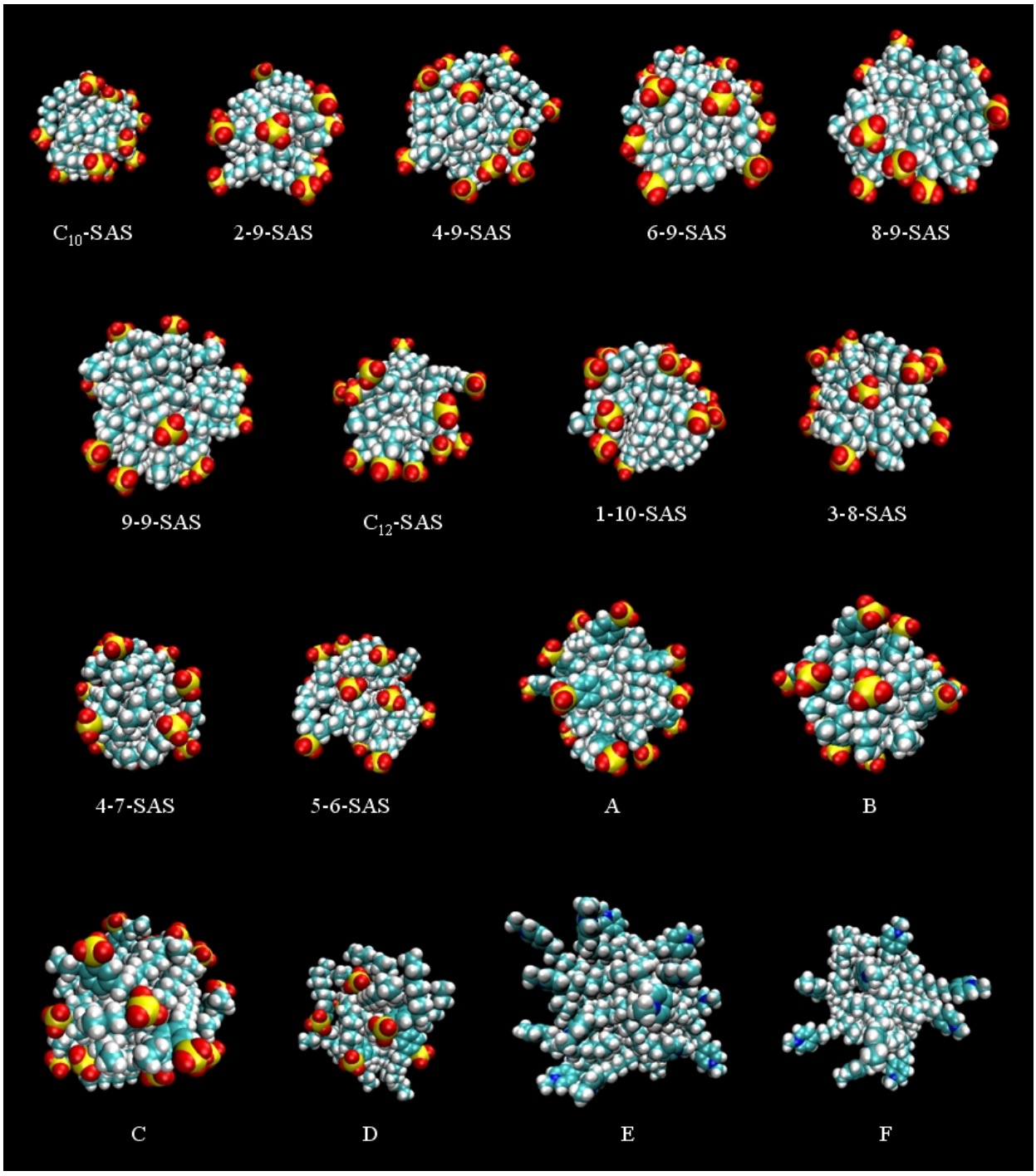


Figure 3-3: Snapshots of the post-equilibration structures of the simulated micelles corresponding to each of the ionic linear and branched surfactants considered in this thesis. For clarity, water molecules and counterions are not shown. (Color code: red – oxygen, yellow – sulfur, light blue – carbon, white – hydrogen, and dark blue – nitrogen.)

carried out for the ionic linear and branched surfactants considered here (results not reported). In particular, I found that the transfer free energy, $g_{tr,CS-MT}$, computed using the MD simulation results, depends weakly on the aggregation number of the simulated micelle, a finding that is consistent with the assumption made in Section 2.2.

## 3.4 Data Analysis Method

### 3.4.1 Definition of Hydration

In Chapters 1 and 2, I discussed the importance of quantifying the degree of hydration of surfactants in the bulk water and micellar states. Before implementing the new CS–MT modeling approach presented in Section 2.2, below, I describe the specific methodology used to determine the degree of hydration from the simulation data. Specifically, the definition of hydration is based on the number of contacts with "hydrating" atoms, as discussed in Section 2.2.2. I have adopted this definition of hydration because the hydrophobic effect results from changes in the hydrogen-bonding or coordinate-bonding network of the aqueous solution that are induced by the presence of nonpolar, hydrophobic moieties. Contact of a hydrophobic group with water atoms, with hydrogen-bonding atoms in a surfactant molecule, or with a charged ion in solution may break, or perturb, the hydrogen-bonding network of water. In the CS–MT model, one approximates all hydrating contacts as having the same free energy, as long as they are counted in the same environment (that is, either in the bulk water environment or in the micellar environment). The implications of this approximation for modeling surfactant micellization in aqueous solution were discussed in detail by Stephenson et al. [59, 60].

### 3.4.2 Analysis of the Bulk Water and Micelle Simulation Results

To quantify the degree of hydration of an atomic group in the surfactant molecule during a bulk water simulation, the number of hydrating contacts that it experiences during the course of a simulation run must be counted. For the ionic linear and branched surfactants considered here, contacts with water atoms, with ions, and with hydrogen-bonding groups in the surfactant head should each be counted as contributing to hydration, as discussed in Section 2.2.2. In analyzing the simulation

data, a contact was defined as two atoms being separated by less than a set distance (the "cutoff distance") at any time during the simulation, where one of the two atoms should be chosen as the hydrating atom defined in Section 3.4.1. The other atom should be the central atom of an atomic group in the surfactant molecule, such as the carbon atom in a hydrocarbon group, the carbon atom in a benzene carbon group, or the sulfur atom in a sulfonate group. Note that both in the bulk water and in the micelle simulations, hydrating contacts between two atoms within the same surfactant molecule are not considered as hydrating contacts because they do not reflect intermolecular interactions between surfactant molecules. In addition, note that use of the location of the central atom of an atomic group to represent the location of the entire group is consistent with the method used to determine the cutoff distance using the radial distribution function (RDF) between a hydrating atom and the central atom of an atomic group in the surfactant molecule (see Section 3.4.3). It is also noteworthy that using the location of the central atom to represent the location of the entire atomic group differs from a united-atom approach, an approach where the hydrogen atoms are not treated explicitly. Note also that the degree of hydration of a hydrophilic group (such as, a sulfonate group) is not required in the CS–MT model (as discussed in Section 2.2). As a result, a cutoff distance was only selected for hydrophobic groups in the surfactant molecule. It is important to recognize that the average number of hydrating contacts counted using the proposed method is directly proportional to the average number of hydrating atoms located within the specified cutoff distance.

Quantification of the degree of hydration of the surfactant molecules during the micelle simulations was carried out in a similar manner, including using the same cutoff distance chosen to identify hydrating contacts. After counting the hydrating contacts in the bulk water and in the micellar states, I proceeded to analyze the hydration information using the metric introduced to quantify the fractional hydration of group $i$, $f_i$, in Section 2.2.2. As expected intuitively, I found that $f_i$ is significantly smaller than unity for a hydrophobic group in the surfactant molecule, indicating that fewer contacts with hydrating atoms are experienced in the micellar state than in the bulk water environment.

### 3.4.3 Cutoff Distance Selection by Analyzing Radial Distribution Functions

#### Molecular Significance of Radial Distribution Functions and Cutoff Distances

To select the cutoff distance used to define hydrating contacts between atoms, one should only quantify the *local* water environment of each hydrophobic group, since beyond this *local* water environment, the *bulk* water molecules are weakly affected by the hydrophobic groups. Specifically, the *local* water environment of each hydrophobic group consists of the nearest-neighbor hydrating atoms that are strongly affected by the hydrophobic groups, while the effect of these hydrophobic groups is much weaker on hydrating atoms located beyond this local environment.

The effect of hydrophobic groups on hydrating atoms can be quantified by plotting the population of hydrating atoms around them using radial distribution functions (RDF's) (see below). With this in mind, a cutoff distance should be selected such that only nearest-neighbor hydrating atoms contribute hydrating contacts to a hydrophobic group. However, to ensure that good contact statistics is obtained, the selected cutoff distance should be at least as large as the sum of the van der Waals radii of a $CH_3$ group (belonging to the surfactant hydrophobic tail) and a hydrogen atom (belonging to a water molecule), or 0.35 nm. The sensitivity of the CS–MT modeling results to variations in the specific value of the cutoff distance chosen was studied by Stephenson et al. [58] when simulating planar and curved oil aggregates. In particular, $g_{tr,CS-MT}$ values for oil aggregates calculated using the CS–MT modeling approach (see Section 2.2) were found to depend weakly on the value of the cutoff distance [58]. Furthermore, Stephenson et al. concluded that by choosing the smallest value of the cutoff distance that yields good statistics, only nearest-neighbor contacts with hydrating atoms come into play, and the dependence of $f_i$ on micelle curvature is minimized (nevertheless, note that $f_i$ is still curvature-dependent) [58]. As discussed in Section 2.2, the effect of curvature on $g_{tr,CS-MT}$ is accounted for explicitly in the CS–MT model, and therefore, no additional curvature dependence is needed.

Radial distribution functions (RDF's) have been used extensively to investigate interatomic interactions [78, 85, 91, 95, 111, 152–156]. In particular, RDF's have been used to probe water structure and population around hydrophobic moieties [85, 111, 152–155]. Typically, to quantify water population around an atomic group of interest, RDF's have been used to determine the cutoff distance required to compute the "hydration number". The hydration number is defined as the

number of nearest-neighbor water molecules (typically represented by the oxygen atoms in the water molecules) present within a certain cutoff distance (referred to as the "first hydration shell") around the atomic group of interest [154, 156]. Note that the concept of "hydration number" is somewhat different from that of "the number of hydrating contacts" introduced in Section 2.2.2, in that the former includes only water molecules while the latter includes *all* the hydrating atoms. Nevertheless, RDF's can also be used to determine cutoff distances in order to count the number of hydrating contacts (see below).

The pair correlation function, $g_{A-B}(r)$, is defined as the density RDF of atoms of type B located at a radial distance r from a central atom of type A, and quantifies the probability of finding B atoms (the target atoms) at a distance $r$ from the A atom (the central atom) which is located at the origin of the spherical coordinate system. In particular, in the MD simulation analysis, the volume around the central A atom is divided into very thin shells of thickness $\Delta r$, where the central spherical surface in the $i$th layer is located at a distance $r_i$ from the origin (see Figure 3-4). The concept of the layer-by-layer approach used to determine the density RDF and the number RDF (to be discussed later) is illustrated in Figure 3-4. The density RDF at $r_i$, $g_{A-B}(r_i)$, is defined as the ratio of $\langle \rho_{A-B}(r_i) \rangle$, the local density of B atoms in the $i$th layer, that is, at a distance $r_i$ from the A atom, and $\langle \rho_B \rangle$, the average density of B atoms corresponding to a total of $N_B$ B atoms contained in the cubic simulation cell of volume $\langle V_{cell} \rangle$. Specifically,

$$g_{A-B}(r_i) = \frac{\langle \rho_{A-B}(r_i) \rangle}{\langle \rho_B \rangle} \tag{3.1}$$

where

$$\langle \rho_{A-B}(r_i) \rangle = \frac{\langle N_{A-B}(r_i) \rangle}{4\pi r_i^2 \Delta r} \tag{3.2}$$

where $\langle N_{A-B}(r_i) \rangle$ is the number of B atoms in the $i$th layer, of thickness $\Delta r$, at distance $r_i$ from the A atom, referred to as the number RDF, and

$$\langle \rho_B \rangle = \frac{N_B}{\langle V_{cell} \rangle} \tag{3.3}$$

Note that "$\langle\ \rangle$" in Eqs. 3.1 – 3.3 indicates a time-averaged quantity obtained from the MD simulations. The concept of the number RDF, indicating the method used to count the number of

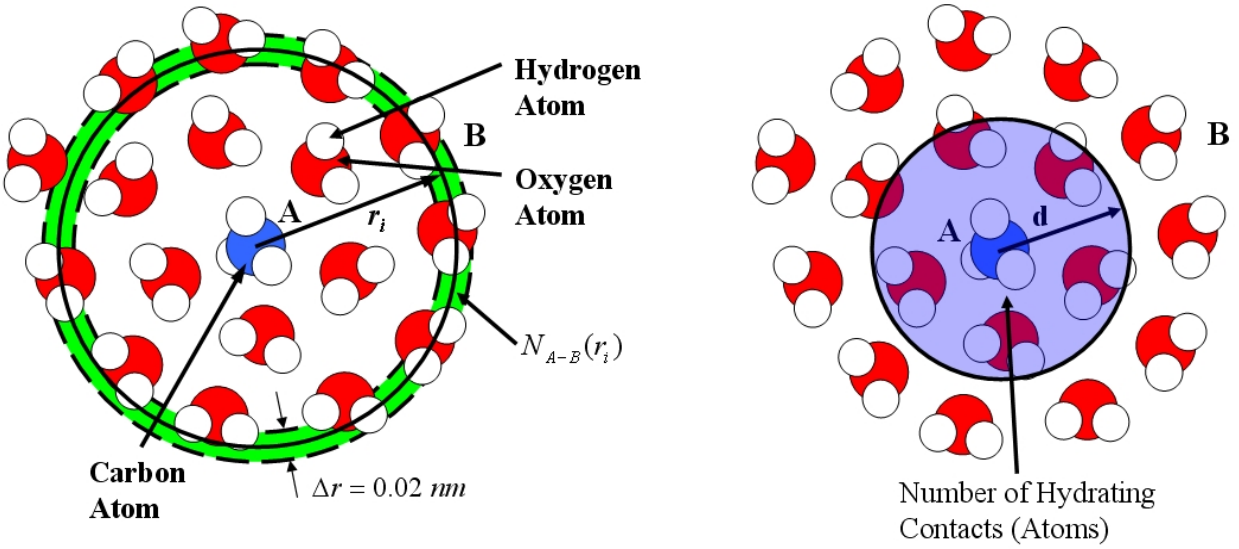


Figure 3-4: On the left: illustration of the number RDF (the green ring region at $r_i$) of hydrogen and oxygen atoms (the B atoms) with respect to a methyl group (the A atom), corresponding to one simulation time frame. On the right: illustration of the method used to count the number of hydrating contacts which involves counting the number of hydrating atoms within a cutoff distance $d$ (that is, within the sphere of radius $d$).

hydrating contacts, is also illustrated in Figure 3-4. Note that $\Delta r = 0.02$ nm was chosen such that it is much smaller than the size of any atoms in the simulation cell (typically, of the order of 0.1 nm) in order to generate very thin layers, yet large enough to yield good statistics. Although different $\Delta r$ values result in RDF curves of varying smoothness, the predicted cutoff distance was found to be independent of the $\Delta r$ value. Note that $N_B$, the total number of B atoms in the simulation cell, is computed using information reported in Table 3.2 (it is equal to the total number of water molecules, if B represents the water oxygen atoms, or equal to twice the total number of water molecules, if B represents the water hydrogen atoms). Note also that since all the MD simulations were conducted in the $NPT$ ensemble, the simulation cell volume $V_{cell}$ is a function of the simulation time, and therefore, a time-averaged cell volume $\langle V_{cell} \rangle$ should be used in Eq. 3.3. Since the MD simulation directly outputs $g_{A-B}(r_i)$, $\langle N_{A-B}(r_i) \rangle$ can be computed by combining Eqs. 3.2, 3.1, and 3.3 as follows:

$$\langle N_{A-B}(r_i) \rangle = \langle \rho_{A-B}(r_i) \rangle 4\pi r_i^2 \Delta r = g_{A-B}(r_i) \langle \rho_B \rangle 4\pi r_i^2 \Delta r = \frac{4\pi r_i^2 \Delta r}{\langle V_{cell} \rangle} g_{A-B}(r_i) N_B \qquad (3.4)$$

**Calculating the Cutoff Distance Using Radial Distribution Functions**

Marcus used number RDF's to compute the cutoff distance (the location of the first hydration shell) when determining solvation (hydration) numbers [157]. Instead, other researchers have used density RDF's to compute the cutoff distance [154, 156]. In Figure 3-5, sample density RDF and number RDF curves of oxygen atoms in water molecules with respect to: (i) the sulfur atom in the hydrophilic anionic sulfonate group (top row), and (ii) the carbon atom with the hydrophobic $CH_3$ group (bottom row) are illustrated. Note that pronounced first peaks and first valleys are observed in both the density and the number RDF curves of the water oxygen atoms with respect to the hydrophilic sulfonate group, reflecting both the strong hydrogen-bonding and electrostatic ordering effects induced by the hydrophilic anionic group [85, 111, 152–155, 157]. On the other hand, significantly less pronounced first peaks and first valleys are observed in both the density and the number RDF curves of the water oxygen atoms with respect to the hydrophobic $CH_3$ group, reflecting the fact that the hydrophobic ordering effect induced by the $CH_3$ group is weaker than the hydrogen-bonding and electrostatic ordering effects induced by the hydrophilic sulfonate group [85, 111, 152–155].

In Figure 3-5, all the RDF curves have a value of zero until $r_i \simeq 0.30$ nm, reflecting the steric hinderance when $r_i \lesssim 0.30$ nm that prevents close proximity between the water oxygen atom and the sulfur atom in the sulfonate group as well as between the water oxygen atom and the carbon atom in the $CH_3$ group. When $r_i$ exceeds 0.30 nm, the RDF curves increases, reflecting the fact that, at these $r_i$ values, increasing number of water oxygen atoms can begin to approach the sulfur atom in the sulfonate group as well as the carbon atom in the $CH_3$ group. Figure 3-5 (top row) shows a distinct first peak at $r_{\max}$ in both the density and the number RDF curves corresponding to the hydrophilic group, indicating the most probable location of the nearest-neighbor water oxygen atoms. Following the first peak, there is a first valley at $r_{\min}$ in both the density and the number RDF curves, reflecting the depletion of the water oxygen atoms which occurs between the first and the second hydration layers. Following the first valley at $r_{\min}$, one observes a second peak and a second valley which are not as pronounced as the first two, indicating that the ordering diminishes as the distance from the hydrophilic group increases. As a result, the region extending beyond the second valley can be viewed as a bulk water environment (the curve should approach a horizontal

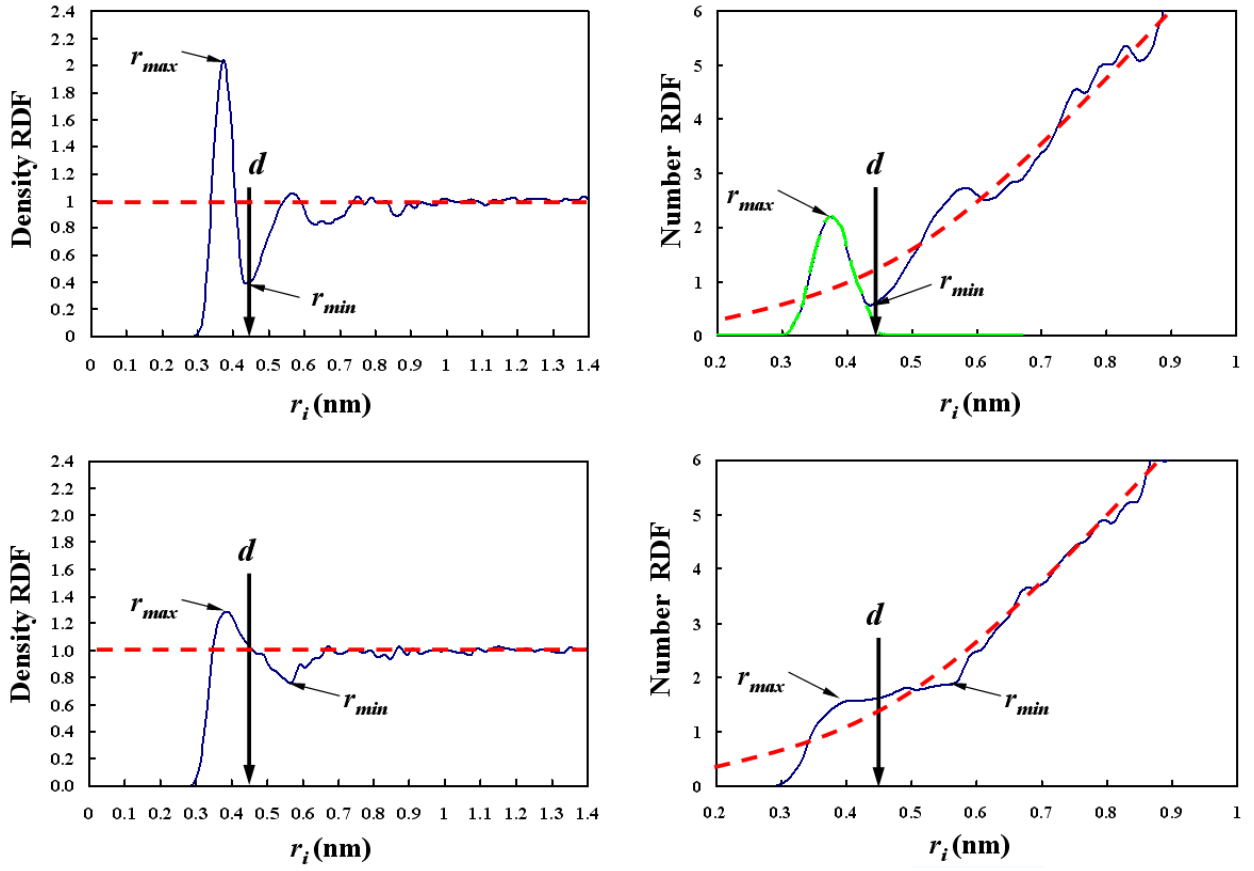


Figure 3-5: Sample density RDF's (left column) and corresponding number RDF's (right column) of water oxygen atoms with respect to: (i) the sulfur atom in the hydrophilic anionic sulfonate group (top row), and (ii) the carbon atom in the hydrophobic $CH_3$ group (bottom row). A symmetric distribution (green dashed curve) of the water oxygen atoms is depicted in the number RDF plot for the hydrophilic sulfonate group. The area under the green dashed curve represents the hydration number. The red dashed horizontal lines and curves indicate the RDF's for the bulk water environment. Note that the locations of $r_{\max}$ and $r_{\min}$ are assigned in the density RDF plots and are also shown in the number RDF plots at the same locations. The cutoff distance $d$ for the hydrophilic sulfonate group was determined using the two methods discussed in this section — one using the density RDF curve, and the other using the number RDF curve. As discussed in the text, the cutoff distance $d$ for the hydrophobic $CH_3$ group was selected to be equal to the cutoff distance $d$ for the hydrophilic sulfonate group.

line of unity in the density RDF plot (the red dashed line), corresponding to a quadratic curve in the number RDF plot (the red dashed curve)). A similar behavior is observed in the density and the number RDF curves corresponding to the hydrophobic group, although the second peak and the second valley are less pronounced in this case. Note that the first peaks at $r_{\max}$, the first valleys at $r_{\min}$, and the second peak are located at similar positions in both the density and the number RDF curves corresponding to the hydrophilic groups (see Figure 3-5, top row).

In order to count all the water molecules in the first hydration shell (which corresponds to the hydration number) around the hydrophilic group, a cutoff distance $d$ is typically assigned at the position of the first valley of the density RDF curve [154, 156]. This frequently made cutoff selection is based on the assumption that the number distribution of the nearest-neighbor water molecules should be symmetric with respect to the location of the first peak (that is, it should behave like a bell-shaped distribution centered around the first peak) [157]. As shown in Figure 3-5 (top row), for the hydrophilic group, the symmetric distribution curve of the nearest-neighbor water molecules (the green dashed curve) matches very well the number RDF curve around the first peak. As a result, the integral of this symmetric distribution curve (corresponding to the area under this curve) should be equal to the hydration number. As discussed earlier, due to the similarity between the density and the number RDF curves in the case of the hydrophilic group (see Figure 3-5, top row), instead of locating the cutoff distance by analyzing the number RDF curve as described above, it is more convenient to simply locate the cutoff distance at the position of the first valley in the density RDF curve (for example, as shown in Figure 3-5, top row, both methods yield the same value of $d = r_{\min} \simeq 0.45$ nm).

On the other hand, the situation is very different for the density and the number RDF curves in the case of the hydrophobic group (see Figure 3-5, bottom row), where less pronounced peaks and valleys are observed (although there is a noticeable first peak at $r_{\max}$ and a noticeable shallow first valley at $r_{\min}$ in the density RDF curve). As a result, it is no longer possible to match the number RDF curve to a symmetric distribution curve around $r_{\max}$. Indeed, an examination of Figure 3-5 (bottom row) reveals that the left half of a symmetric distribution curve could match very well the number RDF curve, but that the right half of a symmetric distribution curve could not match at all the number RDF curve. This inability to fully match the number RDF curve with a symmetric distribution curve reflects the disordering of the hydrating atoms as they crowd around the hy-

drophobic group at distances beyond $r_{\max}$ [85, 111, 152–155]. Accordingly, the method involving use of the number RDF curve to calculate the cutoff distance discussed above is not applicable in the hydrophobic group case. In addition, in the hydrophobic group case, the conventional method involving use of the density RDF curve to calculate the cutoff distance becomes questionable. With this in mind, as a first approximation, I have selected the cutoff distance for the hydrophobic group to be equal to the cutoff distance for the hydrophilic group, that is, $d = 0.45$ nm (see below).

As discussed earlier, in the case of the hydrophobic group, the first peak at $r_{\max}$ in the density RDF curve indicates the most probable location of the nearest-neighbor water oxygen atoms (see Figure 3-5, bottom row). Following the first peak, the first valley at $r_{\min}$ in the density RDF curve reflects a noticeable depletion of the water oxygen atoms. Accordingly, if the cutoff distance $d$, was smaller than $r_{\max}$, then the number of nearest-neighbor water oxygen atoms would be undercounted due to the exclusion of the water oxygen atoms located at, or beyond, $r_{\max}$. This is also true in the case of the hydrophilic group, that is, $d$ should be larger than $r_{\max}$ to ensure that the number of nearest-neighbor hydrating atoms is not undercounted. Furthermore, if the cutoff distance $d$ was located beyond the first valley at $r_{\min}$, then the number of nearest-neighbor water oxygen atoms would be overcounted because of the inclusion of bulk water oxygen atoms which are weakly affected by the hydrophobic group. As discussed earlier, in the case of the hydrophilic group, the cutoff distance selection criterion is very rigorous, and yields a cutoff distance $d \simeq r_{\min}$ in the density RDF curve. This reflects the clear distinction between the first layer and the second layer of hydrating atoms in the hydrophilic group case. However, in the case of the hydrophobic group, the first valley at $r_{\min}$ is so shallow that the distinction between the first layer and the second layer of hydrating atoms is not as clear. In fact, due to the disordering of the hydrating atoms around the hydrophobic group, one could expect that the first layer and the second layer of hydrating atoms should overlap slightly with each other. Therefore, hydrating atoms counted for distance smaller than $r_{\min}$ not only include the first layer of hydrating atoms but also include some of the hydrating atoms in the second layer. Accordingly, in the case of the hydrophobic group, the cutoff distance $d$ should be smaller than $r_{\min}$ to ensure that the number of nearest-neighbor hydrating atoms is not overcounted.

With all of the above in mind, to determine the sensitivity of the CS–MT modeling results (specifically, the ability to predict CMC's, see Chapter 5) to the value of the cutoff distance se-

lected, several different cutoff distance values were tested, including $d = 0.40$, $0.45$, $0.50$, and $0.55$ nm. These $d$ values were selected because they satisfy $r_{\max} < d < r_{\min}$ in the density RDF curve (that is, $d$ falls between 0.40 and 0.55 nm), and as explained above, the actual cutoff distance value should be within this range. In order to simplify the testing procedure, the sensitivity test was carried out only in the case of 2-9-SAS. I found that a larger cutoff distance yields a higher predicted CMC, while a smaller cutoff distance yields a lower predicted CMC (results not shown). The increase in the predicted CMC as $d$ increases is due to the fact that a larger $d$ value yields a higher $f_i$ value for the surfactant tail group, and a lower $f_i$ value for the surfactant head group. This results in the overprediction of the $\hat{g}_{dehydr}$ contribution (see Section 2.2.3) which overcomes the underprediction of the $\hat{g}_{hydr}$ contribution (see Section 2.2.4), leading to a slight overprediction of $g_{tr,CS-MT}$. This overprediction further results in a slight overprediction of $g^*_{mic}$ and associated higher predicted CMC (see Sections 2.1.1 and 2.2.1). In addition, the results of the sensitivity test show that the predicted CMC using $d = 0.45$ nm agrees best with the experimental CMC of 2-9-SAS. Clearly, selecting $d = 0.45$ nm for the hydrophobic group is not as rigorous as in the case of the hydrophilic group, and requires further investigation.

In summary, all the CS–MT modeling results reported in this thesis were generated using a cutoff distance of $d = 0.45$ nm (see Chapter 5). Interestingly, cutoff distances used to compute hydration (coordination) numbers of various chemical species reported in the literature vary from 0.35 nm to 0.50 nm [78, 91, 95, 156] (for different simulation methods and parameters). However, one should keep in mind that only some of the reported cutoff distances were selected based on rigorous density RDF results, while the majority of the reported cutoff distances were selected without providing any clear justification.

### 3.4.4 Error Analysis in Counting Hydrating Contacts

An estimate of the standard error in counting hydrating contacts for each group of atoms in the ionic linear and branched surfactants considered was obtained through the use of block averaging [158, 159]. In block averaging, the standard error is computed from the variance between averages of blocks of data, and the block size is increased until the standard error estimate becomes constant. To assist in identifying this asymptotic value for the simulation data reported

here, a two-exponential function was fit to the block average curve [158, 159]. Block averaging is useful to analyze correlated data, such as the data obtained from an MD simulation. Data gathering simulation runs for the ionic linear and branched surfactants considered here in the bulk water and in the micellar states were conducted for sufficient time to ensure that the uncertainty in each counted hydrating contact was sufficiently small, typically less than 5%.

The block averaging approach described above provides an accurate estimate of the standard error of the results of a single simulation. However, it is also typically desirable to run multiple independent simulations to estimate the run-to-run variance. If the run-to-run variance is much larger than the variance estimated from a single simulation, it indicates that insufficient sampling has been done [148, 160]. This problem has been commented upon in the context of free-energy calculations using computer simulations [145, 148]. Recently, Stephenson et al. conducted additional independent bulk water and aggregate simulations of oil molecules to determine the run-to-run variance [58], and found that it is comparable in magnitude to the block average estimates of the standard error for each oil molecule. Accordingly, and because of the high computational cost associated with conducting such simulations, independent simulations were not deemed necessary for the ionic linear and branched surfactants simulated as part of this thesis. Nevertheless, additional studies are needed to validate the results of reference [58] when simulating ionic linear and branched surfactants.

# Chapter 4

# Surfactant Property Inputs Required to Implement the CS–MT Modeling Approach

## 4.1 Head and Tail Identifications Based on Micelle Simulations

As discussed in Section 1.3.2, the surfactant head and tail in a self-assembled micelle are key inputs required to implement the MT modeling approach. This information is required for both the traditional MT modeling approach (to compute $g_{tr}$ and $g_{int}$) and the CS–MT modeling approach (to compute $\hat{g}_{hydr}$), as discussed in Sections 2.1.2 and 2.2.4, respectively. Various approaches were developed in the past to identify surfactant heads and tails based on: (i) experimental evidence (see Section 1.2.2) [49, 61], or (ii) MD simulations of surfactant molecules at a flat water–oil interface (see Section 1.3.2) [57]. However, MD simulations of surfactant molecules at a *flat* water–oil interface do not take into consideration the curvature of the micelle surface. In addition, in the case of branched surfactants considered in this thesis, it is unclear which oil type one should use to best represent a bulk phase of branched surfactant tails.

With these challenges in mind, Stephenson et al. carried out MD simulations of surfactant molecules in a bulk water environment and in a micellar environment, and concluded that a cutoff value of the fractional hydration of each atomic group $i$, $f_i = 0.60$, could be utilized to distinguish surfactant heads from surfactant tails [59, 60]. However, this head/tail identification method is

not satisfactory because it depends on the degree of hydration of the surfactant molecule in the bulk water environment, while physically, it should only depend on the degree of hydration in the micellar environment. In addition, the cutoff value may depend on the curvature of the micelle surface, and therefore, a single cutoff value may not be generally applicable for different simulated micelle sizes.

With the limitations above in mind, I developed a new method for head and tail identification that utilizes RDF's obtained from the surfactant micelle simulations. Specifically, in Section 4.1.1, an extension of the Gibbs dividing surface approach to represent the micelle core–water interface using surfactant micelle simulations is discussed. In Section 4.1.2, the location of each atomic group in a surfactant molecule using the same micelle simulations is discussed. Finally, in Section 4.1.3, the notion of assigning neutral groups, in addition to surfactant head and tail groups, is discussed, including presenting the head/tail identification results.

### 4.1.1 Extension of the Gibbs Dividing Surface Approach

As discussed above, in the modified CS–MT modeling approach presented in this thesis, a new approach for head and tail identification is formulated which only makes use of surfactant micelle simulations. Two key outputs from the micelle simulations are the density RDF and the number RDF (see Section 3.4.3) of hydrating atoms (the oxygen and the hydrogen atoms in water, the counterions, and the hydrating atoms in the surfactant molecules, such as the oxygen atoms in the sulfonate group and the nitrogen atom in the pyridinium group), evaluated with respect to the micelle center of mass (COM). Note that relatively simple, radially-dependent RDF's were utilized here (no angular dependence), and therefore, a spherical micelle geometry is required in the MD simulations, and was adopted here. In the case of other micelle geometries, such as cylinders, bilayers, or ellipsoids, more complex RDF's need to be utilized (see Section 6.2.4).

The concept of the number RDF and a sample density RDF plot of hydrating atoms with respect to the micelle COM are illustrated in Figure 4-1 (top row). The density RDF and the number RDF shown in Figure 4-1 were calculated using Eqs. 3.1 and 3.4, with A referring to the micelle COM and B referring to the hydrating atoms. Note that the layer thickness, $\Delta r = 0.05$ nm, used here is larger than the $\Delta r$ value used in Section 3.4.3 in order to increase the computational efficiency, yet

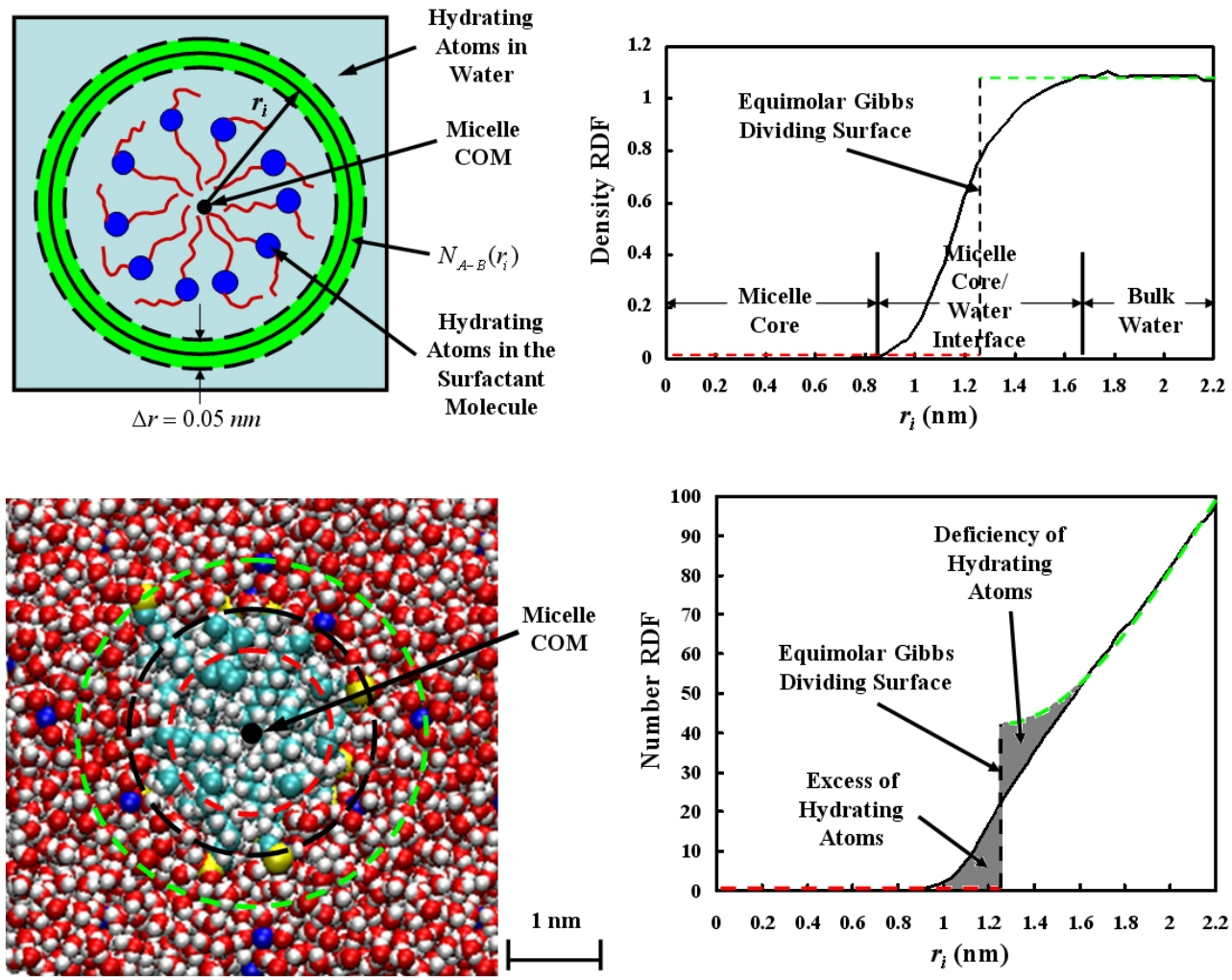


Figure 4-1: Top left: illustration of the number RDF (the green ring region at $r_i$) of hydrating atoms (the light blue region and the dark blue circles) with respect to the micelle COM, corresponding to one simulation time frame. Top right: sample density RDF of hydrating atoms with respect to the micelle COM. The green dashed line represents the conceptual pure hydrating atom phase. The red dashed line represents the conceptual pure micelle-core phase. The black dashed line denotes the location of the equimolar Gibbs dividing surface. Bottom left: MD simulation snapshot of an equilibrated $C_{12}$-SAS micelle (color code: red – oxygen, yellow – sulfur, light blue – carbon, white – hydrogen, and dark blue – sodium ion). The green dashed circle separates the bulk water and the micelle core–water interface phases. The red dashed circle separates the micelle core–water interface and the micelle core phases. The black dashed circle denotes the location of the equimolar Gibbs dividing surface. Bottom right: the number RDF corresponding to the density RDF on the top right. The two grey areas represent the excess and the deficiency of hydrating atoms.

small enough to generate fine layers.

Density RDF's have been used extensively to quantify the population of water molecules around a micellar aggregate [77, 78, 91, 109], including providing information about the hydration state of each atomic group in the surfactant molecule upon incorporation into a micelle. As shown in Figure 4-1 (top right), in general, the density RDF curve can be divided into three phases in terms of the hydrating atom density, including: (i) the micelle core (for $r_i \leqslant 0.86$ nm), where there are no hydrating atoms and their density approaches zero, (ii) the finite-thickness micelle core–water interface ($0.86$ nm $\leqslant r_i \leqslant 1.67$ nm), where the hydrating atom density increases from zero to the bulk aqueous density, and (iii) the bulk aqueous solution (for $r_i > 1.67$ nm), where hydrating atoms are weakly perturbed by the micelle. As can be seen, the real micelle core–water interface is not strictly sharp, as assumed in the CS–MT model, but instead, possesses finite thickness. As a result, in the context of the CS–MT model where absolute head and tail assignments are made, a theoretical model is required to replace the finite-thickness interface with the sharp interface shown in Figure 4-1 (top right).

With the above need in mind, I made use of the similarity between the density RDF of hydrating atoms and the Gibbs adsorption curve for a two-component system [103]. Specifically, I selected the equimolar Gibbs dividing surface to represent the sharp micelle core–water interface adopted in the CS–MT model to make surfactant head and tail identifications. As shown in Figure 4-1 (top right), the equimolar Gibbs dividing surface separates the conceptual, pure micelle-core phase (no hydrating atoms, the red dashed line) from the conceptual pure hydrating atom phase (the green dashed line). In the real three-phase micellar system, as opposed to to the conceptual, two-phase micellar system, there is an excess and a deficiency of hydrating atoms which need to be assigned to the equimolar Gibbs dividing surface in order to make the conceptual and the real systems identical (see Figure 4-1, bottom right). Note that a Gibbs dividing surface may be located anywhere within the finite-thickness interface depending on the specific surface excess quantities required, such as the "Gibbs surface of tension" [103, 161]. With this in mind, I have chosen the equimolar Gibbs dividing surface (referred to hereafter as the "dividing surface") to be located at $r_i = l$, such that the excess and the deficiency of hydrating atoms are the same (in Figure 4-1, bottom right; note that this corresponds to the two grey areas being equal in the number RDF plot). When this approach is applied to the number RDF plot, it yields a value of $l = 1.25$ nm (see Figure 4-1, right column).

I have selected the number RDF-based approach outlined above to calculate the location of the dividing surface, $l$, for the various ionic linear and branched surfactants considered in this thesis. The results of these calculations are reported in Figure 4-2 (see the horizontal black dashed lines). Note that in Figure 4-2, I also report: (i) $L_i$, the expected location of each atomic group $i$ in a surfactant molecule (denoted by the red dots), (ii) $\sigma_i$, one standard deviation with respect to $L_i$ (denoted by the blue markers), and (iii) the head group, neutral group, and tail group assignments for the various ionic linear and branched surfactants considered. These results are further discussed in Sections 4.1.2 and 4.1.3.

Figure 4-2 shows that $l$ varies between about 1.0 nm to 1.4 nm for the various ionic linear and branched surfactants considered here, due to differences in the size of the simulated surfactant micelle (this impacts the micelle aggregation number as well as the total number of surfactant hydrocarbon groups). The general trend is that $l$ increases when the micelle size increases. Specifically, (a) for the first series of x-y-SAS branched surfactants ($y = 9$), $l$ increases when the total number of hydrocarbon groups ($x+y$) increases, (b) for the second series of x-y-SAS branched surfactants ($x + y = 11$), $l$ remains approximately constant because the total number of hydrocarbon groups is constant, and (c) for the complex branched surfactants (A to F), $l$ increases when both the total number of hydrocarbon groups and the micelle aggregation number increase. Note that the value of $l$ for surfactant D is not reported in Figure 4-2, because of the non-regular ellipsoidal micelle geometry in the MD simulation of this surfactant.

The error in calculating the location of the dividing surface, $l$, reflects primarily the method used to equate the excess and the deficiency of hydrating atoms which utilizes a layer-by-layer approach. In addition, note that different sampling of simulation frames may result in different $l$ values for each sampling time considered; however, this difference was assumed to be negligible (see Section 3.4.4). Clearly, additional studies are needed for branched surfactant simulations to further substantiate this assumption. As a result, the error in $l$ is approximately one half of the layer thickness, that is, $\Delta l = 0.025$ nm. Accordingly, the $\Delta l$ value is negligible relative to that of $\sigma_i$ (typically between 0.3 nm and 0.6 nm, see Section 4.1.2), and was not considered in the head, neutral, and tail group assignment procedure discussed in Section 4.1.3.

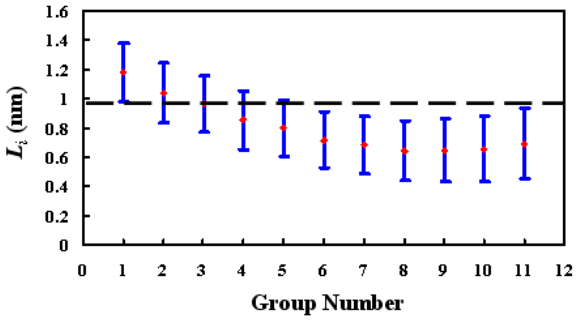


$C_{10}$-SAS

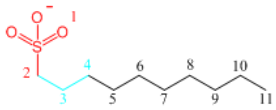

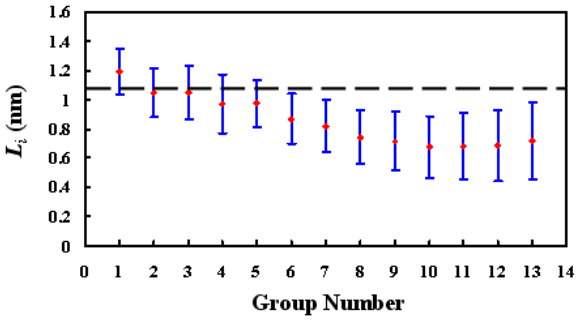


2-9-SAS

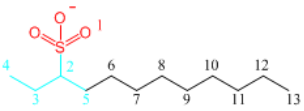

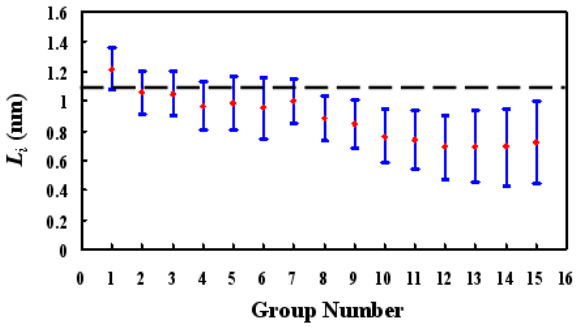


4-9-SAS

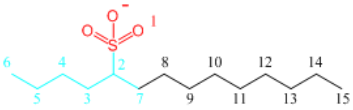

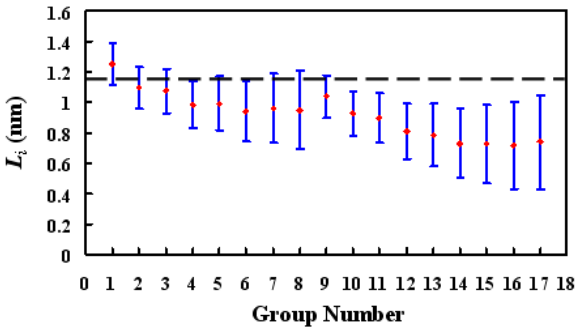


6-9-SAS

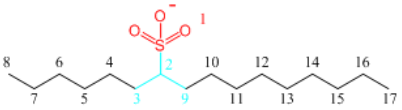

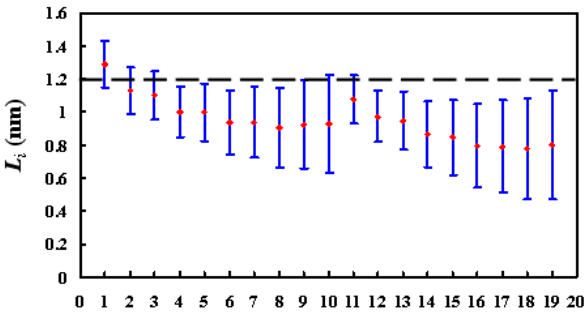


8-9-SAS

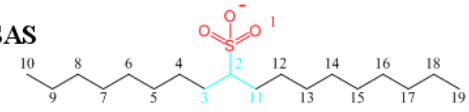

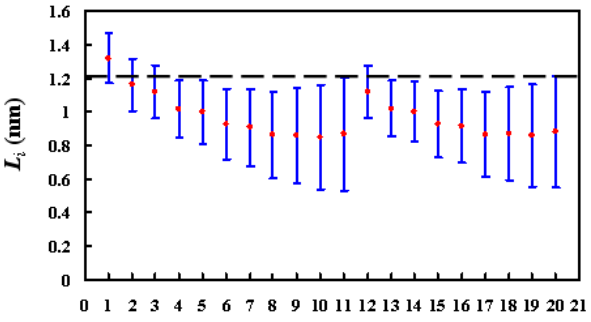


9-9-SAS

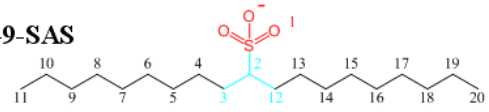

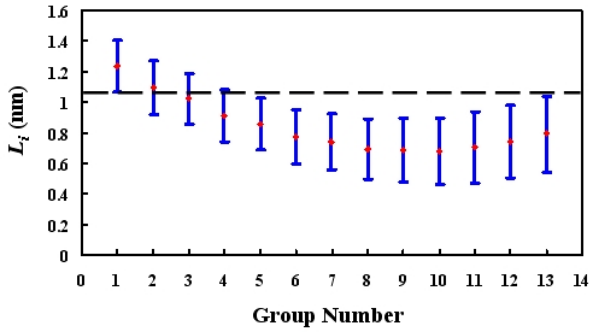


$C_{12}$-SAS

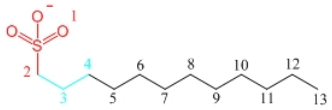

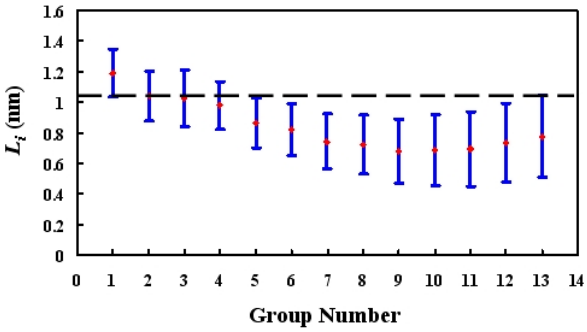


1-10-SAS

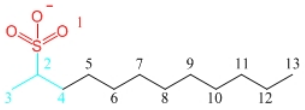

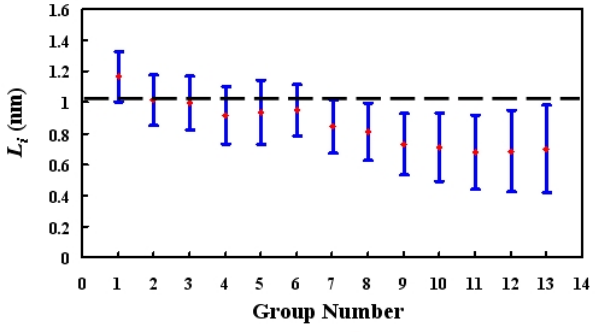


3-8-SAS

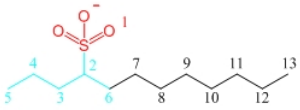

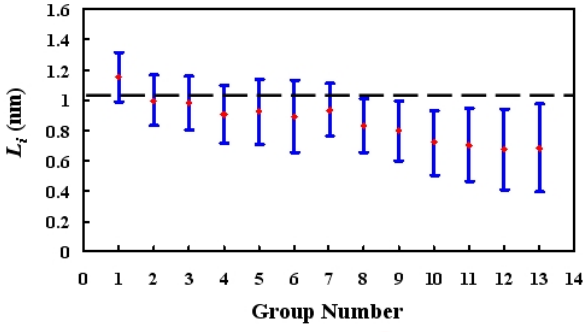


4-7-SAS

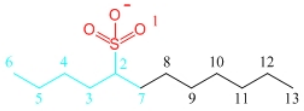

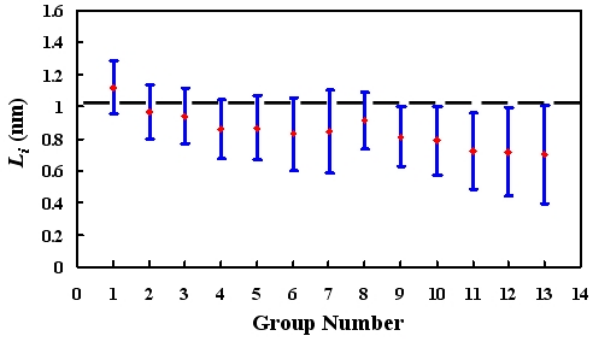


5-6-SAS

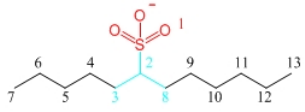

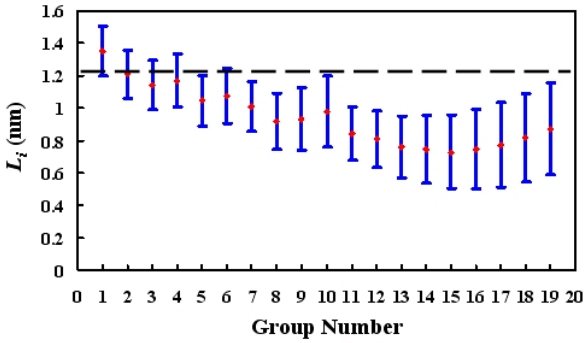


Surfactant A

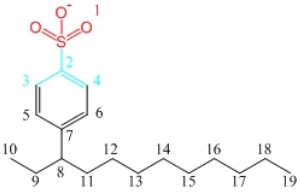

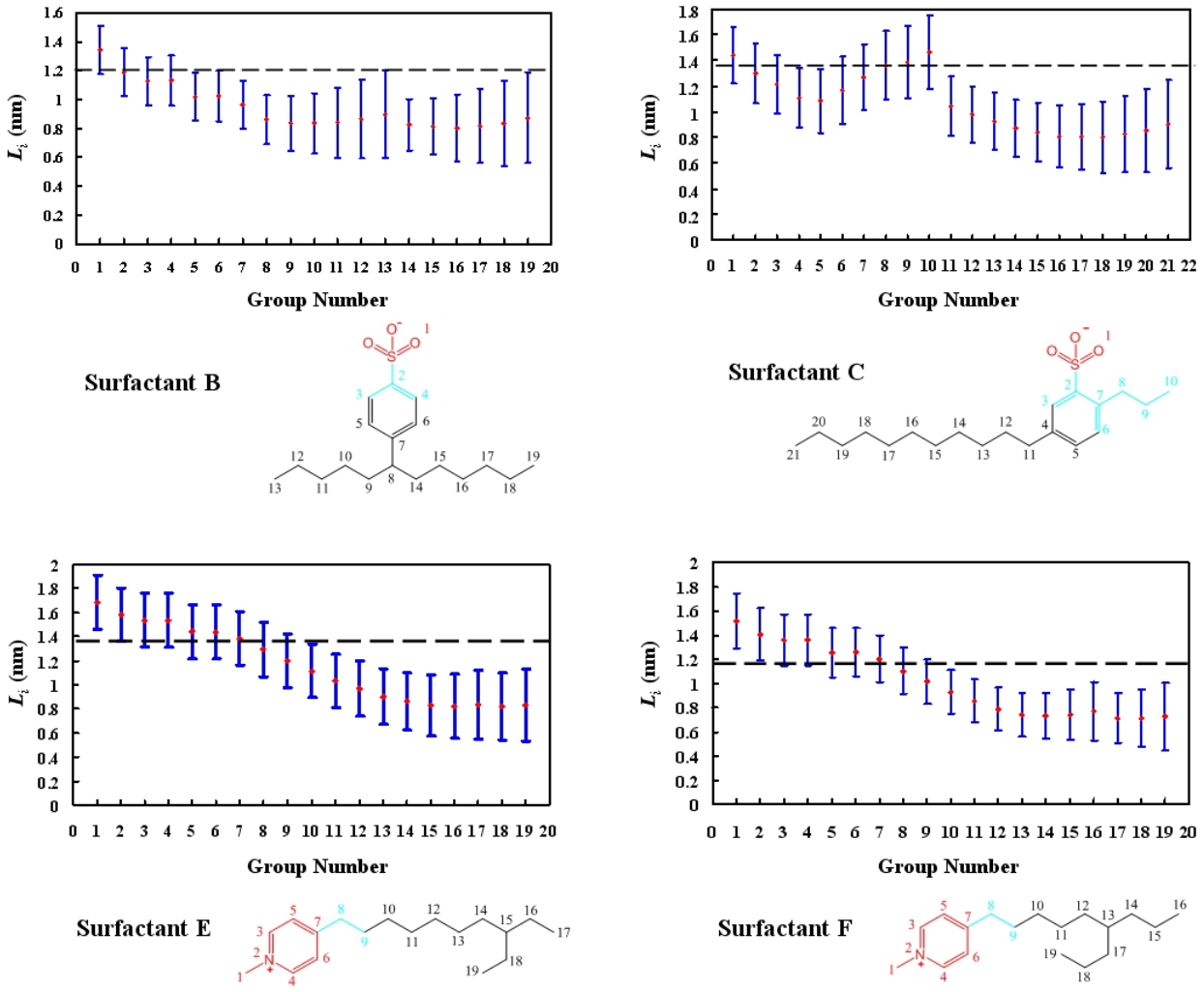


Figure 4-2: Head and tail identification results for the various ionic linear and branched surfactants considered in this thesis. The horizontal black dashed lines denote $l$ — the locations of the equimolar Gibbs dividing surfaces. The red dots denote $L_i$, the expected location of surfactant group $i$. The blue markers denote $\sigma_i$, one standard deviation from the expected location of group $i$. The chemical structures of the various ionic linear and branched surfactant considered are shown below each plot, including the various group numbers (color code: red – head groups, light blue – neutral groups, and black – tail groups).

### 4.1.2 Location of Atomic Group $i$ in the Surfactant Molecule

After calculating the location of the dividing surface, $l$, representing the conceptual, sharp micelle core–water interface, I proceeded to calculate the expected location of each atomic group $i$ in the surfactant molecule, $L_i$, with respect to the micelle COM. By comparing the relative values of $L_i$ and $l$, it is possible to determine if group $i$ is head, tail, or neutral (see Section 4.1.3). To calculate $L_i$, one can analyze the detailed micelle structure using the number RDF of each atomic group $i$ in the surfactant molecule with respect to the micelle COM. Note that the normalized number RDF, $\langle \widetilde{N}_{A-B}(r_i) \rangle$, rather than the original number RDF, $\langle N_{A-B}(r_i) \rangle$, introduced in Section 3.4.3, was used to calculate $L_i$, because it is equivalent to the probability density function associated with finding an atomic group (see below for details). The value of $\langle \widetilde{N}_{A-B}(r_i) \rangle$ was calculated by normalizing the original number RDF by $N_B$, the total number of atomic groups of type $i$ present in the micelle simulation cell (that is, the various micelle aggregation numbers listed in Table 3.2). The number RDF, $\langle N_{A-B}(r_i) \rangle$, was calculated using the procedure described in Section 3.4.3. Specifically, Eq. 3.4 was used with $\Delta r = 0.05$ nm, where in the present case, A refers to the micelle COM, and B refers to atomic groups of type $i$ in the surfactant micelle. This yields:

$$\langle \widetilde{N}_{A-B}(r_i) \rangle = \frac{\langle N_{A-B}(r_i) \rangle}{N_B} = \frac{4\pi r_i^2 \Delta r}{\langle V_{cell} \rangle} g_{A-B}(r_i) \tag{4.1}$$

where the various variables are defined in Section 3.4.3.

To illustrate the use of Eq. 4.1, the normalized number RDF's of five representive atomic groups in ionic branched surfactant A were calculated and are reported in Figure 4-3. Note that the position of a peak in the normalized number RDF curve indicates the position where most of the atomic groups will locate (recall that there are $N_B$ atomic groups of type $i$ in a micelle comprising $N_B$ surfactant molecules), while the expected location indicates where one expects atomic groups of type $i$ to be located. As can be seen, the normalized number RDF's of the carbon atoms in the surfactant hydrocarbon tail broaden as the distance of the carbon atom from the sulfonate head group increases. In addition, as expected, the normalized number RDF of the C2 atom is similar to that of the sulfur atom, while the normalized number RDF's of the other carbon atoms extend further towards the micelle COM [77, 78, 91, 109]. As discussed earlier, the normalized number RDF reported here is equivalent to the probability density function associated with finding an

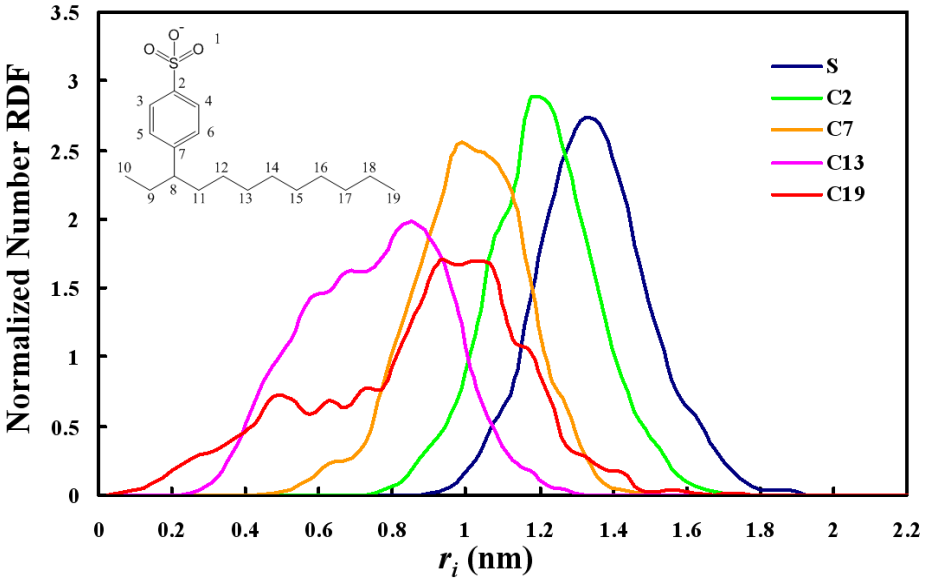


Figure 4-3: Normalized number RDF of five representive atomic groups (S: sulfur atom in the sulfonate group, C2, C7, C13, and C19: four carbon atoms in the hydrocarbon groups indicated by their locations in the surfactant molecule, where the chemical structure is shown in the top left corner of the RDF plot) in surfactant A with respect to the spherical micelle COM.

atomic group $i$ within a layer of thickness $\Delta r$. In other words, the area under each normalized RDF curve is equal to unity, and therefore, can be used to determine $L_i$ — the expected location of atomic group $i$ in a surfactant molecule with respect to the micelle COM. Specifically,

$$L_i = \sum_{i}^{n} \langle \widetilde{N}_{A-B}(r_i) \rangle r_i = \sum_{i}^{n} \frac{4\pi r_i^3 \Delta r}{\langle V_{cell} \rangle} g_{A-B}(r_i) \tag{4.2}$$

where $n$ is the total number of layers in the micelle simulation cell, determined by the layer thickness, $\Delta r = 0.05$ nm (which is small enough to generate fine layers), and the size of the micelle simulation cell. Note that an increase in the value of $n$, or a decrease in the value of $\Delta r$, does not make a noticeable difference in the calculation of $L_i$.

The expected locations, $L_i$, of each atomic group $i$ in the various ionic linear and branched surfactant considered here were calculated using Eq. 4.2, and are reported in Figure 4-2 (see the red dots). As can be seen, in general, $L_i$ is larger for the charged head groups (such as the sulfonate groups in x-y-SAS and in surfactants A to C, as well as the pyridinium groups in surfactants E and

F) and smaller for those hydrocarbon groups located farther away from the surfactant ionic head. This reflects the tendency of the ionic hydrophilic groups to reside farther away from the micelle COM, and the tendency of the hydrocarbon groups to reside closer to the micelle COM.

Recognizing that the location of each atomic group in the surfactant molecule spans a certain $r_i$ range along the distance to the micelle COM (see Figure 4-3), it is important to quantify this range. For this purpose, I have used the standard deviation, $\sigma_i$, characterizing the location of atomic group $i$ in a surfactant molecule with respect to the micelle COM. Note that the chosen standard deviation, $\sigma_i$, is defined with respect to the expected value, $L_i$, and not with respect to the error in the data analysis. In other words,

$$\sigma_i = \sqrt{\left(\sum_i^n \langle \widetilde{N}_{A-B}(r_i)\rangle r_i^2\right) - L_i^2} = \sqrt{\left(\sum_i^n \frac{4\pi r_i^4 \Delta r}{\langle V_{cell}\rangle} g_{A-B}(r_i)\right) - L_i^2} \tag{4.3}$$

where the various variables were defined in Section 3.4.3. Note that, by definition, an atomic group $i$ locates most probably within one standard deviation from its expected location, that is, between $(L_i - \sigma_i)$ and $(L_i + \sigma_i)$. In the case of an atomic group $i$ characterized by a normal distribution with respect to $r_i$, and having an expected location at $L_i$ and a standard deviation of $\sigma_i$, the probability that it will be located between $(L_i - \sigma_i)$ and $(L_i + \sigma_i)$ is quite high, about $68\%$.

The standard deviations in the locations of the various atomic groups in each ionic linear and branched surfactant considered here were determined using Eq. 4.3, and are reported in Figure 4-2 (see the blue markers). As can be seen, in general, charged head groups (such as the sulfonate groups in x-y-SAS and in surfactants A to C, as well as the pyridinium groups in surfactants E and F) are pinned at the micelle core–water interface and have relative small $\sigma_i$ values. On the other hand, the hydrocarbon groups farther away from the charged head group tend to have larger $\sigma_i$ values, which reflects the enhanced mobility of the end groups of the surfactant molecules (such as the $CH_3$ group at the end of a hydrocarbon chain which possesses increased mobility inside the micelle core). Note that the values of $L_i$ and $\sigma_i$ for surfactant D are not reported in Figure 4-2, because of the non-regular ellipsoidal micelle geometry in the MD simulation of this surfactant.

### 4.1.3 Assignment of Surfactant Neutral Groups in Addition to Surfactant Head and Tail Groups

As discussed in Section 1.3.2, some atomic groups in the surfactant molecule tend to reside near the micelle core–water interface. These groups cannot be identified unambiguously as being part of the surfactant head or the surfactant tail, since they are neither as dehydrated as those groups which belong to the surfactant tail nor as hydrated as those groups which belong to the surfactant head. After calculating the expected location of the dividing surface (that is, $l$, where the conceptual, sharp micelle core–water interface is located) and the locations of each atomic group $i$ (characterized by $L_i$ and $\sigma_i$) for the various ionic linear and branched surfactants considered here (see Figure 4-2), I found that: (i) all the charged head groups (group 1 in Figure 4-2; note, however, that in the case of the $C_{10}$-SAS and $C_{12}$-SAS linear surfactants, the $CH_2$ group adjacent to group 1 is also included as part of the charged head group) are expected to locate above the dividing surface ($L_i > l$), that is, they are very likely to be fully hydrated and be part of the surfactant head, as previously reported using a non-rigorous analysis [48, 49], (ii) most of the hydrocarbon groups (such as groups 6 to 14 in 2-9-SAS, groups 5 to 13 in $C_{12}$-SAS, and groups 5 to 20 in surfactant B, shown in Figure 4-2) are expected to locate within more than one standard deviation below the dividing surface ($(L_i + \sigma_i) < l$), that is, they are very likely to reside in the micelle core and be part of the surfactant tail, and (iii) some of the hydrocarbon groups adjacent to the ionic surfactant heads are located right at, or at most within one standard deviation below the dividing surface ($L_i \leq l \leq (L_i + \sigma_i)$), that is, they are likely to reside in the micelle core while nevertheless having a reasonable probability to reside outside of the micelle core–water interface. Accordingly, these groups have been designated as "neutral atom" groups.

Based on this important finding, the following new procedure was adopted to assign surfactant groups: (a) group $i$ having $L_i > l$ is assigned to be part of the surfactant head, (b) group $i$ having $L_i \leq l \leq (L_i+\sigma_i)$ is assigned to be a neutral group, and (c) group $i$ having $(L_i+\sigma_i) < l$ is assigned to be part of the surfactant tail. In particular, in the case of an atomic group characterized by a normal distribution with respect to $r_i$, the probability that it will be located in the micelle core is: (i) below $50\%$, if the atomic group is assigned to be part of the surfactant head, (ii) between $50\%$ and $84\%$, if the atomic group is assigned to be a neutral group, and (iii) above $84\%$, if the atomic group

is assigned to be part of the surfactant tail. The implementation of this new procedure to assign head groups, tail groups, and neutral groups for the various ionic linear and branched surfactant considered in this thesis is reported in Figure 4-2, where, in the various chemical structures shown, red denotes head groups, light blue denotes neutral groups, and black denotes tail groups (for exemptions, see below).

A modified MT model, which includes a generalized packing calculation to account for neutral groups, was developed in collaboration with J. D. Mendenhall in the Blankschtein group to model the free energy of micellization of surfactants possessing conventional head and tail groups in addition to neutral groups (details not reported in this thesis). As discussed in Section 2.2.4, only surfactant tail groups contribute to $\hat{g}_{hydr}$. However, since neutral groups do reside more often in the micelle core (with a probability between $50\%$ and $84\%$ if this neutral group is characterized by a normal distribution), I have also included them in the calculation of $\hat{g}_{hydr}$. Note that assigning an atomic group as a neutral group does not preclude it from becoming a head group or a tail group, but instead, allows for all three possibilities. Accordingly, a sufficient number of neutral groups should be assigned to allow flexibility in the packing model calculations, while not exceeding the current computational demands.

Additional examination of Figure 4-2 reveals that similar to the linear surfactant case ($C_{10}$-SAS and $C_{12}$-SAS), for the branched surfactants, the charged groups are always part of the surfactant head. However, the hydrocarbon groups adjacent to the charged groups (group 2 in x-y-SAS and in surfactants A to C, as well as group 8 in surfactants E and F) are not part of the surfactant head (unlike in the linear surfactant case, where group 2 is also part of the surfactant head), but instead, they are neutral groups. Interestingly, in the linear surfactant case, the two $CH_2$ groups (groups 3 and 4) adjacent to the $CH_2$ group which is adjacent to the charged head group are not part of the surfactant tail (contrary to the assignment made in the traditional MT model [48, 49]), but instead, they are neutral groups. Nevertheless, as discussed earlier, neutral groups do reside more often in the micelle core (with a probability between $50\%$ and $84\%$), and therefore, in the case of the linear surfactants ($C_{10}$-SAS and $C_{12}$-SAS), neutral groups were still considered to be part of the surfactant tail when implementing the CS–MT modeling approach, following the traditional approach to assign surfactant heads and tails (see Section 1.2.2).

Several other hydrocarbon groups close to the charged head group were also assigned as neutral

groups: (i) for the x-y-SAS branched surfactants, the two $CH_2$ groups adjacent to the CH group were assigned as neutral groups, (ii) for the x-y-SAS surfactants with relative short side chains (such as 2-9-SAS, 4-9-SAS, 1-10-SAS, 3-8-SAS, and 4-7-SAS), the entire side chain resides at the micelle core–water interface, and therefore, all the groups were assigned as neutral groups, (iii) for surfactants A and B, the two benzene carbon groups adjacent to the top benzene carbon group were assigned as neutral groups, (iv) for surfactant C with relative short side chains, although one end of the side chain is expected to locate beyond the dividing surface, as discussed earlier, in order to allow flexibility in the packing model, the entire side chain and several benzene carbon groups close to the sulfonate head and the side chain were assigned as neutral groups, (v) for surfactant D with no results reported, the assignment is similar to that for surfactant C in order to cover all the possibilities in the packing model, where the entire side chain and several benzene carbon groups (same locations as in surfactant C) were assigned as neutral groups, and (vi) for surfactants E and F, the two $CH_2$ groups adjacent to the charged pyridinium group were assigned as neutral groups.

It is important to note that although the use of various simulated spherical micelle sizes (corresponding to various micelle surface curvatures) in the MD simulation resulted in different values of $l$, $L_i$, and $\sigma_i$ for each ionic linear and branched surfactant considered in this thesis (results not reported), I found that the head, neutral, and tail group identification results are weakly dependent on the curvature of the simulated micelle surface, which highlights the advantage of the novel head/neutral/tail identification method developed in this thesis relative to the various other methods developed in the past [49, 57, 59–61].

## 4.2 Estimation of Four Surfactant Geometric Parameters Based on the Head/Neutral/Tail Group Assignments

On the basis of the head/neutral/tail group assignments discussed in Section 4.1.3, four geometric parameters were estimated for each surfactant considered and used as inputs in the CS–MT modeling approach [48, 57, 60, 61, 96]. The four geometric parameters include: (i) $a_h$, the cross-sectional area of the surfactant head, which is required to calculate $g_{st}$ (see Section 2.1), (ii) $a_0$, the interfacial area shielded by the surfactant head at the micelle core–water interface, which is required

to calculate $g_{int}$ and $\hat{g}_{int}$ (see Sections 2.1.2 and 2.2.1), (iii) $d_{charge}$, the distance from the location of the charge in the surfactant head to the beginning of the surfactant tail, which is required to calculate $g_{elec}$ (see Section 2.1), and (iv) $l_{hg}$, the length of the surfactant head, or the distance from the tip of the surfactant head to the beginning of the surfactant tail, which is required to calculate $g_{elec}$ (see Section 2.1). These four geometric parameters are listed in Table 4.1 for the various ionic linear and branched surfactants considered in this thesis, and were estimated based on the surfactant chemical structures and the head/neutral/tail group assignments reported in Figure 4-2.

As discussed in Section 4.1.3, due to the high tendency of neutral groups to reside in the micelle core, they were assumed to be part of the surfactant tail when estimating $d_{charge}$, $l_{hg}$, and $a_h$ (for the x-y-SAS surfactants, the area of a sulfonate group; for surfactants A to D, the area of a benzene sulfonate group; and for surfactants E and F, the area of a pyridinium group). Note that the neutral group assumption made here results in the largest possible estimated values of $d_{charge}$, $l_{hg}$, and $a_h$. When estimating $a_0$, the neutral groups were assumed to shield the micelle core–water interface because they do reside near this interface. For the linear surfactants and for surfactants E and F, $a_0$ was estimated based on the cross-sectional area of a single $CH_2$ group (about 21 $Å^2$), because the neutral groups (groups 3 and 4 in $C_{10}$-SAS and $C_{12}$-SAS, and groups 8 and 9 in surfactants E and F) are part of a single hydrocarbon chain. For most of the x-y-SAS branched surfactants (except for 1-10-SAS, where the side chain is negligible), both the primary chain and the side chain contribute to $a_0$, and as a result, $a_0$ was estimated to be twice the $a_0$ value in the case of a single hydrocarbon chain (about 42 $Å^2$). For surfactants A to D, since the interface is located on the benzene ring (part of the benzene ring consists of neutral groups, see Figure 4-2), $a_0$ was estimated to be the same as $a_0$ for the linear surfactants because the cross-sectional area of a benzene ring is only slightly larger than that of a single hydrocarbon chain. It is important to stress that I found that large variations in $a_0$ result in small variations in the predicted $g^*_{mic}$. This is due to the fact that $g_{int}$ in Eq. 2.9 and $\hat{g}_{int}$ in Eq. 2.14 appear to cancel each other out in the calculation of $g^*_{mic}$, particularly, in cases where the that the geometry of the simulated micelle is the same as that of the optimal micelle. With this in mind, the assumptions made in the calculation of $a_0$ should not greatly affect the CMC's predicted using the CS–MT modeling approach.

| Surfactant Type | $a_h$ [Å]$^2$ | $a_0$ [Å]$^2$ | $d_{charge}$ [Å] | $l_{hg}$ [Å] | $\sigma_0$ [mN/m] |
|---|---|---|---|---|---|
| **$C_{10}$-SAS** | 23 | 21 | 5.0 | 6.4 | 50.11 |
| **2-9-SAS** | 23 | 42 | 3.9 | 5.1 | 50.85 |
| **4-9-SAS** | 23 | 42 | 3.9 | 5.1 | 50.69 |
| **6-9-SAS** | 23 | 42 | 3.9 | 5.1 | 49.73 |
| **8-9-SAS** | 23 | 42 | 3.9 | 5.1 | 49.73 |
| **9-9-SAS** | 23 | 42 | 3.9 | 5.1 | 49.73 |
| **$C_{12}$-SAS** | 23 | 21 | 5.0 | 6.4 | 51.11 |
| **1-10-SAS** | 23 | 21 | 3.9 | 5.1 | 50.50 |
| **3-8-SAS** | 23 | 42 | 3.9 | 5.1 | 50.85 |
| **4-7-SAS** | 23 | 42 | 3.9 | 5.1 | 50.85 |
| **5-6-SAS** | 23 | 42 | 3.9 | 5.1 | 48.72 |
| **Surfactant A** | 25 | 21 | 4.5 | 6.0 | 48.00 |
| **Surfactant B** | 25 | 21 | 4.5 | 6.0 | 48.00 |
| **Surfactant C** | 25 | 21 | 4.5 | 6.0 | 47.00 |
| **Surfactant D** | 25 | 21 | 4.5 | 6.0 | 47.00 |
| **Surfactant E** | 20 | 21 | 5.0 | 8.0 | 50.40 |
| **Surfactant F** | 20 | 21 | 5.0 | 8.0 | 50.40 |

Table 4.1: The four estimated surfactant geometric parameters ($a_h$, $a_0$, $d_{charge}$, and $l_{hg}$) and interfacial tensions required to implement the CS-MT modeling approach.

## 4.3 Interfacial Tension Predictions Using Group-Contribution Methods

As discussed in Sections 2.1.2 and 2.2.1, $\sigma_0$, the interfacial tension between a surfactant tail phase and water at a flat interface, is required as an input in the CS–MT modeling approach. The empirical correlation discussed in Section 2.1.2 was used to determine $\sigma_0$ for the linear surfactants ($C_{10}$-SAS and $C_{12}$-SAS) and for the x-y-SAS branched surfactants (see Table 4.1). However, for the complex branched surfactants with aromatic groups, a suitable empirical correlation, or experimental $\sigma_0$ values, are not available. Therefore, a group-contribution method was developed by combining the parachor method [162, 163] and the Girifalco-Good equation [164] to estimate $\sigma_0$ for these complex branched surfactants. Note that the *parachor* does not have a physicochemical basis; however, it is useful as a parameter to estimate a range of chemical-structure related properties, especially those related to liquid-liquid interactions.

The parachor method is commonly used to estimate the surface tension of a liquid, $\gamma$, as fol-

lows:

$$\gamma = \left( \frac{parachor}{5V_{scale}} \right)^4 \tag{4.4}$$

where $V_{scale}$ is the scaled volume of a molecule and is given by the sum of the contributions of its contituent atoms as defined by Girolami, where the H atom contributes 1 and the C atom contributes 2 to the value of $V_{scale}$ (note that only H and C atoms are present in the surfactant hydrocarbon tails considered in this thesis) [165]. A very simple method was developed by McGowan to estimate the *parachor*, employing only the atomic contributions of the various $i$ type atoms, $A_i$, and the number of covalent bonds, $N_{bonds}$, in the molecule considered [163]. Specifically,

$$parachor = \sum n_i A_i - 19 N_{bonds} \tag{4.5}$$

where $n_i$ is the number of atoms of type $i$, $A_i = 24.7$ for an H atom, and $A_i = 47.6$ for a C atom.

After estimating the surface tension, $\gamma$, of the surfactant tail phase using Eqs. 4.4 and 4.5, I used the Girifalco-Good equation [164] to estimate the tail/water interfacial tension, $\sigma_0$, as follows:

$$\sigma_0 = \gamma + \gamma_w - 2\Phi\sqrt{\gamma\gamma_w} \tag{4.6}$$

where $\gamma_w = 72$ mN/m is the surface tension of water, and $\Phi$ is a function parameterized to estimate the interfacial tension ($\Phi = 0.55$ for aliphatic hydrocarbons and $\Phi = 0.72$ for aromatic hydrocarbons). In the case of complex branched surfactant tails consisting of both aliphatic hydrocarbons and aromatic hydrocarbons, an average $\Phi$ value can be estimated using the following simple group-contribution method:

$$\Phi = \frac{\sum n_j \Phi_j}{\sum n_j} \tag{4.7}$$

where $n_j$ is the number of hydrocarbon groups of type $j$, and $\Phi_j$ is the $\Phi$ value corresponding to the hydrocarbon group of type $j$. The estimated interfacial tensions of the various ionic linear and branched surfactants considered are reported in Table 4.1. Recognizing that only those surfactant tail groups which are most likely to reside in the micelle core should be considered in the calculation of $\sigma_0$, the neutral groups, which may sometimes reside on the micelle core–water interface, were not considered for the purpose of estimating the interfacial tension of the tail phase. Note also that it is reasonable to estimate $\sigma_0$ based solely on the primary hydrocarbon chain if the

side chain and the primary chain are similar in length [166]. Therefore, the $\sigma_0$ values of some of the x-y-SAS surfactant tails (such as 6-9-SAS, 8-9-SAS, 9-9-SAS, and 5-6-SAS) were estimated based solely on the primary hydrocarbon chain. The $\sigma_0$ values estimated for the ionic linear and branched surfactants considered here yield predicted CMC's which are in good agreement with the experimental CMC values (see Chapter 5). Note that large variations in $\sigma_0$ may result in noticeable variations in the predicted CMC's. Accordingly, the $\sigma_0$ values need to be estimated as accurately as possible, including testing the sensitivity of the predicted CMC's to the $\sigma_0$ values used.

# Chapter 5

# Prediction of Degrees of Hydration and Critical Micelle Concentrations of Branched Surfactants Using the CS–MT Modeling Approach

## 5.1 Prediction of Fractional Degrees of Hydration Using Molecular Dynamics (MD) Simulations

As discussed in Section 2.2.2, in order to quantify the hydrophobic effect in the context of the CS–MT model, one needs to input the fractional degrees of hydration, $f_i$, of every group $i$ in the surfactant molecule of interest. In this section, I present MD simulation predictions of the average fractional degree of hydration, $f_i$ (see Eq. 2.16 in Section 2.2.2) for the x-y-SAS branched surfactants (see Section 5.1.1) and for the complex ionic branched surfactants (see Section 5.1.2) considered in this thesis.

### 5.1.1 Simulated Fractional Hydration Profiles of the x-y-SAS Branched Surfactants

Figure 5-1 shows the simulated fractional hydration profiles of the first series of x-y-SAS branched surfactants ($y = 9$, see Section 3.1), and Figure 5-2 shows the simulated fractional hydration profiles of the second series of x-y-SAS branched surfactants ($x + y = 11$, see Section 3.1). In addition, for comparison, the simulated fractional hydration profiles of the two linear surfactants ($C_{10}$-SAS and $C_{12}$-SAS) are shown in Figures 5-1 and 5-2, respectively. The $f_i$ results shown in Figures 5-1 and 5-2 were generated using MD simulations, as discussed in Section 3.4.2.

For discussion purposes, 4-9-SAS and 9-9-SAS were selected as representatives of the first series of the x-y-SAS branched surfactants ($y = 9$, see Figure 5-1). These two surfactants were selected because 4-9-SAS possesses a very asymmetric surfactant tail, while 9-9-SAS possesses a perfectly symmetric surfactant tail. This tail asymmetry is a key characteristic of the first series of x-y-SAS branched surfactants ($y = 9$), where as the length of the side chain increases, the surfactant tail structure becomes more symmetric with respect to the sulfonate group. As shown in Figure 5-1, the charged sulfonate group in 4-9-SAS and 9-9-SAS has the highest average $f_i$ value of 0.98. The CH group (group 2) adjacent to the sulfonate group and the two $CH_2$ groups adjacent to that CH group (groups 3 and 7 in 4-9-SAS and groups 3 and 12 in 9-9-SAS) are quite hydrated, with an average $f_i$ value of 0.69. The rest of the hydrocarbon groups in the primary and side chains in 4-9-SAS and 9-9-SAS are much less hydrated, with an average $f_i$ value of 0.31. The length of the shorter, side chain is a key feature affecting the hydration profiles of the x-y-SAS branched surfactants ($y = 9$), due to its impact on the local structure of water. Although the primary chains in 4-9-SAS and 9-9-SAS are equal in length, the side chain is much shorter than the primary chain in 4-9-SAS, while the side chain and the primary chain have the same length in 9-9-SAS. As a result, the fractional degrees of hydration of the shorter, side chain and the longer, primary chain, separated by the sulfonate group on the hydrocarbon tail, are different for 4-9-SAS and 9-9-SAS. In the case of 4-9-SAS, the hydrocarbon groups in the side chain and in the primary chain (excluding the two $CH_2$ groups adjacent to the CH group), have different hydration states: the groups in the primary chain (groups 8 to 15, with an average $f_i = 0.29$) are less hydrated than the groups in the side chain (groups 4 to 6, with an average $f_i = 0.43$) because the side chain is much shorter

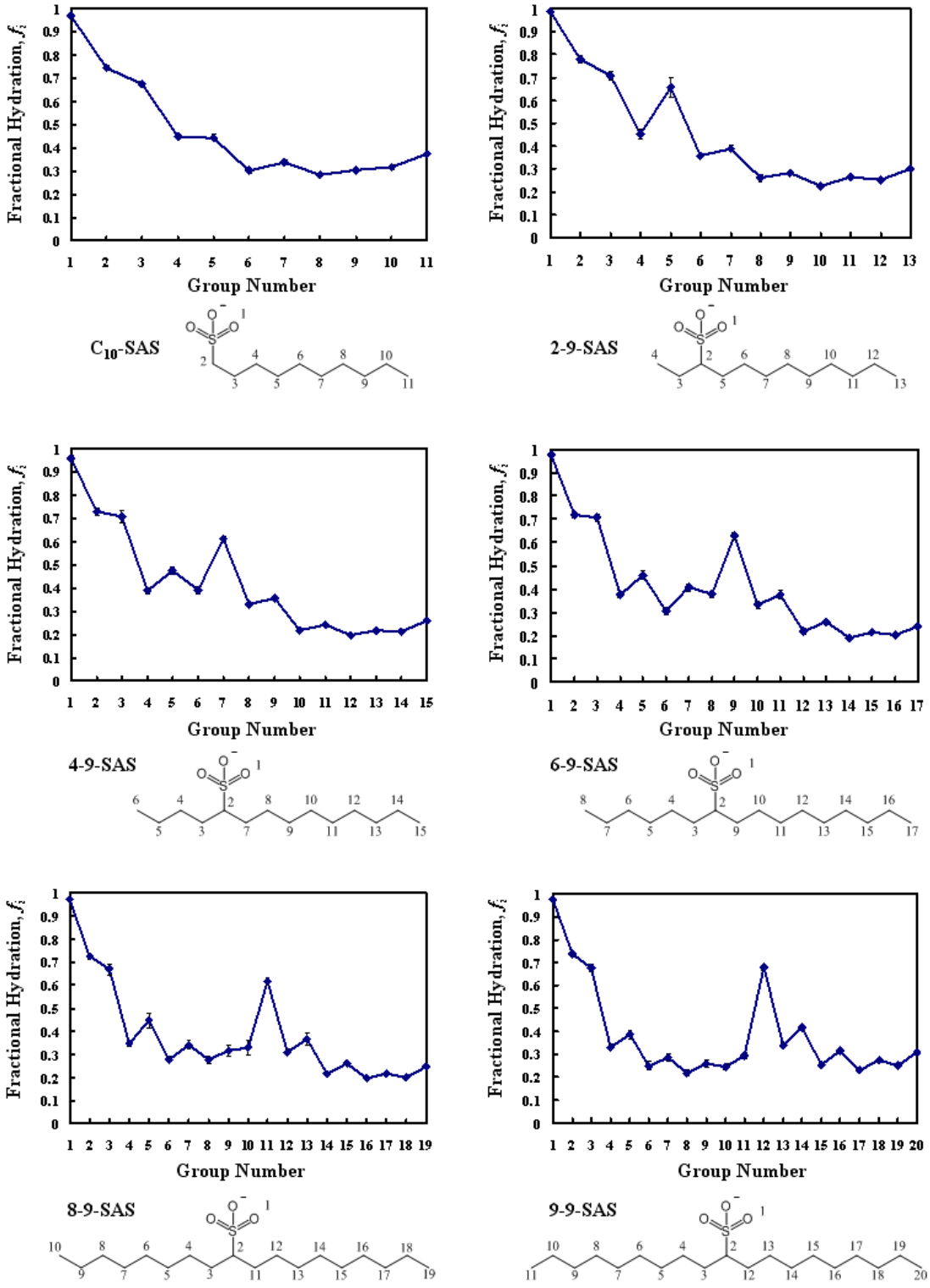


Figure 5-1: Simulated average fractional degree of hydration, $f_i$, of each group $i$ in the first series of x-y-SAS branched surfactants ($y = 9$), with the chemical structures shown below the $f_i$ plots. The error bars correspond to the standard error of the mean, as computed through block averaging of the computer simulation data (see Section 3.4.4).

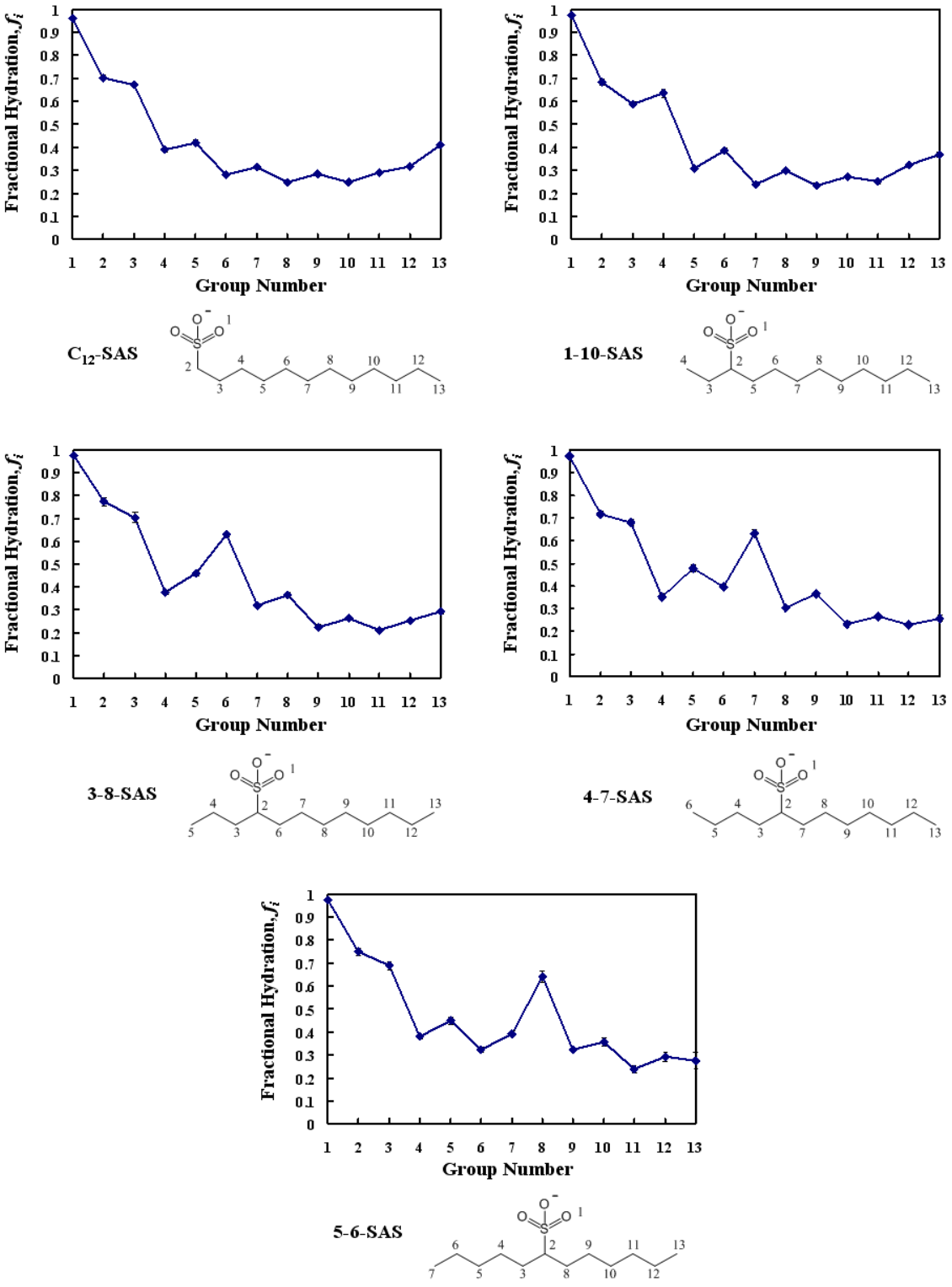


Figure 5-2: Simulated average fractional degree of hydration, $f_i$, of each group $i$ in the second series of x-y-SAS branched surfactants ($x + y = 11$), with the chemical structures below the $f_i$ plots. The error bars shown correspond to the standard error of the mean, as computed through block averaging of the computer simulation data (see Section 3.4.4).

than the primary chain. On the other hand, in the case of 9-9-SAS, nearly perfect symmetry of the hydration states of the two chains is observed due to the symmetric structure of the surfactant molecule ($x = y = 9$). Note that the average $f_i$ values of the terminal hydrocarbon groups (groups 12 to 15 in 4-9-SAS and groups 19 and 20 in 9-9-SAS) increase slightly towards the end of the surfactant tail. The observed increase reflects use of a micelle aggregation number that is too small in the MD simulations, for which the micelle core-minor radius, $l_c$, is small relative to the fully-extended length of the surfactant tail, $l_{\max}$. As a result, the terminal hydrocarbon groups tend to extend beyond the micelle COM and are able to establish additional hydrating contacts. Similar $f_i$ trends are observed for the terminal hydrocarbon groups in all the ionic linear and branched surfactants considered in this thesis (see Figures 5-1, 5-2, and 5-3).

For discussion purposes, 2-9-SAS and 5-6-SAS were selected as representatives of the second series of x-y-SAS branched surfactants ($x+y = 11$). Note that 2-9-SAS is a member of both series of x-y-SAS branched surfactants. These two surfactants were selected for discussion because 2-9-SAS possesses a very asymmetric surfactant tail, while 5-6-SAS possesses a relatively symmetric surfactant tail. This tail asymmetry is a key characteristic of the second series of x-y-SAS branched surfactants ($x+y = 11$), where as the sulfonate group moves towards the center of the hydrocarbon chain, the surfactant tail structure becomes more symmetric. Similar to the first series of x-y-SAS branched surfactants, as shown in Figure 5-1 in the case of 2-9-SAS and in Figure 5-2 in the case of 5-6-SAS, the charged sulfonate group in both surfactants has the highest average $f_i$ value of 0.98. The CH group (group 2) adjacent to the sulfonate group and the two $CH_2$ groups adjacent to that CH group (groups 3 and 5 in 2-9-SAS and groups 3 and 8 in 5-6-SAS) are also highly hydrated, with an average $f_i$ value of 0.71. The rest of the hydrocarbon groups in 2-9-SAS and 5-6-SAS are significantly less hydrated, with an average $f_i$ value of 0.32. The location of the charged sulfonate group on the linear hydrocarbon backbone is a key feature affecting the hydration profiles of the x-y-SAS branched surfactants ($x + y = 11$), due to its impact on the local structure of water. The sulfonate group in 2-9-SAS is closer to one end of the hydrocarbon chain than the sulfonate group in 5-6-SAS. As a result, the fractional degrees of hydration of the shorter, side chain and the longer, primary chain, separated by the sulfonate group on the hydrocarbon tail, are different for 2-9-SAS and 5-6-SAS. In the case of 2-9-SAS, the trends are similar to those observed in the first series, where groups 6 to 13 in the primary chain, with an average $f_i = 0.29$, are less hydrated

than group 4 in the side chain, with $f_i = 0.45$, because the charged sulfonate group is closer to one end of the hydrocarbon chain. In the case of 5-6-SAS, the trend is the same as in 2-9-SAS, but the hydration difference between the side chain and the primary chain is smaller. Specifically, the average hydration state of groups 4 to 7 in the side chain, with an average $f_i = 0.39$, is comparable to that of groups 9 to 13 in the primary chain, with an average $f_i = 0.31$, because the charged sulfonate group is located near the center of the hydrocarbon chain.

The two reference linear alkyl sulfonates ($C_{10}$-SAS and $C_{12}$-SAS) have fractional hydration profiles similar to those of other ionic linear surfactants (including SDS, CTAB, and DTAB), which were discussed recently by Stephenson et al. [60]. As shown in Figures 5-1 and 5-2, the charged sulfonate group in $C_{10}$-SAS and $C_{12}$-SAS has the highest average $f_i$ value of 0.97. In addition, the $f_i$ value of group $i$ in the linear alkyl sulfonate tail depends on the position of group $i$ relative to the sulfonate group (for additional details, see Stephenson et al. [60]).

### 5.1.2 Simulated Fractional Hydration Profiles of the Complex Ionic Branched Surfactants

Figure 5-3 shows the simulated fractional hydration profiles of the six complex ionic branched surfactants (surfactants A to F, see Section 3.1) considered in this thesis.

Similar to the $f_i$ values of the x-y-SAS branched surfactants shown in Figures 5-1 and 5-2, Figure 5-3 shows that the charged sulfonate groups of surfactants A and B have the highest average $f_i$ value of 0.95. Some of the benzene groups adjacent to the sulfonate group (groups 2 to 4) are also highly hydrated (with an average $f_i = 0.70$) in both surfactants. The rest of the benzene groups (groups 5 to 7), located farther away from the sulfonate group, are less hydrated (with an average $f_i = 0.55$) in both surfactants. In comparing surfactants A and B, the benzene sulfonate group in surfactant A is closer to one end of the linear hydrocarbon chain than the benzene sulfonate group in surfactant B. As a result, the fractional degrees of hydration of the shorter, side chain and the longer, primary chain, separated by the benzene sulfonate group on the hydrocarbon tail, are different for each surfactant. In the case of surfactant A, the trends are similar to those observed in the second x-y-SAS branched surfactant series (see Figure 5-2), where the groups in the primary chain (groups 11 to 19, with an average $f_i = 0.24$) are slightly less hydrated than the groups in the

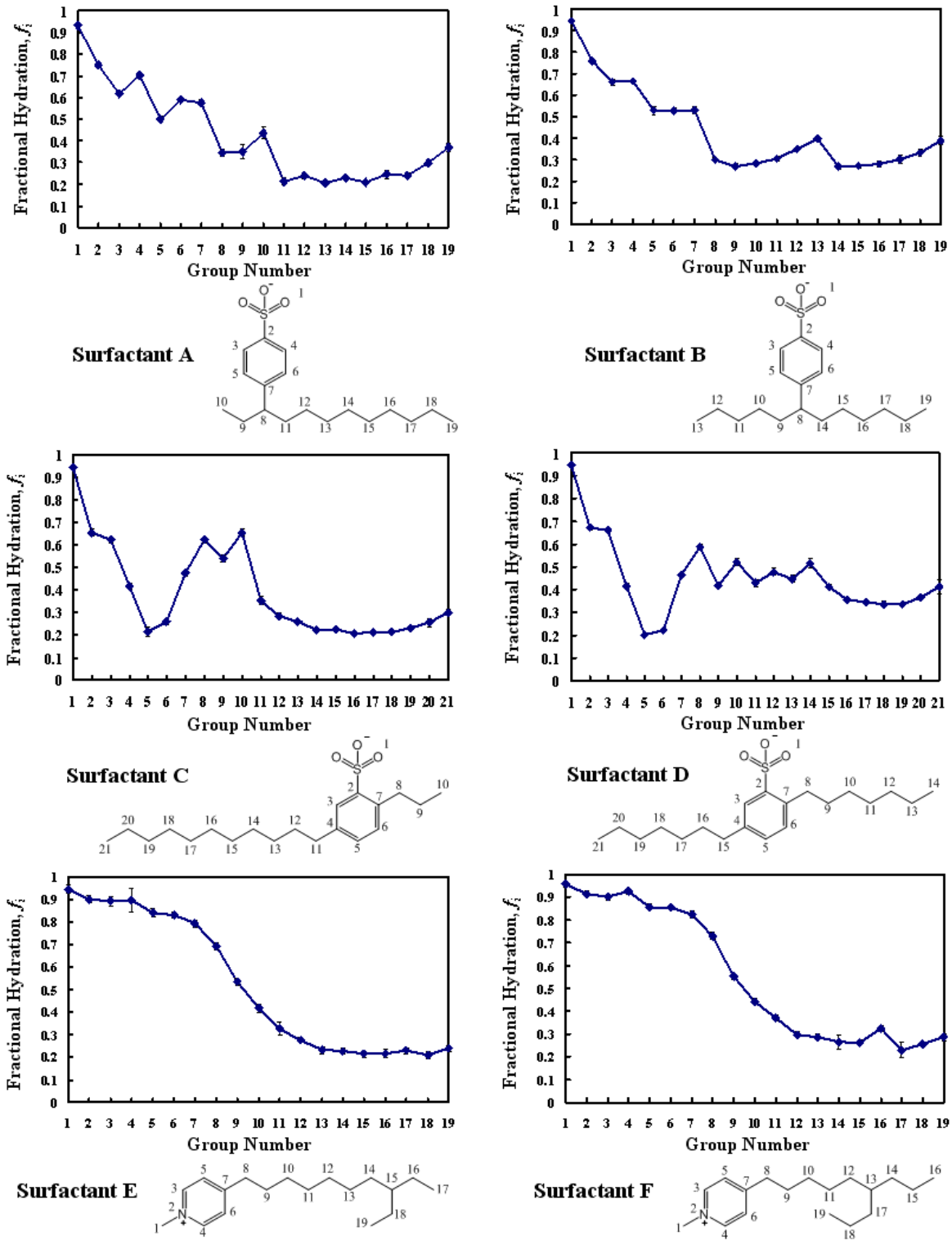


Figure 5-3: Simulated average fractional degree of hydration, $f_i$, of each group $i$ in the complex ionic branched surfactants considered in this thesis, with the chemical structures shown below the $f_i$ plots. The error bars correspond to the standard error of the mean, as computed through block averaging of the computer simulation data (see Section 3.4.4).

side chain (groups 9 and 10, with an average $f_i = 0.39$) because the charged benzene sulfonate group is closer to one end of the hydrocarbon chain. In the case of surfactant B, the trend is the same as with surfactant A, but the hydration difference between the side chain and the primary chain is very small. Specifically, the hydration state of the side chain (groups 9 to 13, with an average $f_i = 0.33$) is comparable to that of the primary chain (groups 14 to 19, with an average $f_i = 0.31$), because the benzene sulfonate group is located near the center of the hydrocarbon chain.

As shown in Figure 5-3, similar to surfactants A and B, the charged sulfonate groups in surfactants C and D have the highest fractional degrees of hydration values (with an average $f_i = 0.95$). Some of the benzene groups (groups 2, 3, and 7) adjacent to the sulfonate group are also highly hydrated (with an average $f_i = 0.61$) in both surfactants. The rest of the benzene groups (groups 4 to 6), located farther away from the sulfonate group, are much less hydrated in both surfactants (with an average $f_i = 0.28$), as a result of the shielding of hydrating atoms by the two branched tails. In surfactant C, the side chain, which is closer to the charged sulfonate group, is much shorter than the primary chain, while in surfactant D, the side and the primary chains have equal lengths. As a result, in surfactant C, the $f_i$ values of the shorter, side chain (groups 8 to 10, with an average $f_i = 0.62$) are much higher than those of the longer, primary chain (groups 11 to 21, with an average $f_i = 0.27$). Although in surfactant D the side chain and the primary chain have equal lengths, the side chain is closer to the charged sulfonate group, and as a result, the $f_i$ values of the side chain (groups 8 to 14, with an average $f_i = 0.48$) are slightly higher than those of the primary chain (groups 15 to 21, with an average $f_i = 0.38$).

As shown in Figure 5-3, the charged pyridinium groups in surfactants E and F have the highest fractional degrees of hydration values (with an average $f_i = 0.87$). Similar to the linear ionic surfactants (see Section 5.1.1), the degree of hydration of group $i$ in the branched alkyl pyridinium tail is a function of its location relative to the pyridinium head, due to the shorter side chain being very close to the end of the longer primary chain. As a result, in surfactants E and F, the difference between the $f_i$ values corresponding to the different branching structures is negligible (groups 8 to 19 in both surfactants have very similar average $f_i$ values).

## 5.2 Predicting the Micellization Behavior of the x-y-SAS Branched Surfactants

The CS–MT and the traditional MT modeling approaches were used to predict various aspects of the micellization behavior of: (a) the first series of x-y-SAS branched surfactants ($y = 9$) in aqueous solution at 45°C, and (b) the second series of x-y-SAS surfactants ($x+y = 11$) in aqueous solution at 40°C. CS–MT modeling results for the *simulated* micelles are reported in Table 5.1, and include: (i) $\hat{g}_{dehydr}$ (using Eq. 2.17 in Section 2.2.3), (ii) $\hat{g}_{hydr}$ (using Eq. 2.18 in Section 2.2.4), (iii) $\hat{g}_{int}$ (using Eq. 2.9 in Section 2.1.2), and (iv) $g_{tr,CS-MT}$ (using Eq. 2.14 in Section 2.2.1). CS–MT modeling results for $\hat{g}_{dehydr}$ and $\hat{g}_{hydr}$ were obtained using the simulated $f_i$ values reported in Section 5.1. In addition, the surfactant characteristics discussed in Chapter 4 (the simulated surfactant head/neutral/tail assignments, and the estimated values of $a_h$, $a_0$, $d_{charge}$, $l_{hg}$, and $\sigma_0$) were used to compute various free-energy contributions discussed in this section and in Section 5.3. In Table 5.1, I have also reported the traditional MT model predictions of $g_{tr}$ (using Eq. 2.7 in Section 2.1.2) to allow comparison with $g_{tr,CS-MT}$. Note that the traditional MT model predictions of $g_{tr}$ were made under the assumption that the ionic group (in this case, the sulfonate group) and the hydrocarbon group adjacent to it (specifically, the $CH_2$ group in $C_{10}$-SAS and $C_{12}$-SAS, and the CH group in the x-y-SAS branched surfactants) are part of the surfactant head, following the traditional approach to assign surfactant heads and tails (see Section 1.2.2).

In Tables 5.2 and 5.3, I have reported CS–MT and traditional MT modeling results for micelles of the *optimal* shape and size. As discussed in Section 2.1.1, at the optimal micelle shape and size, $g_{mic}$ attains its minimum value ($g^*_{mic}$). Both the CS–MT model and the traditional MT model yield identical predictions for the optimal micelle shape and size. As discussed in Section 2.2.1, this reflects the fact that $g_{tr}$, the only contribution to $g_{mic}$ that differs in the two models, does not depend on micelle shape and size.

In Table 5.2, I have reported predictions using the CS–MT model and the traditional MT model of: (i) the micelle shape (that is, the shape factor, $S$; see Section 2.1.1), (ii) the number-average micelle aggregation number, $n$ (see Section 2.1.1), and (iii) the various free-energy contributions to $g_{mic}$, including $g_{int}$, $g_{pack}$, $g_{st}$, $g_{elec}$, and $g_{ent}$ (see Section 2.1.2). Note that, as indicated above, both the CS–MT model and the traditional MT model yield identical predictions for the optimal

| Surfactant Type | $\hat{g}_{dehydr}\ [k_BT]$ | $\hat{g}_{hydr}\ [k_BT]$ | $\hat{g}_{int}\ [k_BT]$ | $g_{tr,CS-MT}\ [k_BT]$ | $g_{tr}\ [k_BT]$ |
|---|---|---|---|---|---|
| **$C_{10}$-SAS** | $-9.59 \pm 0.05$ | $1.02 \pm 0.01$ | $5.82$ | $-14.56 \pm 0.05$ | $-15.08$ |
| **2-9-SAS** | $-12.68 \pm 0.11$ | $1.40 \pm 0.02$ | $4.94$ | $-16.32 \pm 0.11$ | $-18.05$ |
| **4-9-SAS** | $-15.03 \pm 0.10$ | $1.86 \pm 0.02$ | $5.94$ | $-19.11 \pm 0.10$ | $-20.78$ |
| **6-9-SAS** | $-17.02 \pm 0.11$ | $2.38 \pm 0.04$ | $6.84$ | $-21.47 \pm 0.12$ | $-23.63$ |
| **8-9-SAS** | $-19.45 \pm 0.16$ | $3.04 \pm 0.06$ | $7.80$ | $-24.21 \pm 0.17$ | $-26.49$ |
| **9-9-SAS** | $-20.26 \pm 0.12$ | $3.50 \pm 0.05$ | $8.27$ | $-25.03 \pm 0.13$ | $-27.92$ |
| **$C_{12}$-SAS** | $-12.02 \pm 0.05$ | $1.19 \pm 0.01$ | $6.57$ | $-17.41 \pm 0.05$ | $-18.05$ |
| **1-10-SAS** | $-12.68 \pm 0.07$ | $0.95 \pm 0.01$ | $5.77$ | $-17.50 \pm 0.07$ | $-18.05$ |
| **3-8-SAS** | $-12.78 \pm 0.07$ | $1.58 \pm 0.02$ | $5.09$ | $-16.29 \pm 0.07$ | $-18.05$ |
| **4-7-SAS** | $-12.88 \pm 0.08$ | $1.60 \pm 0.02$ | $5.34$ | $-16.62 \pm 0.09$ | $-18.05$ |
| **5-6-SAS** | $-12.61 \pm 0.16$ | $1.88 \pm 0.05$ | $5.51$ | $-16.24 \pm 0.16$ | $-18.05$ |

Table 5.1: CS-MT and traditional MT modeling results for the simulated ionic x-y-SAS branched surfactant micelles considered in this thesis. CS-MT model predictions of $\hat{g}_{dehydr}$, $\hat{g}_{hydr}$, $\hat{g}_{int}$, and $g_{tr,CS-MT}$ were made as described in Section 2.2. The uncertainties reported for the CS-MT model predictions correspond to the standard error of the mean in predicting $g_{tr,CS-MT}$, as computed through block averaging of the computer simulation data (see Section 3.4.4). Traditional MT modeling predictions of $g_{tr}$ are presented to allow comparison with $g_{tr,CS-MT}$.

| Surfactant Type | Shape | $n$ | $g_{int}\ [k_BT]$ | $g_{pack}\ [k_BT]$ | $g_{st}\ [k_BT]$ | $g_{elec}\ [k_BT]$ | $g_{ent}\ [k_BT]$ |
|---|---|---|---|---|---|---|---|
| **$C_{10}$-SAS** | Sph | 27 | 3.82 | 2.42 | 0.85 | 2.47 | $-0.82$ |
| **2-9-SAS** | Cyl | 14 | 2.44 | 3.18 | 0.99 | 3.71 | $-1.02$ |
| **4-9-SAS** | Sph | 13 | 5.00 | 3.76 | 0.37 | 2.53 | $-0.53$ |
| **6-9-SAS** | Sph | 13 | 6.20 | 3.99 | 0.28 | 2.46 | $-0.38$ |
| **8-9-SAS** | Sph | 13 | 7.50 | 4.25 | 0.22 | 2.37 | $-0.23$ |
| **9-9-SAS** | Sph | 13 | 8.09 | 4.21 | 0.21 | 2.26 | $-0.18$ |
| **$C_{12}$-SAS** | Sph | 40 | 4.22 | 2.47 | 0.80 | 3.46 | $-0.83$ |
| **1-10-SAS** | Sph | 13 | 4.57 | 2.90 | 0.65 | 2.89 | $-0.73$ |
| **3-8-SAS** | Cyl | 12 | 3.05 | 3.57 | 0.85 | 3.25 | $-0.98$ |
| **4-7-SAS** | Cyl | 8 | 4.05 | 3.56 | 0.66 | 2.89 | $-0.91$ |
| **5-6-SAS** | Cyl | 6 | 4.65 | 3.72 | 0.56 | 2.34 | $-0.87$ |

Table 5.2: CS-MT modeling results for the optimal ionic x-y-SAS branched surfactant micelles considered in this thesis. Note that the traditional MT modeling results are almost identical in this case (see the text for details).

| | $g^*_{mic}$ $[k_BT]$ (CMC [mM]) | | |
|---|---|---|---|
| **Surfactant Type** | CS–MT Model | Traditional MT Model | Experimental |
| **$C_{10}$-SAS** | $-6.83 \pm 0.05$ $(60.05 \pm 3.08)$ | $-7.35$ $(35.70)$ | $-7.24$ $(39.80)$ |
| **2-9-SAS** | $-7.92 \pm 0.11$ $(20.19 \pm 2.35)$ | $-9.65$ $(3.58)$ | $-8.00$ $(18.60)$ |
| **4-9-SAS** | $-8.97 \pm 0.10$ $(7.06 \pm 0.75)$ | $-10.64$ $(1.33)$ | $-9.01$ $(6.76)$ |
| **6-9-SAS** | $-9.92 \pm 0.12$ $(2.73 \pm 0.35)$ | $-12.08$ $(0.32)$ | $-10.42$ $(1.66)$ |
| **8-9-SAS** | $-11.11 \pm 0.17$ $(0.83 \pm 0.16)$ | $-13.39$ $(0.09)$ | $-12.35$ $(0.24)$ |
| **9-9-SAS** | $-11.44 \pm 0.13$ $(0.60 \pm 0.11)$ | $-14.33$ $(0.03)$ | $-13.34$ $(0.09)$ |
| **$C_{12}$-SAS** | $8.29 \pm 0.05$ $(13.95 \pm 0.71)$ | $-8.93$ $(7.35)$ | $-8.58$ $(10.40)$ |
| **1-10-SAS** | $-8.22 \pm 0.07$ $(14.96 \pm 1.08)$ | $-8.77$ $(8.63)$ | $-8.22$ $(14.90)$ |
| **3-8-SAS** | $-7.56 \pm 0.07$ $(28.94 \pm 2.10)$ | $-9.32$ $(4.99)$ | $-7.78$ $(23.20)$ |
| **4-7-SAS** | $-7.39 \pm 0.09$ $(34.30 \pm 3.23)$ | $-8.82$ $(8.21)$ | $-7.58$ $(28.30)$ |
| **5-6-SAS** | $-6.86 \pm 0.16$ $(58.27 \pm 10.11)$ | $-8.67$ $(9.54)$ | $-7.34$ $(36.10)$ |

Table 5.3: CS-MT and traditional MT modeling results for the optimal ionic x-y-SAS branched surfactant micelles considered in this thesis. The CS-MT and the traditional MT model predictions of the optimal $g_{mic}$, denoted as $g^*_{mic}$, were obtained using the values of $g_{tr,CS-MT}$ and $g_{tr}$ reported in Table 5.1 as inputs to Eqs. 2.5 and 2.15, respectively. The CS-MT and the traditional MT model predicted CMC's were computed using Eq. 2.4, corresponding to the predicted $g^*_{mic}$ values. The experimental $g^*_{mic}$ values were inferred from the experimental CMC's using Eq. 2.4. The uncertainties reported for the CS-MT model predictions correspond to the standard error of the mean in predicting $g_{tr,CS-MT}$, as computed through block averaging of the computer simulation data (see Section 3.4.4).

micelle shape and size, and as a result, the free-energy contributions listed in (iii) are also identical.

In Table 5.3, I have reported: (i) the CS–MT model predictions of $g^*_{mic}$ and the CMC (using Eq. 2.15 in Section 2.2.1 and Eq. 2.4 in Section 2.1.1, respectively), (ii) the traditional MT predictions of $g^*_{mic}$ and the CMC (using Eq. 2.5 in Section 2.1.2 and Eq. 2.4 in Section 2.1.1, respectively), and (iii) the experimental CMC's and $g^*_{mic}$ values (inferred from the experimental CMC's) [127, 167].

For the x-y-SAS branched surfactants considered, as well as for the $C_{10}$-SAS and $C_{12}$-SAS linear surfactants, the values of $g_{int}$ computed for the optimal micelles (see Table 5.2) are slightly lower than the values of $\hat{g}_{int}$ computed for the simulated micelles (see Table 5.1). This reflects: (i) the small difference between the simulated (see Table 3.2 in Section 3.3.2) and the optimal micelle aggregation numbers (for spherical micelles consisting of the $C_{10}$-SAS and $C_{12}$-SAS linear surfactants, as well as for spherical micelles consisting of the 4-9-SAS, 6-9-SAS, 8-9-SAS, 9-9-SAS, and 1-10-SAS branched surfactants), and (ii) the difference between the simulated (all spherical) and the optimal micelle shapes (for cylindrical micelles consisting of the 2-9-SAS, 3-8-SAS, 4-7-SAS, and 5-6-SAS branched surfactants). The free-energy contributions, $g_{int}$, $g_{pack}$, $g_{st}$,

$g_{elec}$, and $g_{ent}$ (see Table 5.2), although all much smaller in magnitude than $g_{tr,CS-MT}$ and $g_{tr}$ (see Table 5.1), all contribute significantly to $g_{mic}$.

For the first series of x-y-SAS surfactants ($y = 9$), both the predicted and the experimental CMC's decrease as the length of the shorter, side chain, $x$, increases (see Figure 5-4 and Table 5.3). This trend is mainly due to the increase in the magnitude of $g_{tr,CS-MT}$ (or of $g_{tr}$ in the traditional MT model) as the total hydrocarbon chain length increases (see Table 5.1). For comparison, the $C_{10}$-SAS linear surfactant which does not possess a side chain, has a higher CMC than those of all the members of the first series of x-y-SAS surfactants ($y = 9$, see Figure 5-4 and Table 5.3). Figure 5-4 also shows that the CMC's predicted using the CS–MT model are higher than the experimental CMC's, with the overprediction increasing as the length of the side chain becomes comparable to that of the primary chain. Nevertheless, as Figure 5-4 indicates, the predictions are at worst a factor of 7 from the experimental CMC's, which indicates good predictive ability in view of the exponential dependence of the predicted CMC on $g^*_{mic}$ (see Eq. 2.4 in Section 2.1.1). The observed overprediction may reflect inaccuracies in the surfactant property inputs that were used in the CS–MT model, including the *trans/gauche* potential energy difference used in the packing model [97–99], the interfacial tension, $\sigma_0$, estimated based on the length of the primary chain (see Section 4.6), and the interfacial area shielded by the surfactant head, $a_0$ (see Section 4.2). In addition, another possible reason for the observed overprediction may be that the micelle aggregation number is quite low (as small as 13, see Table 5.2). In that case, some of the approximations made in the MT theory, including smearing discrete charges on the micelle surface and packing of the surfactant tails using a mean-field approach, may cease to be valid at these low aggregation numbers.

Figure 5-4 also shows that the CMC's predicted using the traditional MT model are underpredicted (at worst by a factor of 6). This reflects considering most of the neutral groups to be part of the surfactant tail (leading to a larger magnitude of $g_{tr}$, and hence, to a more negative value of $g^*_{mic}$). In view of this underprediction, fewer number of neutral groups should be considered to be part of the surfactant tail when implementing the traditional MT model in order to obtain good CMC predictions (however, additional studies are needed to substantiate this claim, see Section 6.2.4). Nevertheless, the CMC's of the $C_{10}$-SAS linear surfactant, as well as the 8-9-SAS and 9-9-SAS branched surfactants, predicted using the traditional MT model, are in very good agreement with

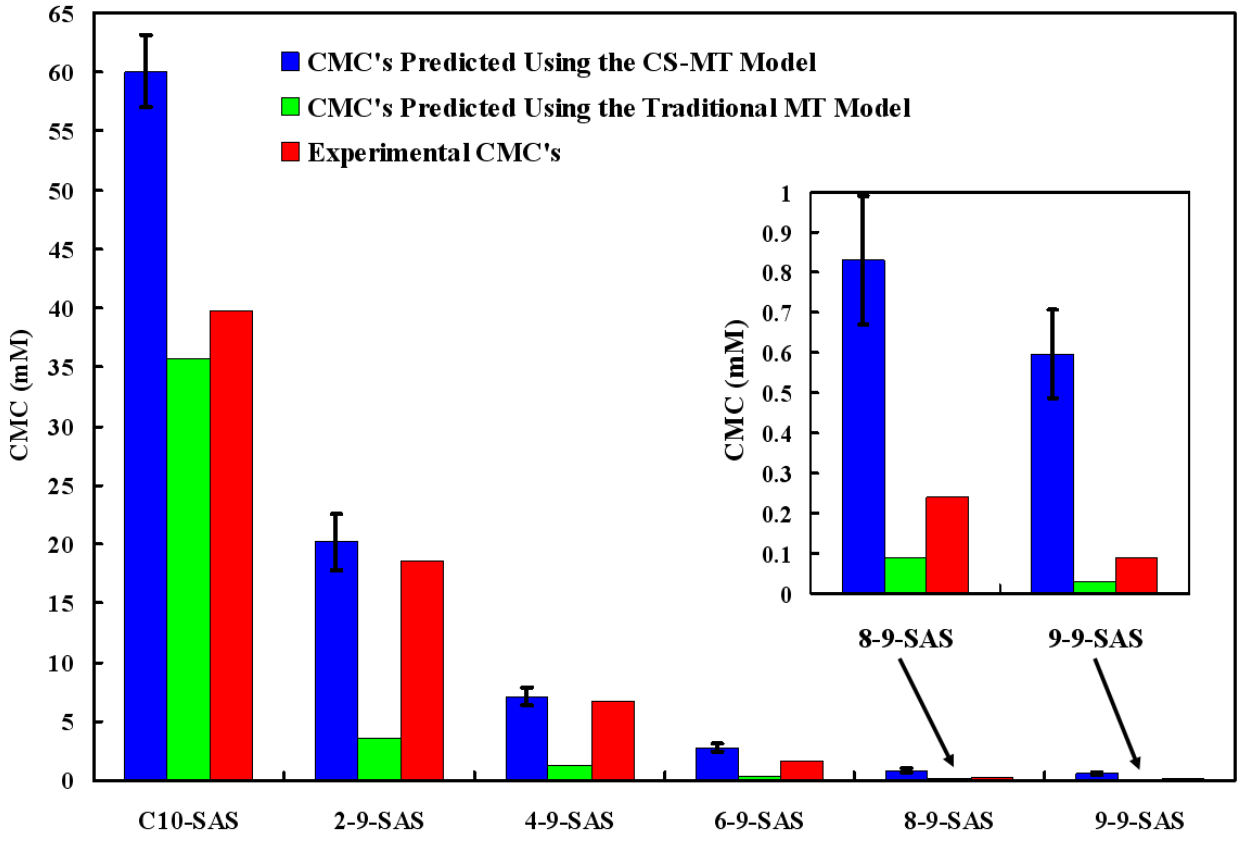


Figure 5-4: CMC's predicted using the CS–MT model (blue) and the traditional MT model (green), as well as the experimental CMC's (red), for the first series of x-y-SAS branched surfactants ($y = 9$). The CMC of the $C_{10}$-SAS linear surfactant is also shown for comparison. The inset CMC plot for 8-9-SAS and 9-9-SAS is shown for clarity. Each error bar corresponds to the standard error of the mean in predicting $g_{tr,CS-MT}$ using the CS–MT model, as reported in Table 5.3.

the experimental CMC's. This reflects the ability of the traditional MT model to predict CMC's of linear surfactants as well as of branched surfactants possessing two very symmetric and long chains (such that the branched surfactant behaves like an effective linear surfactant).

Overall, given the exponential dependence of the CMC on $g^*_{mic}$ (see Eq. 2.4 in Section 2.1.1), the CMC's predicted using both the CS–MT model and the traditional MT model are in good reasonable agreement with the experimental CMC's. Furthermore, for some members of the first series of x-y-SAS surfactants ($y = 9$) possessing short side chains ($x = 2$ to 6), the CMC's predicted using the CS–MT model are closer to the experimental CMC's than those predicted using the traditional MT model (see Figure 5-4).

The optimal micelle shapes and sizes ($n$) predicted for the first series of x-y-SAS branched surfactants ($y = 9$) are reported in Table 5.2. Unfortunately, no experimental information on these two micelle properties is available for comparison. Note that the $g^*_{mic}$ values predicted using the CS–MT model for spherical micelles and for cylindrical micelles are very similar (within $0.5$ kT, results not reported here). Therefore, the optimal micelle shapes predicted for the first series of x-y-SAS branched surfactants ($y = 9$) may not be as accurate. As reported in Table 5.2, regardless of the predicted micelle shape, the optimal micelle aggregation numbers of all the members of the first series of x-y-SAS branched surfactants ($y = 9$) are very similar (14 or 13). This is due to the interplay between the increase in $l_c$ and the increase in the surfactant tail volume as the side chain length, $x$, increases.

For the second series of x-y-SAS branched surfactants ($x + y = 11$, including the $C_{12}$-SAS linear surfactant for comparison), both the predicted (using the CS–MT model) and the experimental CMC's increase as the sulfonate group moves from one end of the hydrocarbon chain towards the center of the hydrocarbon chain (see Figure 5-5 and Table 5.3). Since the sum of the lengths of the side and the primary chains is the same for this second series of x-y-SAS branched surfactants ($x + y = 11$), their $g_{tr,CS-MT}$ values are very similar (see Table 5.1), except for 1-10-SAS, which behaves more like a linear surfactant due to its extremely short side chain (with a $g_{tr,CS-MT}$ value very similar to that of the $C_{12}$-SAS linear surfactant). As a result, the observed increase in the CMC is mainly due to the interplay between the increase in $g_{int}$ and the decreases in both $g_{st}$ and $g_{elec}$ (the surface area per surfactant molecule, $a$, increases as the micelle core-minor radius, $l_c$, decreases, see Section 2.1.1). As shown in Figure 5-5, for the second series of x-y-SAS branched surfactants ($x + y = 11$), the CMC's predicted using the CS–MT model are higher than the experimental CMC's, with the overprediction increasing as the sulfonate group moves closer towards the center of the hydrocarbon chain. Nevertheless, the predicted CMC's are very close to the experimental CMC's (at worst, a factor of 1.6 difference). As discussed earlier for the first series of x-y-SAS branched surfactants ($y = 9$), this overprediction may reflect the same inaccuracies in the surfactant property inputs used in the CS–MT model. In addition, another reason for the observed difference may be that the micelle aggregation number decreases ($n = 6$ for 5-6-SAS) as the sulfonate group moves towards the center of the linear hydrocarbon chain, and in that case, the MT theory may not be accurate for such low aggregation numbers.

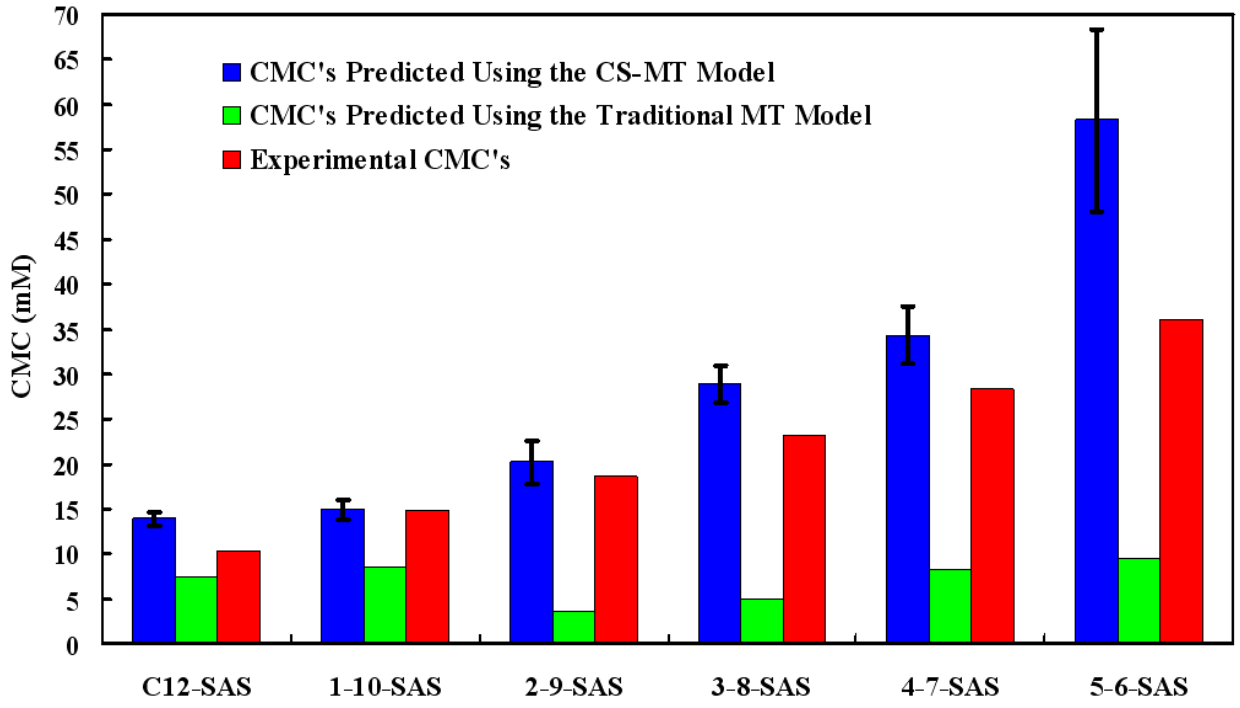


Figure 5-5: CMC's predicted using the CS–MT model (blue) and the traditional MT model (green), as well as the experimental CMC's (red) for the second series of x-y-SAS branched surfactants ($x + y = 11$). The CMC of the $C_{12}$-SAS linear surfactant is also shown for comparison. Each error bar corresponds to the standard error of the mean in predicting $g_{tr,CS-MT}$ using the CS–MT model, as reported in Table 5.3.

In addition, as shown in Figure 5-5, the CMC's predicted using the traditional MT model are lower than the experimental CMC's (at worst by a factor of 5) due to the same reasons discussed earlier for the first series of x-y-SAS branched surfactants ($y = 9$). Nevertheless, the CMC of the $C_{12}$-SAS linear surfactant predicted using the traditional MT model is in very good agreement with the experimental CMC value (see Figure 5-5). Given the exponential dependence of the CMC on $g^*_{mic}$ (see Eq. 2.4 in Section 2.1.1), the CMC's predicted by both the CS–MT model and the traditional MT model are in very good agreement with the experimental CMC's. Overall, for the second series of x-y-SAS branched surfactants ($x+y = 11$), the CS–MT model yields better CMC predictions than the traditional MT model.

The optimal micelle shapes and sizes ($n$) predicted for the second series of x-y-SAS branched surfactants ($x + y = 11$) are also reported in Table 5.2. Again, no experimental information is

available for comparison. Note that there is a transition from a spherical micelle shape (for $C_{12}$-SAS and 1-10-SAS) to a cylindrical micelle shape (for 2-9-SAS, 3-8-SAS, 4-7-SAS, and 5-6-SAS) as the sulfonate group moves towards the center of the hydrocarbon chain. This micelle shape transition is driven by the tendency to decrease the surface area per surfactant molecule, $a$, such that the increase in $g_{int}$ does not exceed the decreases in both $g_{st}$ and $g_{elec}$. As shown in Table 5.2, the predicted optimal micelle aggregation number decreases as the sulfonate group moves towards the center of the hydrocarbon chain, due to the decrease in the micelle core-minor radius, $l_c$, while the surfactant tail volume remains constant.

The predicted optimal micelle shapes and sizes ($n$) for the $C_{10}$-SAS and $C_{12}$-SAS linear surfactants (see Table 5.2) agree well with the experimental results (both surfactants form spherical micelles, with $n \simeq 40$ in the case of $C_{10}$-SAS and $n \simeq 54$ in the case of $C_{12}$-SAS [167]). The reason that $n\,(C_{12}\text{-SAS}) > n\,(C_{10}\text{-SAS})$ (see Table 5.2) is that, for a spherical micelle, $n = \frac{4}{3}\pi l_c^3/V$, where the surfactant tail volume, $V$, is proportional to $l_c$, which leads to $n$ being proportional to $l_c^2$, with $l_c\,(C_{12}\text{-SAS}) > l_c\,(C_{10}\text{-SAS})$.

## 5.3 Predicting the Micellization Behavior of the Complex Ionic Branched Surfactants

The CS–MT and the traditional MT modeling approaches were used to predict various aspects of the micellization behavior of the complex ionic branched surfactants A to F in aqueous solution at 25°C. CS–MT and traditional MT modeling results for the *simulated* micelle are reported in Table 5.4, with each free-energy contribution computed as discussed in Section 5.2. The traditional MT model predictions of $g_{tr}$ were made under the assumption that the ionic group (in this case, the sulfonate group and the pyridinium group) and the hydrocarbon group adjacent to it (in this case, the benzene carbon group in surfactants A to D, and the $CH_2$ group in surfactants E and F) are part of the surfactant head, following the traditional method of assigning surfactant heads and tails (see Section 1.2.2). CS–MT and traditional MT modeling results for the *optimal* micelle are reported in Tables 5.5 and 5.6, where the various free-energy contributions to $g_{mic}$, the predicted $g_{mic}^*$ values and CMC's, and the experimental CMC's and $g_{mic}^*$ values (inferred from the experimental CMC's)

| Surfactant Type | $\hat{g}_{dehydr}\ [k_BT]$ | $\hat{g}_{hydr}\ [k_BT]$ | $\hat{g}_{int}\ [k_BT]$ | $g_{tr,CS-MT}\ [k_BT]$ | $g_{tr}\ [k_BT]$ |
|---|---|---|---|---|---|
| **Surfactant A** | $-17.56 \pm 0.14$ | $4.22 \pm 0.05$ | 9.01 | $-22.34 \pm 0.15$ | $-27.42$ |
| **Surfactant B** | $-17.08 \pm 0.11$ | $5.40 \pm 0.05$ | 9.58 | $-21.26 \pm 0.12$ | $-27.42$ |
| **Surfactant C** | $-20.55 \pm 0.10$ | $3.95 \pm 0.03$ | 7.03 | $-23.63 \pm 0.10$ | $-31.46$ |
| **Surfactant D** | $-18.56 \pm 0.15$ | $5.60 \pm 0.06$ | 11.14 | $-24.49 \pm 0.16$ | $-31.46$ |
| **Surfactant E** | $-15.69 \pm 0.14$ | $2.37 \pm 0.04$ | 6.73 | $-20.05 \pm 0.15$ | $-19.43$ |
| **Surfactant F** | $-14.54 \pm 0.12$ | $2.49 \pm 0.04$ | 8.07 | $-20.12 \pm 0.13$ | $-19.43$ |

Table 5.4: CS-MT and traditional MT modeling results for the simulated complex ionic branched surfactant (A to F) micelles considered in this thesis. CS-MT model predictions of $\hat{g}_{dehydr}$, $\hat{g}_{hydr}$, $\hat{g}_{int}$, and $g_{tr,CS-MT}$ were made as described in Section 2.2. The uncertainties reported for the CS-MT model predictions correspond to the standard error of the mean in predicting $g_{tr,CS-MT}$, as computed through block averaging of the computer simulation data (see Section 3.4.4). Traditional MT modeling predictions of $g_{tr}$ are presented to allow comparison with $g_{tr,CS-MT}$.

| Surfactant Type | Shape | $n$ | $g_{int}\ [k_BT]$ | $g_{pack}\ [k_BT]$ | $g_{st}\ [k_BT]$ | $g_{elec}\ [k_BT]$ | $g_{ent}\ [k_BT]$ |
|---|---|---|---|---|---|---|---|
| **Surfactant A** | Sph | 39 | 6.65 | 2.34 | 0.51 | 4.08 | $-0.72$ |
| **Surfactant B** | Cyl | 43 | 6.07 | 2.59 | 0.83 | 4.35 | $-1.00$ |
| **Surfactant C** | Sph | 32 | 5.43 | 2.84 | 0.62 | 4.98 | $-0.75$ |
| **Surfactant D** | Cyl | 12 | 7.76 | 4.11 | 0.56 | 4.32 | $-0.89$ |
| **Surfactant E** | Cyl | 20 | 4.16 | 2.46 | 1.13 | 4.95 | $-1.11$ |
| **Surfactant F** | Cyl | 15 | 4.86 | 2.65 | 0.94 | 4.59 | $-1.08$ |

Table 5.5: CS-MT modeling results for the optimal complex ionic branched surfactant (A to F) micelles considered in this thesis. Note that the traditional MT modeling results are almost identical in this case (see the text for details).

were obtained as discussed in Section 5.2.

Similar to the case for the x-y-SAS branched surfactants, the values of $g_{int}$ computed for the optimal micelles (see Tables 5.5) are slightly lower than the values of $\hat{g}_{int}$ computed for the simulated micelles (see Table 5.4). This reflects: (i) the small difference between the simulated (see Table 3.2 in Section 3.3.2) and the optimal micelle aggregation numbers (for spherical micelles consisting of surfactants A and C), and (ii) the difference between the simulated (all spherical) and the optimal micelle shapes (for cylindrical micelles containing surfactants B, D, E, and F). Similar to the x-y-SAS branched surfactants discussed in Section 5.2, the free-energy contributions, $g_{int}$, $g_{pack}$, $g_{st}$, $g_{elec}$, and $g_{ent}$ (see Table 5.5), although all much smaller in magnitude than $g_{tr,CS-MT}$ and $g_{tr}$ (see Table 5.4), all contribute significantly to $g_{mic}$.

For surfactants A and B, the total hydrocarbon chain lengths are fixed (similar to the second series of x-y-SAS branched surfactants ($x + y = 11$)), which implies that the values of $g_{tr,CS-MT}$

| | $g^*_{mic}$ $[k_BT]$ (CMC [mM]) | | |
|---|---|---|---|
| **Surfactant Type** | CS–MT Model | Traditional MT Model | Experimental |
| **Surfactant A** | $-10.49 \pm 0.15$ $(1.55 \pm 0.25)$ | $-15.57$ $(0.01)$ | $-10.42$ $(1.66)$ |
| **Surfactant B** | $-9.43 \pm 0.12$ $(4.46 \pm 0.57)$ | $-15.59$ $(0.01)$ | $-9.68$ $(3.47)$ |
| **Surfactant C** | $-11.52 \pm 0.10$ $(0.55 \pm 0.06)$ | $-19.35$ $(0.0002)$ | $-11.25$ $(0.72)$ |
| **Surfactant D** | $-9.64 \pm 0.16$ $(3.62 \pm 0.62)$ | $-16.61$ $(0.003)$ | $-10.22$ $(2.02)$ |
| **Surfactant E** | $-9.46 \pm 0.15$ $(4.33 \pm 0.70)$ | $-8.84$ $(8.05)$ | $-9.60$ $(3.76)$ |
| **Surfactant F** | $-9.17 \pm 0.13$ $(5.78 \pm 0.81)$ | $-8.48$ $(11.53)$ | $-9.39$ $(4.65)$ |

Table 5.6: CS-MT and traditional MT modeling results for the optimal complex ionic branched surfactant (A to F) micelles considered in this thesis. The CS-MT and the traditional MT model predictions of the optimal $g_{mic}$, denoted as $g^*_{mic}$, were obtained using the values of $g_{tr,CS-MT}$ and $g_{tr}$ reported in Table 5.4 as inputs to Eqs. 2.5 and 2.15, respectively. The CS-MT and the traditional MT model predicted CMC's were computed using Eq. 2.4, corresponding to the predicted $g^*_{mic}$ values. The experimental $g^*_{mic}$ values were inferred from the experimental CMC's using Eq. 2.4. The uncertainties reported for the CS-MT model predictions correspond to the standard error of the mean in predicting $g_{tr,CS-MT}$, as computed through block averaging of the computer simulation data (see Section 3.4.4).

for these two surfactants are similar (see Table 5.4). As a result, the reason for the higher CMC of surfactant B, relative to surfactant A (see Table 5.6), is similar to that for the second series of x-y-SAS branched surfactants ($x + y = 11$), that is, the interplay between the increase in $g_{int}$ and the decreases in both $g_{st}$ and $g_{elec}$ (see Section 5.2). As shown in Figure 5-6 and Table 5.6, the CMC is slightly underpredicted for surfactant A, while it is overpredicted for surfactant B (at worst by a factor of 1.3) using the CS–MT model. As discussed above in the case of the x-y-SAS branched surfactants (see Section 5.2), this difference may reflect inaccuracies in the surfactant property inputs used in the CS–MT model. As shown in Figure 5-6 and Table 5.6, the CMC's of surfactants A and B are both greatly underpredicted using the traditional MT model (at worst by a factor of 45) due to the same reasons discussed above in the case of the x-y-SAS branched surfactants (see Section 5.2), that is, most of the neutral groups were considered to be part of the surfactant tail, resulting in an overprediction in the magnitude of $g_{tr}$ and associated more negative value of $g^*_{mic}$. With the above in mind, for surfactants A and B, the CS–MT model is significantly better than the traditional MT model in predicting CMC's, and it also more accurately accounts for the chemical and structural complexities of surfactants A and B.

As the benzene sulfonate group moves towards the center of the hydrocarbon chain, the predicted optimal micelle shape changes from spherical (surfactant A) to cylindrical (surfactant B),

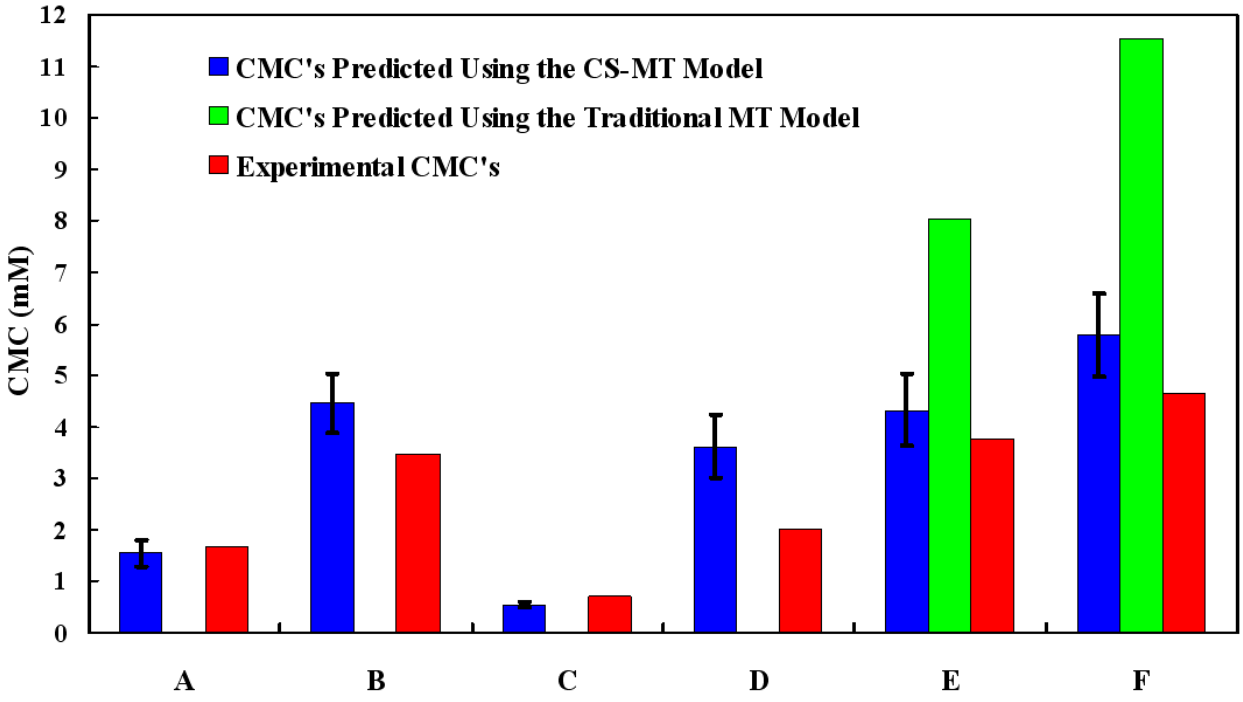


Figure 5-6: CMC's predicted using the CS–MT model (blue) and the traditional MT model (green), as well as the experimental CMC's (red), for the complex ionic branched surfactants A to F. Each error bar corresponds to the standard error of the mean in predicting $g_{tr,CS-MT}$ using the CS–MT model, as reported in Table 5.6. Note that the CMC's predicted using the traditional MT model for surfactants A to D are nearly zero mM (see Table 5.6), and are therefore not visible on the scale used to report the CMC's.

reflecting the tendency to decrease the surface area per surfactant molecule, $a$, such that the increase in $g_{int}$ does not exceed the decreases in both $g_{st}$ and $g_{elec}$, similar to the case of the second series of x-y-SAS branched surfactants ($x + y = 11$; see Section 5.2). The predicted micelle sizes ($n$) of surfactants A and B (see Table 5.5) agree reasonably well with the experimental values ($n \simeq 57$ for surfactant A and $n \simeq 20$ for surfactant B) [167]. As shown in Table 5.5, the predicted optimal aggregation numbers are similar for surfactants A ($n = 39$) and B ($n = 43$) due to the interplay between the decrease in $l_c$ and the elongation of the surfactant micelle as the benzene sulfonate group moves towards the center of the hydrocarbon chain. Contrary to the higher experimental $n$ value of surfactant A, the predicted similar $n$ values of surfactants A and B are probably related to the inability of the current MT theory to accurately model a micelle whose shape deviates slightly from that of a perfect sphere.

For surfactants C and D, although the total hydrocarbon chain lengths are the same, the shorter, side chain in surfactant D tends to swing out of the micelle core (see Section 4.1) and contributes much less to $g_{tr,CS-MT}$. As a result, the CMC of surfactant D is higher than that of surfactant C. In addition, the interplay between the increase in $g_{int}$ and the decreases in $g_{st}$ and $g_{elec}$ plays an important role here, similar to the reason for the CMC differences observed in the second series of x-y-SAS branched surfactants ($x+y=11$; see Section 5.2). As shown in Figure 5-6 and Table 5.6, the CMC is slightly underpredicted for surfactant C and overpredicted for surfactant D (at worst by a factor of 1.8) using the CS–MT model. Similar to the CMC predictions made for surfactants A and B, this probably reflects inaccuracies in the surfactant property inputs used in the CS–MT model.

As shown in Figure 5-6 and Table 5.6, similar to the CMC predictions made for surfactants A and B, the predicted CMC's of surfactants C and D are greatly underpredicted using the traditional MT model (at least by a factor of 670), due to the fact that most of the neutral groups were considered to be part of the surfactant tail, resulting in an overprediction in the magnitude of $g_{tr}$ and associated more negative value of $g^*_{mic}$. Again, as in the case of surfactants A and B, the CS–MT model is significantly better at predicting the CMC's of surfactants C and D than the traditional MT model, and is also able to more accurately account for the chemical and structural complexities of surfactants C and D.

Similar to surfactants A and B, surfactant C forms spherical micelles, while surfactant D forms cylindrical micelles (see Table 5.5), driven by the tendency to decrease the surface area per surfactant molecule, $a$, so that the increase in $g_{int}$ does not exceed the decreases in both $g_{st}$ and $g_{elec}$. The predicted micelle aggregation numbers of surfactants C and D (see Table 5.5) are smaller than the experimental values, with $n \simeq 45$ for surfactant C and $n \simeq 38$ for surfactant D [167]. The higher predicted $n$ value of surfactant C results from the decrease in the micelle core-minor radius, $l_c$, while maintaining a constant value of the surfactant tail volume, similar to the case of the second series of x-y-SAS branched surfactants ($x+y=11$; see Section 5.2).

For surfactants E and F, the total hydrocarbon chain lengths are fixed (similar to the second series of x-y-SAS branched surfactants ($x+y=11$)), indicating that their $g_{tr,CS-MT}$ values should be similar (see Table 5.4). As a result, the reasons responsible for the higher CMC of surfactant F are similar to those in the case of the second series of x-y-SAS branched surfactants ($x+y=11$),

that is, the interplay between the increase in $g_{int}$ and the decreases in both $g_{st}$ and $g_{elec}$ (see Section 5.2). As shown in Figure 5-6 and Table 5.6, for surfactants E and F, the CS–MT model overpredicts the CMC's (at worst by a factor of 1.3). Again, this is most probably due to inaccuracies in the surfactant property inputs used in the CS–MT model.

As shown in Figure 5-6 and Table 5.6, the traditional MT model also overpredicts the CMC's of surfactants E and F (at worst by a factor of 2.5), due to the fact that only one of the neutral groups (group 8, one of the two neutral $CH_2$ groups, is adjacent to the charged pyridinium group) was considered to be part of the surfactant tail (leading to a smaller magnitude of $g_{tr}$ and associated less negative value of $g^*_{mic}$). In the case of surfactants E and F, all the neutral groups should be considered to be part of the surfactant tail when implementing the traditional MT model. Similar to the other complex ionic branched surfactants (A to D), the CS–MT model performs better than the traditional MT model at predicting the CMC's of surfactants E and F, and it also more accurately accounts for the chemical and structural complexities of surfactants E and F.

The predicted optimal micelle shape is a cylinder for both surfactants E and F (see Table 5.5), due to the similarities between the two surfactant tail structures. Again, no experimental information is available to corroborate the shape and $n$ predictions for surfactants E and F. The predicted higher $n$ value of surfactant E relative to surfactant F (see Table 5.5) is due to the decrease in the micelle core-minor radius, $l_c$, while maintaining a constant value of the surfactant tail volume, similar to what I discussed in the case of the second series of x-y-SAS branched surfactants ($x + y = 11$; see Section 5.2).

# Chapter 6

# Conclusions and Future Work

## 6.1 Thesis Summary

The central objective of this thesis has been to demonstrate the validity and accuracy of the CS–MT modeling approach by predicting the aqueous micellar solution properties of seventeen ionic linear and branched surfactants of varying chemical and structural complexity. These branched surfactants comprise eleven secondary alkyl sulfonate surfactants (in addition, two linear alkyl sulfonate surfactants were modeled for comparison), and six complex ionic branched surfactants possessing aromatic groups (see Chapter 3). The molecular-level prediction of micellar solution properties is of great practical value to industrial formulators in reducing the need for tedious and time-consuming experimentation (see Chapter 1). In addition, the development of molecular-based approaches like the CS–MT model improves our fundamental understanding of the phenomenon of surfactant self-assembly, particularly, of the self-assembly of ionic branched surfactants considered in this thesis (see Chapter 1).

To implement the CS–MT model, I have used MD simulations to determine quantitative information about the change in the degree of hydration of each surfactant group that occurs upon surfactant self-assembly (see Chapter 5). A careful study of the local structure of hydrating atoms surrounding various surfactant hydrophobic groups was carried out using the Radial Distribution Function (RDF) approach (see Chapter 3). In addition, I developed a new method to identify surfactant heads and tails by introducing an equimolar Gibbs dividing surface to represent the conceptual micelle core–water interface (see Chapter 4). This assignment of atomic groups to

the surfactant head or tail regions leads to reasonable agreement with the traditional head and tail identification results, with the primary difference being the occasional identification of some surfactant atomic groups being neutral (i.e., residing very close to the dividing surface and not clearly belonging to either the surfactant head or tail regions).

The hydration information obtained from MD simulations was then used to quantify the hydrophobic effect driving surfactant self-assembly in aqueous media (captured in the $g_{tr,CS-MT}$ free-energy contribution), as well as other key inputs to the CS–MT model and to the traditional MT model required to compute the other free-energy contributions (see Chapter 2). To enable a relatively simple estimation of $\hat{g}_{dehydr}$, $\hat{g}_{hydr}$, $\hat{g}_{int}$, as well as of the other free-energy contributions in the case of ionic linear and branched surfactants, a number of approximations were made. After obtaining all the required free-energy contributions, the optimal micellization free energy, $g^*_{mic}$, and the CMC were computed for each surfactant micelle of optimal shape and size (see Chapter 5). The traditional MT model was also used to predict $g_{tr}$, which was compared with $g_{tr,CS-MT}$ predicted using the CS–MT model (see Chapter 5). Use of the traditional MT model required as input the assignment of heads and tails obtained from MD simulations, as well as the implementation of a number of approximations.

Although the CS–MT model enables the prediction of a broad variety of micellar solution properties (the micelle shape, size, and degree of counterion binding) once $g^*_{mic}$ is computed, the CMC was specifically selected for prediction and comparison with the available experimental CMC data, because the CMC depends exponentially on $g^*_{mic}$, and therefore, provides a very sensitive quantitative indicator of the predictive accuracy of the CS–MT model (see Chapter 5). Furthermore, it is noteworthy that for most of the ionic branched surfactants studied, no other experimental information is currently available. Reasonable agreement between the CMC predictions made using the CS–MT model and the experimental CMC's was obtained for all the ionic linear and branched surfactants considered here (see Chapter 5). The CMC's predicted using the CS–MT model were closer to the experimental CMC's than those predicted using the traditional MT model. In addition, the CS–MT model was able to describe the chemical and structural complexities of the ionic branched surfactants studied more accurately than the traditional MT model (see Chapter 5).

The results obtained for the relatively complex ionic branched surfactants possessing aromatic groups illustrates the predictive value of the CS–MT modeling approach: the CMC's predicted

using the CS–MT model are in remarkably good agreement with the experimental CMC's, while the CMC's predicted using the traditional MT model are quite inaccurate (see Chapter 5). With the above in mind, the CS–MT model represents an important advance in predicting the micellization properties of increasingly complex surfactants, such as the branched ionic surfactants considered in this thesis.

## 6.2 Future Research Directions

### 6.2.1 Frame-by-Frame Analysis of MD Simulation Results

As discussed in Section 3.4.4, the block averaging approach provides an accurate estimate of the standard error of the results of a single simulation. However, in order to ensure that sufficient sampling has been performed, it is desirable to run multiple independent simulations to estimate the run-to-run variance and to compare the run-to-run variance with the variance estimated from a single simulation [148, 160]. In past studies, the run-to-run variance has been determined by conducting additional independent bulk water and aggregate simulations of oil molecules [58], and was found to be comparable in magnitude to the block average estimates of the standard error for each oil molecule.

Although independent simulations were not deemed necessary for the ionic linear and branched surfactants simulated as part of this thesis, additional independent bulk water and micelle simulations are required to validate such an assumption. In addition, the analysis of each simulation frame should be useful in validating the above assumption, because the result of each simulation frame analysis can be used to determine both the run-to-run variance and the variance associated with a single simulaton. To implement such a frame-by-frame analysis, it will be necessary to develop a program capable of analyzing each simulation frame, in addition to calculating the run-to-run variance and the variance associated with a single simulation.

In Section 4.1, I developed a new method to identify surfactant heads and tails which utilizes an equimolar Gibbs dividing surface to represent the conceptual micelle core–water interface. Variation in the location of such a dividing surface may result under a different sampling of the simulation frames, and this variation could also be quantified by carrying out the frame-by-frame analysis

described above. Until such an analysis is completed, one can not gauge if this variation is negligible relative to the error associated with the analysis approach used to determine the location of the dividing surface.

### 6.2.2 MD Simulation Studies of Solvent Accessible Surface Areas (SASA's) of Branched Surfactants

In Section 2.2.4, the two microscopic interfacial tensions, $\sigma_{bulk}$ and $\sigma_{core}$, were assumed to be constant and functions of the surfactant alkyl tail length and the curvature (based on MD simulation results for 15 oil aggregates), respectively. However, in the case of the ionic branched surfactants studied in this thesis, these assumptions require further validation by using MD simulation results to obtain the two SASA terms in Eq. 2.19, including $\text{SASA}_{core}$ (in a micelle simulation) and $\text{SASA}_i$ for each surfactant hydrophobic group (in a bulk water simulation).

Such a case-by-case study will require additional work when analyzing MD simulation results for surfactants possessing complex chemical structures and novel atomic groups (i.e., atomic groups other than hydrocarbon groups), where the previous assumptions for estimating $\sigma_{bulk}$ and $\sigma_{core}$ values may not be applicable. This additional work is essential when modeling surfactants that possess: (i) highly branched structures (for example, in Triton X-100), (ii) aromatic groups (for example, in the linear alkyl benzene sulfonate surfactants), (iii) silicone groups (for example, in Silwet L-77), (iv) halocarbon groups (for example, in PFOA, or perfluorooctanoic acid), or (v) combinations of (i) to (iv) above (for example, in Triton X-100, which is both highly branched and contains benzene groups).

### 6.2.3 Validation of Surfactant Property Predictions

In Sections 4.2 and 4.6, a number of approximations were made to determine the surfactant property values used as inputs to the CS–MT model. These properties include: (i) $a_0$, the interfacial area shielded by the surfactant head, and (ii) $\sigma_0$, the interfacial tension between a surfactant tail phase and water at a flat interface.

The designation of neutral groups when identifying surfactant heads and tails complicates the rigorous estimation of $a_0$. A sensitivity analysis on $a_0$ is therefore required in order to evaluate

the accuracy of the CS–MT modeling results. Note that typical values of $a_0$ range between 12 Å and 31 Å for linear nonionic surfactants [59], and between 21 Å and 42 Å for the ionic linear and branched surfactants considered here.

The group-contribution method used to estimate $\sigma_0$, including using Eq. 4.7 to obtain an effective $\Phi$ value, needs further validation. Such validation can be achieved by predicting the $\sigma_0$ values for a homologous series of chemical compounds using the group-contribution method proposed in this thesis (see Section 4.6), followed by comparing the predicted $\sigma_0$ values with the available experimental $\sigma_0$ values. The following homologous series of chemical compounds may be studied: (a) a series of branched alkanes with various branching structures (similar to the alkyl pyridinium iodide surfactants), (b) a series of alkyl benzene molecules with various aromatic compositions (similar to the LAS surfactants), (c) a series of alkyl silicone molecules with various silicon compositions (similar to Silwet L-77), or (d) a series of partially fluorinated hydrocarbons with various fluorocarbon compositions (similar to partially fluorinated surfactants).

However, for surfactants possessing more complex tails composed of multiple chemical structures, like Triton X-100 which is both highly branched and contains benzene groups, a more complex group-contribution method needs to be developed and subsequently validated by comparing the predicted $\sigma_0$ values with the experimental $\sigma_0$ data. Unfortunately, there is a notable lack of available experimental data on interfacial tensions between water and such complex molecules. Similar to the case of $a_0$, a sensitivity test may provide some insight into the accuracy necessary to estimate $\sigma_0$ in order to minimize errors in the predicted micellization properties.

### 6.2.4 Improving Surfactant Head and Tail Identification

In Section 4.1, a new method to identify surfactant head and tail regions was developed using an equimolar Gibbs dividing surface to represent the conceptual micelle core–water interface. This method was applied to a variety of ionic linear and branched surfactants. However, such an approach is based on simulating a *spherical* micelle, for which the RDF's are spherically symmetric and can be readily implemented. In order to extend this simulation-based approach to other regular micelle geometries, such as cylinders and bilayers, RDF's with respect to the axis of a cylinder or with respect to the central plane of a bilayer, respectively, are required. Moreover, for non-

regular micelle geometries, such as ellipsoids, radially-dependent and angular-dependent RDF's are required, which will introduce additional computational complexity into the head and tail identification process.

In the assignment of an atomic group as head, tail, or neutral, the use of one standard deviation to evaluate the range of distribution of each atomic group with respect to the micelle center of mass is a conventional, yet arbitrary choice. This choice results in very good agreement with the traditional surfactant head and tail identification results for all the surfactants considered. In addition, the number of atomic groups identified as neutral groups is kept to a minimum, which enables more effective modeling using the new packing method because a larger number of neutral groups requires a more complex packing model where the free-energy contributions, $g_{tr}$ and $g_{int}$, are directly coupled in the model. Nevertheless, the use of other criteria to assign surfactant heads and tails, based, for example, on comparing the locations of each atomic group and the location of the conceptual micelle core–water interface, may be considered. With this in mind, additional careful future studies in this area may be pursued.

In Sections 4.2, 5.2, and 5.3, the key assumption that all the neutral groups in the surfactant molecule are part of the surfactant tail was made in order to estimate all the surfactant geometric parameters, including $a_h$, $a_0$, $d_{charge}$, $l_{hg}$, and to compute the free-energy contribution $\hat{g}_{hydr}$. Although this assumption yielded good CS–MT predictions, sensitivity tests involving assigning some of these neutral groups to be part of the surfactant head are required to further validate the original assumption. In addition, when estimating $\sigma_0$, the assumption was made that the neutral groups are not part of the surfactant tail to ensure that only those surfactant groups which are most likely in the surfactant tail are accounted for. Clearly, sensitivity tests are also required to validate this assumption.

## 6.3 Concluding Remarks

In this thesis, I have presented a predictive theoretical framework which combines atomistic-level computer simulations and a molecular-thermodynamic approach and enables the molecular-level prediction of the micellization behavior of complex ionic branched surfactants in aqueous solution. In developing this framework, a number of theoretical and computational challenges were

identified and addressed, and a number of areas for future research were also identified. The approaches developed in this thesis to successfully combine computer simulations with molecular-thermodynamic theory in a complementary manner not only extend our ability to make accurate predictions of surfactant micellization behavior in aqueous solution, but also contribute to our fundamental understanding of the thermodynamic processes that underlie surfactant self-assembly. The work presented in this thesis should provide a natural foundation for future research in the area of surfactant self-assembly, and, more generally, should assist future researchers in connecting atomistic-level computer simulation methods with continuum thermodynamic models.

# Bibliography


[1] C. Tanford. *The hydrophobic effect : formation of micelles and biological membranes*. Krieger, Malabar, Fla., 2nd edition, 1991.

[2] Jacob N. Israelachvili. *Intermolecular and surface forces : with applications to colloidal and biological systems*. Academic Press, 1985.

[3] K. Holmberg, B. Jonsson, B. Kronberg, and B. Lindman. *Surfactants and Polymers in Aqueous Solution*. Wiley, 2002.

[4] R. Zana. Micellization of amphiphiles: selected aspects. *Colloids and Surfaces A: Physicochemical and Engineering Aspects*, 123-124:27–35, 1997.

[5] P. H. Elworthy, A. T. Florence, and C. B. Macfarlane. *Solubilization by surface-active agents and its applications in chemistry and the biological sciences*. Chapman & Hall, London, 1968.

[6] S. D. Christian and J. F. Scamehorn. *Solubilization in surfactant aggregates*. Surfactant science series ; v. 55. M. Dekker, New York, 1995.

[7] L. Yurlova, A. Kryvoruchko, and B. Kornilovich. Removal of ni(ii) ions from wastewater by micellar-enhanced ultrafiltration. *Desalination*, 144(1-3):255–260, 2002.

[8] T. Polubesova, S. Nir, D. Zadaka, O. Rabinovitz, C. Serban, L. Groisman, and B. Rubin. Water purification from organic pollutants by optimized micelle-clay systems. *Environmental Science & Technology*, 39(7):2343–2348, 2005.

[9] A. V. Sineva, A. M. Parfenova, and A. A. Fedorova. Adsorption of micelle forming and non-micelle forming surfactants on the adsorbents of different nature. *Colloids and Surfaces a-Physicochemical and Engineering Aspects*, 306(1-3):68–74, 2007.

[10] Z. K. Zhao, F. Liu, W. H. Qiao, Z. S. Li, and L. B. Cheng. Novel alkyl methyl- naphthalene sulfonate surfactants: A good candidate for enhanced oil recovery. *Fuel*, 85(12-13):1815–1820, 2006.

[11] T. Babadagli. Evaluation of the critical parameters in oil recovery from fractured chalks by surfactant injection. *Journal of Petroleum Science and Engineering*, 54(1-2):43–54, 2006.

[12] F. D. S. Curbelo, E. L. Barros, T. V. Dutra, T. N. C. Dantas, and A. I. C. Garnica. Oil recovery by ionic and nonionic surfactants and adsorption in sandstones. *Afinidad*, 63(524):291–295, 2006.

[13] S. A. Hagan, A. G. A. Coombes, M. C. Garnett, S. E. Dunn, M. C. Davis, L. Illum, S. S. Davis, S. E. Harding, S. Purkiss, and P. R. Gellert. Polylactide-poly(ethylene glycol) copolymers as drug delivery systems .1. characterization of water dispersible micelle-forming systems. *Langmuir*, 12(9):2153–2161, 1996.

[14] Clariant functional chemicals - emulsifiers and solubilizers, 2008. http://fun.clariant.com/.

[15] K.M. Pedersen and P.A. Pappalardo. Concentrated aqueous degreasing cleanser. Us patent, Diversey Lever, Inc., July 28 1998.

[16] Y. G. Bogdanova, V. D. Dolzhikova, and B. D. Summ. Wetting in the system polyethylene - aqueous-solution of nonionic surfactant triton x-100. *Vestnik Moskovskogo Universiteta Seriya 2 Khimiya*, 36(3):262–266, 1995.

[17] I. Xiarchos and D. Doulia. Effect of nonionic surfactants on the solubilization of alachlor. *Journal of Hazardous Materials*, 136(3):882–888, 2006.

[18] N. Garti, A. Aserin, E. Wachtel, O. Gans, and Y. Shaul. Water solubilization in nonionic microemulsions stabilized by grafted siliconic emulsifiers. *Journal of Colloid and Interface Science*, 233(2):286–294, 2001.

[19] D. W. Kim and S. T. Noh. Synthesis and surface-active properties of a trisiloxane-modified oligo(propylene oxide-block-ethylene oxide) wetting agent. *Journal of Applied Polymer Science*, 92(5):3292–3302, 2004.

[20] W. Gelbart, A. Ben-Shaul, and D. Roux. *Micelles, membranes, microemulsions, and monolayers*. Partially ordered systems. Springer-Verlag, New York, 1994.

[21] G. Caracciolo, D. Pozzi, G. Mancini, and R. Caminiti. Role of the spacer stereo- chemistry on the structure of solid-supported gemini surfactants aggregates. *Langmuir*, 23(20):10040–10043, 2007.

[22] T. Lu, F. Han, G. R. Mao, G. F. Lin, J. B. Huang, X. Huang, Y. L. Wang, and H. L. Fu. Effect of hydrocarbon parts of the polar headgroup on surfactant aggregates in gemini and bola surfactant solutions. *Langmuir*, 23(6):2932–2936, 2007.

[23] K. Matsuoka, T. Yoshimura, T. Shikimoto, J. Hamada, M. Yamawaki, C. Honda, and K. Endo. Molecular aggregates of partially fluorinated quaternary ammonium salt gemini surfactants. *Langmuir*, 23(22):10990–10994, 2007.

[24] L. Wattebled and A. Laschewsky. Effects of organic salt additives on the behavior of dimeric ("gemini") surfactants in aqueous solution. *Langmuir*, 23(20):10044–10052, 2007.

[25] L. M. Zhou, X. H. Jiang, Y. T. Li, Z. Chen, and X. Q. Hu. Synthesis and properties of a novel class of gemini pyridinium surfactants. *Langmuir*, 23(23):11404–11408, 2007.

[26] J. N. Israelachvili, D. J. Mitchell, and B. W. Ninham. Theory of self-assembly of hydrocarbon amphiphiles into micelles and bilayers. *Journal of the Chemical Society- Faraday Transactions II*, 72:1525–1568, 1976.

[27] J. N. Israelachvili, D. J. Mitchell, and B. W. Ninham. Theory of self-assembly of lipid bilayers and vesicles. *Biochimica Et Biophysica Acta*, 470(2):185–201, 1977.

[28] R. Nagarajan and E. Ruckenstein. Aggregation of amphiphiles as micelles or vesicles in aqueous-media. *Journal of Colloid and Interface Science*, 71(3):580–604, 1979.

[29] J. J. H. Nusselder, T. J. Degroot, M. Trimbos, and J. B. F. N. Engberts. Effect of alkyl chain stiffness and branching on the properties of micelles formed from 1-methyl-4-(c-12-alkyl)pyridinium iodide surfactants. *Journal of Organic Chemistry*, 53(11):2423–2426, 1988.

[30] S. Ozeki and S. Ikeda. The viscosity behavior of aqueous nacl solutions of dodecyldimethylammonium chloride and the flexibility of its rod-like micelle. *Journal of Colloid and Interface Science*, 77(1):219–231, 1980.

[31] S. Ghosh and D. Blankschtein. The role of sodium dodecyl sulfate (sds) micelles in inducing skin barrier perturbation in the presence of glycerol. *Journal of Cosmetic Science*, 58(2):109–133, 2007.

[32] A. Shiloach and D. Blankschtein. Predicting micellar solution properties of binary surfactant mixtures. *Langmuir*, 14(7):1618–1636, 1998.

[33] R. Nagarajan and E. Ruckenstein. Theory of surfactant self-assembly - a predictive molecular thermodynamic approach. *Langmuir*, 7(12):2934–2969, 1991.

[34] G. Gunnarsson, B. Jonsson, and H. Wennerstrom. Surfactant association into micelles - an electrostatic approach. *Journal of Physical Chemistry*, 84(23):3114–3121, 1980.

[35] B. Jonsson and H. Wennerstrom. Thermodynamics of ionic amphiphile-water systems. *Journal of Colloid and Interface Science*, 80(2):482–496, 1981.

[36] J. B. Hayter. A self-consistent theory of dressed micelles. *Langmuir*, 8(12):2873–2876, 1992.

[37] R. Nagarajan. Molecular theory for mixed micelles. *Langmuir*, 1(3):331–341, 1985.

[38] R. Nagarajan. Micellization, mixed micellization and solubilization - the role of interfacial interactions. *Advances in Colloid and Interface Science*, 26(2-4):205–264, 1986.

[39] R. Nagarajan. Solubilization in aqueous solutions of amphiphiles. *Current Opinion in Colloid & Interface Science*, 1(3):391–401, 1996.

[40] R. Nagarajan. Solubilization by amphiphilar aggregates. *Current Opinion in Colloid & Interface Science*, 2(3):282–293, 1997.

[41] R. Nagarajan, M. A. Chaiko, and E. Ruckenstein. Locus of solubilization of benzene in surfactant micelles. *Journal of Physical Chemistry*, 88(13):2916–2922, 1984.

[42] R. Nagarajan and E. Ruckenstein. Critical micelle concentration - transition point for micellar size distribution - statistical thermodynamical approach. *Journal of Colloid and Interface Science*, 60(2):221–231, 1977.

[43] R. Nagarajan and E. Ruckenstein. Solubilization as a separation process. *Separation Science and Technology*, 16(10):1429–1465, 1981.

[44] E. Ruckenstein and J. A. Beunen. Effect of counterion binding on micellization. *Langmuir*, 4(1):77–90, 1988.

[45] M. A. Chaiko, R. Nagarajan, and E. Ruckenstein. Solubilization of single-component and binary-mixtures of hydrocarbons in aqueous micellar solutions. *Journal of Colloid and Interface Science*, 99(1):168–182, 1984.

[46] A. Shiloach and D. Blankschtein. Measurement and prediction of ionic/nonionic mixed micelle formation and growth. *Langmuir*, 14(25):7166–7182, 1998.

[47] A. Shiloach and D. Blankschtein. Prediction of critical micelle concentrations and synergism of binary surfactant mixtures containing zwitterionic surfactants. *Langmuir*, 13(15):3968–3981, 1997.

[48] V. Srinivasan and D. Blankschtein. Effect of counterion binding on micellar solution behavior: 1. molecular-thermodynamic theory of micellization of ionic surfactants. *Langmuir*, 19(23):9932–9945, 2003.

[49] V. Srinivasan and D. Blankschtein. Effect of counterion binding on micellar solution behavior: 2. prediction of micellar solution properties of ionic surfactant-electrolyte systems. *Langmuir*, 19(23):9946–9961, 2003.

[50] I. Reif, M. Mulqueen, and D. Blankschtein. Molecular-thermodynamic prediction of critical micelle concentrations of commercial surfactants. *Langmuir*, 17(19):5801–5812, 2001.

[51] N. Zoeller, L. Lue, and D. Blankschtein. Statistical-thermodynamic framework to model nonionic micellar solutions. *Langmuir*, 13(20):5258–5275, 1997.

[52] M. Mulqueen and D. Blankschtein. Prediction of equilibrium surface tension and surface adsorption of aqueous surfactant mixtures containing zwitterionic surfactants. *Langmuir*, 16(20):7640–7654, 2000.

[53] M. Mulqueen and D. Blankschtein. Theoretical and experimental investigation of the equilibrium oil-water interfacial tensions of solutions containing surfactant mixtures. *Langmuir*, 18(2):365–376, 2002.

[54] M. Mulqueen, S. S. Datwani, K. J. Stebe, and D. Blankschtein. Dynamic surface tensions of aqueous surfactant mixtures: Experimental investigation. *Langmuir*, 17(24):7494–7500, 2001.

[55] M. Mulqueen, K. J. Stebe, and D. Blankschtein. Dynamic interfacial adsorption in aqueous surfactant mixtures: Theoretical study. *Langmuir*, 17(17):5196–5207, 2001.

[56] Y. J. Nikas, S. Puvvada, and D. Blankschtein. Surface tensions of aqueous nonionic surfactant mixtures. *Langmuir*, 8(11):2680–2689, 1992.

[57] B. C. Stephenson, K. Beers, and D. Blankschtein. Complementary use of simulations and molecular-thermodynamic theory to model micellization. *Langmuir*, 22(4):1500–1513, 2006.

[58] B. C. Stephenson, A. Goldsipe, K. J. Beers, and D. Blankschtein. Quantifying the hydrophobic effect. 1. a computer simulation-molecular-thermodynamic model for the self-assembly of hydrophobic and amphiphilic solutes in aqueous solution. *Journal of Physical Chemistry B*, 111(5):1025–1044, 2007.

[59] B. C. Stephenson, A. Goldsipe, K. J. Beers, and D. Blankschtein. Quantifying the hydrophobic effect. 2. a computer simulation-molecular-thermodynamic model for the micellization

of nonionic surfactants in aqueous solution. *Journal of Physical Chemistry B*, 111(5):1045–1062, 2007.

[60] B. C. Stephenson, K. J. Beers, and D. Blankschtein. Quantifying the hydrophobic effect. 3. a computer simulation-molecular-thermodynamic model for the micellization of ionic and zwitterionic surfactants in aqueous solution. *Journal of Physical Chemistry B*, 111(5):1063–1075, 2007.

[61] S. Puvvada and D. Blankschtein. Molecular-thermodynamic approach to predict micellization, phase-behavior and phase-separation of micellar solutions .1. application to nonionic surfactants. *Journal of Chemical Physics*, 92(6):3710–3724, 1990.

[62] A. R. Leach. *Molecular modelling : principles and applications*. Prentice Hall, Harlow, England ; New York, 2nd edition, 2001.

[63] D. van der Spoel, E. Lindahl, B. Hess, A. van Buuren, E. Apol, P. Meulenhoff, D. Tieleman, A. Sijbers, K. Feenstra, R. van Drunen, , and H. Berendsen. *Gromacs User Manual version 3.2*, 2005. www.gromacs.org.

[64] L. A. Rodriguez-Guadarrama, S. K. Talsania, K. K. Mohanty, and R. Rajagopalan. Thermodynamics of aggregation of amphiphiles in solution from lattice monte carlo simulations. *Langmuir*, 15(2):437–446, 1999.

[65] C. M. Care and T. Dalby. Packing entropy in micelle self-assembly. *Europhysics Letters*, 45(1):38–44, 1999.

[66] R. G. Larson. Monte-carlo simulation of microstructural transitions in surfactant systems. *Journal of Chemical Physics*, 96(11):7904–7918, 1992.

[67] R. G. Larson, L. E. Scriven, and H. T. Davis. Monte-carlo simulation of model amphiphilic oil-water systems. *Journal of Chemical Physics*, 83(5):2411–2420, 1985.

[68] M. A. Floriano, E. Caponetti, and A. Z. Panagiotopoulos. Micellization in model surfactant systems. *Langmuir*, 15(9):3143–3151, 1999.

[69] B. Smit, K. Esselink, P. A. J. Hilbers, N. M. Vanos, L. A. M. Rupert, and I. Szleifer. Computer-simulations of surfactant self-assembly. *Langmuir*, 9(1):9–11, 1993.

[70] B. Smit, P. A. J. Hilbers, K. Esselink, L. A. M. Rupert, N. M. Vanos, and A. G. Schlijper. Computer-simulations of a water oil interface in the presence of micelles. *Nature*, 348(6302):624–625, 1990.

[71] B. Smit, P. A. J. Hilbers, K. Esselink, L. A. M. Rupert, N. M. Vanos, and A. G. Schlijper. Structure of a water oil interface in the presence of micelles - a computer-simulation study. *Journal of Physical Chemistry*, 95(16):6361–6368, 1991.

[72] J. B. Maillet, V. Lachet, and P. V. Coveney. Large scale molecular dynamics simulation of self-assembly processes in short and long chain cationic surfactants. *Physical Chemistry Chemical Physics*, 1(23):5277–5290, 1999.

[73] S. J. Marrink, D. P. Tieleman, and A. E. Mark. Molecular dynamics simulation of the kinetics of spontaneous micelle formation. *Journal of Physical Chemistry B*, 104(51):12165–12173, 2000.

[74] R. Pool and P. G. Bolhuis. Accurate free energies of micelle formation. *Journal of Physical Chemistry B*, 109(14):6650–6657, 2005.

[75] K. J. Schweighofer, U. Essmann, and M. Berkowitz. Simulation of sodium dodecyl sulfate at the water-vapor and water-carbon tetrachloride interfaces at low surface coverage. *Journal of Physical Chemistry B*, 101(19):3793–3799, 1997.

[76] C. D. Bruce, M. L. Berkowitz, L. Perera, and M. D. E. Forbes. Molecular dynamics simulation of sodium dodecyl sulfate micelle in water: Micellar structural characteristics and counterion distribution. *Journal of Physical Chemistry B*, 106(15):3788–3793, 2002.

[77] C. D. Bruce, S. Senapati, M. L. Berkowitz, L. Perera, and M. D. E. Forbes. Molecular dynamics simulations of sodium dodecyl sulfate micelle in water: The behavior of water. *Journal of Physical Chemistry B*, 106(42):10902–10907, 2002.

[78] A. D. Mackerell. Molecular-dynamics simulation analysis of a sodium dodecyl-sulfate micelle in aqueous-solution - decreased fluidity of the micelle hydrocarbon interior. *Journal of Physical Chemistry*, 99(7):1846–1855, 1995.

[79] H. Dominguez. Computer simulation studies of surfactant monolayer mixtures at the water/oil interface: charge distribution effects. *Journal of Colloid and Interface Science*, 274(2):665–672, 2004.

[80] H. Dominguez and M. L. Berkowitz. Computer simulations of sodium dodecyl sulfate at liquid/liquid and liquid/vapor interfaces. *Journal of Physical Chemistry B*, 104(22):5302–5308, 2000.

[81] J. Gao, W. Ge, G. H. Hu, and J. H. Li. From homogeneous dispersion to micelles - a molecular dynamics simulation on the compromise of the hydrophilic and hydrophobic effects of sodium dodecyl sulfate in aqueous solution. *Langmuir*, 21(11):5223–5229, 2005.

[82] S. Bogusz, R. M. Venable, and R. W. Pastor. Molecular dynamics simulations of octyl glucoside micelles: Structural properties. *Journal of Physical Chemistry B*, 104(23):5462–5470, 2000.

[83] J. Bocker, J. Brickmann, and P. Bopp. Molecular-dynamics simulation study of an n-decyltrimethylammonium chloride micelle in water. *Journal of Physical Chemistry*, 98(2):712–717, 1994.

[84] A. R. Rakitin and G. R. Pack. Molecular dynamics simulations of ionic interactions with dodecyl sulfate micelles. *Journal of Physical Chemistry B*, 108(8):2712–2716, 2004.

[85] S. Pal, S. Balasubramanian, and B. Bagchi. Identity, energy, and environment of interfacial water molecules in a micellar solution. *Journal of Physical Chemistry B*, 107(22):5194–5202, 2003.

[86] B. C. Stephenson, A. Goldsipe, and D. Blankschtein. Molecular dynamics simulation and thermodynamic modeling of the self-assembly of the triterpenoids asiatic acid and madecassic acid in aqueous solution. *Journal of Physical Chemistry B*, 112(8):2357–2371, 2008. Times Cited: 0 Article English Cited References Count: 59 265js.

[87] B. C. Stephenson, K. A. Stafford, K. J. Beers, and D. Blankschtein. Application of computer simulation free-energy methods to compute the free energy of micellization as a function of micelle composition. 1. theory. *J. Phys. Chem. B*, 112(6):1634–1640, 2008.

[88] B. C. Stephenson, K. A. Stafford, K. J. Beers, and D. Blankschtein. Application of computer simulation free-energy methods to compute the free energy of micellization as a function of micelle composition. 2. implementation. *J. Phys. Chem. B*, 112(6):1641–1656, 2008.

[89] S. Mohanty, H. T. Davis, and A. V. McCormick. Complementary use of simulations and free energy models for ctab/nasal systems. *Langmuir*, 17(22):7160–7171, 2001.

[90] B. C. Stephenson, C. O. Rangel-Yagui, A. Pessoa, L. C. Tavares, K. Beers, and D. Blankschtein. Experimental and theoretical investigation of the micellar-assisted solubilization of ibuprofen in aqueous media. *Langmuir*, 22(4):1514–1525, 2006.

[91] J. C. Shelley, M. Sprik, and M. L. Klein. Molecular-dynamics simulation of an aqueous sodium octanoate micelle using polarizable surfactant molecules. *Langmuir*, 9(4):916–926, 1993.

[92] I. I. Vaisman and M. L. Berkowitz. Local structural order and molecular associations in water dmso mixtures - molecular-dynamics study. *Journal of the American Chemical Society*, 114(20):7889–7896, 1992.

[93] W. L. Jorgensen, J. Gao, and C. Ravimohan. Monte-carlo simulations of alkanes in water - hydration numbers and the hydrophobic effect. *Journal of Physical Chemistry*, 89(16):3470–3473, 1985.

[94] A. Langham and Y. Kaznessis. Simulation of the n-terminus of hiv-1 glycoprotein 41000 fusion peptide in micelles. *Journal of Peptide Science*, 11(4):215–224, 2005.

[95] T. Wymore, X. F. Gao, and T. C. Wong. Molecular dynamics simulation of the structure and dynamics of a dodecylphosphocholine micelle in aqueous solution. *Journal of Molecular Structure*, 486:195–210, 1999.

[96] A. Goldsipe and D. Blankschtein. Modeling counterion binding in ionic-nonionic and ionic-zwitterionic binary surfactant mixtures. *Langmuir*, 21(22):9850–9865, 2005.

[97] A. Ben-Shaul and I. Szleifer. Chain organization and thermodynamics in micelles and bilayers. 1. theory. *Journal of Chemical Physics*, 83(7):3597–3611, 1985.

[98] I. Szleifer, A. Ben-Shaul, and W. M. Gelbart. Chain organization and thermodynamics in micelles and bilayers. 2. model-calculations. *Journal of Chemical Physics*, 83(7):3612–3620, 1985.

[99] I. Szleifer, A. Ben-Shaul, and W. M. Gelbart. Statistical thermodynamics of molecular-organization in mixed micelles and bilayers. *Journal of Chemical Physics*, 86(12):7094–7109, 1987.

[100] V. Srinivasan and D. Blankschtein. Prediction of conformational characteristics and micellar solution properties of fluorocarbon surfactants. *Langmuir*, 21(4):1647–1660, 2005.

[101] R. Smith and C. Tanford. Hydrophobicity of long-chain alkyl carboxylic-acids, as measured by their distribution between heptane and aqueous-solutions. *Proceedings of the National Academy of Sciences of the United States of America*, 70(2):289–293, 1973. Times Cited: 139 Article English Cited References Count: 17 O7855.

[102] T. R. Carale, Q. T. Pham, and D. Blankschtein. Salt effects on intramicellar interactions and micellization of nonionic surfactants in aqueous-solutions. *Langmuir*, 10(1):109–121, 1994. Times Cited: 51 Article English Cited References Count: 57 Mt810.

[103] J. W. Gibbs. *The Scientific Papers of J. W. Gibbs*, volume 1. Dover, New York, 1961.

[104] R.C. Tolman. Consideration of the gibbs theory of surface tension. *Journal of Chemical Physics*, 16:758–774, 1948.

[105] F.O. Koenig. On the thermodynamic relation between surface tension and curvature. *Journal of Chemical Physics*, 18:449–459, 1950.

[106] F. P. Buff. The spherical interface. i. thermodynamics. *Journal of Chemical Physics*, 19:1591–1594, 1951.

[107] R. Aveyard, B.J. Briscoe, and J. Chapman. Adhesion at the alkane/water and ester/water interfaces. *Journal of the Chemical Society, Faraday Transactions 1*, 68:10–16, 1972.

[108] R. Glaser. *Biophysics*. Springer, 2001.

[109] B. Jonsson, O. Edholm, and O. Teleman. Molecular-dynamics simulations of a sodium octanoate micelle in aqueous-solution. *Journal of Chemical Physics*, 85(4):2259–2271, 1986.

[110] K. Lum, D. Chandler, and J. D. Weeks. Hydrophobicity at small and large length scales. *Journal of Physical Chemistry B*, 103(22):4570–4577, 1999.

[111] D. Chandler. Interfaces and the driving force of hydrophobic assembly. *Nature*, 437(7059):640–647, 2005.

[112] R. B. Hermann. Theory of hydrophobic bonding. ii. correlation of hydrocarbon solubility in water with solvent cavity surface area. *Journal of Physical Chemistry*, 76(19):2754–2759, 1972.

[113] J. A. Reynolds, D. B. Gilbert, and C. Tanford. Empirical correlation between hydrophobic free-energy and aqueous cavity surface-area. *Proceedings of the National Academy of Sciences of the United States of America*, 71(8):2925–2927, 1974.

[114] R. Granet and S. Piekarski. Surface and micellar properties of sodium 1-alkyl decane sulfonates. *Colloids and Surfaces*, 33(3-4):321–336, 1988.

[115] H. Azira and A. Tazerouti. Micellar behavior of anionic surfactants with sulfonate function in aqueous solutions. *Journal of Surfactants and Detergents*, 10(3):185–190, 2007.

[116] P. D. T. Huibers, V. S. Lobanov, A. R. Katritzky, D. O. Shah, and M. Karelson. Prediction of critical micelle concentration using a quantitative structure-property relationship approach .2. anionic surfactants. *Journal of Colloid and Interface Science*, 187(1):113–120, 1997.

[117] L. J. Magid, R. Triolo, J. S. Johnson, and W. C. Koehler. Small-angle neutron-scattering measurements on micellar solutions of sodium alkylbenzenesulfonates having branched

alkyl-groups. *Journal of Physical Chemistry*, 86(2):164–167, 1982. Times Cited: 31 Letter English Cited References Count: 26 My912.

[118] J. G. Ma, B. J. Boyd, and C. J. Drummond. Positional isomers of linear sodium dodecyl benzene sulfonate: Solubility, self-assembly, and air/water interfacial activity. *Langmuir*, 22(21):8646–8654, 2006.

[119] N. M. van Os, G. J. Daane, and T. A. B. M. Bolsman. The effect of chemical-structure upon the thermodynamics of micellization of model alkylarenesulfonates .1. sodium para-(x-decyl)benzenesulphonate isomers. *Journal of Colloid and Interface Science*, 115(2):402–409, 1987.

[120] Y. Barakat, L. N. Fortney, R. S. Schechter, W. H. Wade, S. H. Yiv, and A. Graciaa. Criteria for structuring surfactants to maximize solubilization of oil and water .2. alkyl benzene sodium sulfonates. *Journal of Colloid and Interface Science*, 92(2):561–574, 1983.

[121] J. B. Lavigne and M. F. Hughes. Unsymmetrical dialkylbenzene mixtures. Us patent, Chevron Research Company, Sep 16 1966.

[122] E. M. Johnson, G. D. Murray, and F. E. Hardy. Liquid detergent compositions for removal of cooked-on food soils. Us patent, The Procter & Gamble Company, Nov 01 1977.

[123] E. Fanghanel, W. Ortman, K. Behrmann, S. Willscher, N. J. Turro, and I. R. Gould. Photochemical primary processes of xanthene dyes .7. xanthene dyes as probes for the characterization of anionic micelles. *Journal of Physical Chemistry*, 91(13):3700–3703, 1987.

[124] I. VanDerWoude, A. Wagenaar, A. A. P. Meekel, M. B. A. TerBeest, M. H. J. Ruiters, J. B. F. N. Engberts, and D. Hoekstra. Novel pyridinium surfactants for efficient, nontoxic in vitro gene delivery. *Proceedings of the National Academy of Sciences of the United States of America*, 94(4):1160–1165, 1997.

[125] J. J. H. Nusselder and J. B. F. N. Engberts. Surfactant structure and aggregate morphology - the urge for aggregate stability. *Journal of the American Chemical Society*, 111(13):5000–5002, 1989.

[126] J. J. H. Nusselder and J. B. F. N. Engberts. A search for a relation between aggregate morphology and the structure of 1,4-dialkylpyridinium halide surfactants. *Journal of Organic Chemistry*, 56(19):5522–5527, 1991.

[127] J. J. H. Nusselder and J. B. F. N. Engberts. Relation between surfactant structure and properties of spherical micelles - 1-alkyl-4-alkylpyridinium halide surfactants. *Langmuir*, 7(10):2089–2096, 1991.

[128] K. Bijma, E. Rank, and J. B. F. N. Engberts. Effect of counterion structure on micellar growth of alkylpyridinium surfactants in aqueous solution. *Journal of Colloid and Interface Science*, 205(2):245–256, 1998.

[129] K. Bijma, M. J. Blandamer, and J. B. F. N. Engberts. Effect of counterions and headgroup hydrophobicity on properties of micelles formed by alkylpyridinium surfactants. 2. microcalorimetry. *Langmuir*, 14(1):79–83, 1998.

[130] D. Van der Spoel, E. Lindahl, B. Hess, G. Groenhof, A. E. Mark, and H. J. C. Berendsen. Gromacs: Fast, flexible, and free. *Journal of Computational Chemistry*, 26(16):1701–1718, 2005.

[131] W. L. Jorgensen, D. S. Maxwell, and J. Tirado-Rives. Development and testing of the opls all-atom force field on conformational energetics and properties of organic liquids. *Journal of the American Chemical Society*, 118(45):11225–11236, 1996.

[132] H. J. C. Berendsen, J. R. Grigera, and T. P. Straatsma. The missing term in effective pair potentials. *Journal of Physical Chemistry*, 91(24):6269–6271, 1987.

[133] C. M. Breneman and K. B. Wiberg. Determining atom-centered monopoles from molecular electrostatic potentials - the need for high sampling density in formamide conformational-analysis. *Journal of Computational Chemistry*, 11(3):361–373, 1990.

[134] J. Foresman and A. Frisch. *Exploring Chemistry with Electronic Structure Methods*. Gaussian, Inc., Pittsburgh, Pennsylvania, 1996.

[135] D. L. Mobley, E. Dumont, J. D. Chodera, and K. A. Dill. Comparison of charge models for fixed-charge force fields: Small-molecule hydration free energies in explicit solvent. *Journal of Physical Chemistry B*, 111(9):2242–2254, 2007.

[136] C. T. Lee, W. T. Yang, and R. G. Parr. Development of the colle-salvetti correlation-energy formula into a functional of the electron-density. *Physical Review B*, 37(2):785–789, 1988.

[137] B. Miehlich, A. Savin, H. Stoll, and H. Preuss. Results obtained with the correlation-energy density functionals of becke and lee, yang and parr. *Chemical Physics Letters*, 157(3):200–206, 1989.

[138] A. D. Becke. Density-functional thermochemistry .3. the role of exact exchange. *Journal of Chemical Physics*, 98(7):5648–5652, 1993.

[139] P. C. Hariharan and J. A. Pople. Influence of polarization functions on molecular-orbital hydrogenation energies. *Theoretica Chimica Acta*, 28(3):213–222, 1973.

[140] R. C. Binning and L. A. Curtiss. Compact contracted basis-sets for 3rd-row atoms - ga-kr. *Journal of Computational Chemistry*, 11(10):1206–1216, 1990.

[141] T. Clark, J. Chandrasekhar, G. W. Spitznagel, and P. V. Schleyer. Efficient diffuse function-augmented basis-sets for anion calculations .3. the 3-21+g basis set for 1st-row elements, li-f. *Journal of Computational Chemistry*, 4(3):294–301, 1983.

[142] T. Darden, D. York, and L. Pedersen. Particle mesh ewald - an n.log(n) method for ewald sums in large systems. *Journal of Chemical Physics*, 98(12):10089–10092, 1993.

[143] U. Essmann, L. Perera, M. L. Berkowitz, T. Darden, H. Lee, and L. G. Pedersen. A smooth particle mesh ewald method. *Journal of Chemical Physics*, 103(19):8577–8593, 1995.

[144] M. R. Shirts, J. W. Pitera, W. C. Swope, and V. S. Pande. Extremely precise free energy calculations of amino acid side chain analogs: Comparison of common molecular mechanics force fields for proteins. *Journal of Chemical Physics*, 119(11):5740–5761, 2003.

[145] M. R. Shirts and V. S. Pande. Solvation free energies of amino acid side chain analogs for common molecular mechanics water models. *Journal of Chemical Physics*, 122(13):134508, 2005.

[146] E. B. Wilson, J. C. Decius, and P. C. Cross. *Molecular vibrations*. McGraw-Hill, 1955. Reprinted by Dover 1980.

[147] K. Nakamoto. *Infrared and Raman spectra of inorganic and coordination compounds*. Wiley, 5th edition, 1997.

[148] J. P. Ryckaert, G. Ciccotti, and H. J. C. Berendsen. Numerical-integration of cartesian equations of motion of a system with constraints - molecular-dynamics of n-alkanes. *Journal of Computational Physics*, 23(3):327–341, 1977.

[149] H. J. C. Berendsen, J. P. M. Postma, W. F. Vangunsteren, A. Dinola, and J. R. Haak. Molecular-dynamics with coupling to an external bath. *Journal of Chemical Physics*, 81(8):3684–3690, 1984.

[150] P. Jedlovszky, I. Varga, and T. Gilanyi. Adsorption of apolar molecules at the water liquid-vapor interface: A monte carlo simulations study of the water-n-octane system. *Journal of Chemical Physics*, 119(3):1731–1740, 2003.

[151] F. Eisenhaber, P. Lijnzaad, P. Argos, C. Sander, and M. Scharf. The double cubic lattice method - efficient approaches to numerical-integration of surface-area and volume and to dot surface contouring of molecular assemblies. *Journal of Computational Chemistry*, 16(3):273–284, 1995.

[152] I. I. Vaisman, F. K. Brown, and A. Tropsha. Distance dependence of water-structure around model solutes. *Journal of Physical Chemistry*, 98(21):5559–5564, 1994.

[153] P. Linse. Molecular-dynamics simulation of a dilute aqueous-solution of benzene. *Journal of the American Chemical Society*, 112(5):1744–1750, 1990.

[154] W. L. Jorgensen and C. J. Swenson. Optimized intermolecular potential functions for amides and peptides - hydration of amides. *Journal of the American Chemical Society*, 107(6):1489–1496, 1985.

[155] R. L. Mancera and A. D. Buckingham. Temperature effects on the hydrophobic hydration of ethane. *Journal of Physical Chemistry*, 99(40):14632–14640, 1995.

[156] P. K. Mehrotra and D. L. Beveridge. Structural-analysis of molecular solutions based on quasi-component distribution-functions - application to [h2co]aq at 25-degrees-c. *Journal of the American Chemical Society*, 102(13):4287–4294, 1980.

[157] Y Marcus. *Introduction to Liquid State Chemistry*. Wiley, Chichester, 1977.

[158] H. Flyvbjerg and H. G. Petersen. Error-estimates on averages of correlated data. *Journal of Chemical Physics*, 91(1):461–466, 1989.

[159] B. Hess. Determining the shear viscosity of model liquids from molecular dynamics simulations. *Journal of Chemical Physics*, 116(1):209–217, 2002.

[160] J. S. Bader and D. Chandler. Computer-simulation study of the mean forces between ferrous and ferric ions in water. *Journal of Physical Chemistry*, 96(15):6423–6427, 1992.

[161] A. J. M. Yang, J. H. Gibbs, and P. D. Fleming. Molecular theory of surface-tension. *Bulletin of the American Physical Society*, 20(3):305–305, 1975.

[162] M. Reinhard and A. Drefahl. *Handbook for Estimating Physicochemical Properties of Organic Compounds*. Wiley, 1999.

[163] O. Exner. Additive physical properties. iii. re-examination of the additive character of parachor. *Collect. Czech. Chem. Commun.*, 32:24–54, 1967.

[164] L. A. Girifalco and R. J. Good. A theory for the estimation of surface and interfacial energies. i. derivation and application to interfacial tension. *Journal of Physical Chemistry*, 61(7):904–909, 1957.

[165] G. S. Girolami. A simple back of the envelope method for estimating the densities and molecular volumes of liquids and solids. *Journal of Chemical Education*, 71(11):962–964, 1994.

[166] T. A. Camesano and R. Nagarajan. Micelle formation and cmc of gemini surfactants: a thermodynamic model. *Colloids and Surfaces a-Physicochemical and Engineering Aspects*, 167(1-2):165–177, 2000.

[167] N. M. van Os, J. R. Haak, and L. A. M. Rupert. *Physico-Chemical Properties of Selected Anionic, Cationic and Nonionic Surfactants*. Elsevier: New York, 1993.